HYDRAULIC STABILITY OF MULTI-LAYERED SAND-FILLED GEOTEXTILE TUBE BREAKWATERS UNDER WAVE ATTACK

by

Herman Jacobus Kriel

Thesis presented in partial fulfilment of the requirements for the degree of Master of Science in the Faculty of Engineering at Stellenbosch University

Port and Coastal Engineering
Civil Engineering
Supervisor: Mr Geoff Toms
December 2012

Declaration

By submitting this thesis electronically, I declare that the entirety of the work contained therein is my own, original work, that I am the owner of the copyright thereof (unless to the extent explicitly otherwise stated) and that I have not previously in its entirety or in part submitted it for obtaining any qualification.

_____

Herman Jacobus Kriel

Date: _____

Abstract

Current understanding of the hydraulic stability of a stacked geotextile tube structure under wave attack is limited. Failure mechanisms that lead to instability are complicated and there is, as yet, no generic approved design method.

2D physical modelling in the large wave/current flume of the Stellenbosch University was done to test various set-up and hydraulic conditions to determine the hydraulic stability of a stacked geotextile tube structure against wave attack. Sixty-five test runs of approximately 1,000 waves each were run. Modelling was done on two different scales that had good similitude, despite the fact that the same geotextile and fill material were used in both.

The results provided by the physical modelling gave wave conditions larger than anticipated for hydraulic stability. It was found that the term “failure” was too loosely defined in most cases and that, depending on the definition of structure failure the severity of the wave conditions at failure increased substantially. Sliding was found to be the key failure mechanism for a structure constructed from stacked, 80% sand filled, geotextile tubes. The crest tube receives the most severe loading and is the critical tube in the structure. Structures with double tube crests were found to be negligibly more stable than structures with single tube crests, but reduce energy transmission to the leeside of the structure. Impact loading of the structure combined with wave transmission over the structure explained the wave force on the crest tube of the structure.

A modified Goda (1974) method incorporating a wave reduction factor for wave transmission and an angle descriptive of the crest tube position were used. The descriptive angle was derived from results obtained from the physical modelling.

The use of this method provides results that correlate well with those found in the physical modelling and with results obtained in previous research. The method has the additional advantage that it is less constrained by limitations for application than those of previous studies.

.

Opsomming

Die begrip van die hidroliese stabiliteit van ’n struktuur gebou uit gepakte geotekstielsandbuise teen golf aanval, is tans beperk. Faal meganismes wat lei tot die onstabiliteit van ’n struktuur is ingewikkeld en daar is geen generiese aanvaarde ontwerp metode tans in gebruik nie.

2D fisiesemodellering is in die groot golfkanaal van die Universiteit Stellenbosch uitgevoer. ’n Verskeidenheid van struktuur-uitlegte en hidroliese toestande is getoets om die hidroliese stabiliteit van die struktuur teen golf aanval te bepaal. ’n Totaal van 65 toetse van ongeveer 1,000 golwe elk is voltooi. Modellering is op twee verskillende skale gedoen, wat goed vergelyk het ten spyte van die feit dat dieselfde geotekstiel en vul materiaal in albei gebruik is.

Resultate verkry vanaf die fisiese modellering het groter as verwagte golftoestande vir hidroliese stabiliteit gegee. Dit is gevind dat die definisie van faal (mislukking) in die meeste gevalle swak beskryf is en dat, afhangende van wat as faal van die struktuur beskou word, die golftoestande aansienlik beïnvloed word. Die skuif van die buise is die hoof faal meganisme vir ’n gepakte geotekstielbuis-struktuur met ’n vulpersentasie van 80%. Die buis op die kruin van die struktuur word die swaarste belas en is die kritiese buis in die struktuur. Strukture met dubbel buis kruine is onbeduidend meer stabiel as dié met slegs ’n enkele buis as kruin. Die energie wat na die lysy van die struktuur oorgedra word, is egter beduidend minder. Impak belasting van die struktuur gekombineer met golf-transmissie oor die struktuur, verduidelik die stabiliteit van die buis op die kruin van die struktuur.

’n Gemodifiseerde Goda (1974) metode met ’n golfverminderigs faktor word gebruik om golf-transmissie oor die struktuur te akkommodeer, saam met ’n hoek wat beskrywend is van die posisie van die kruin buis. Die beskrywende hoek is afgelei uit resultate verkry uit die fisiesemodellering.

Hierdie metode gee resultate wat goed korreleer met dié verskaf deur die fisiese modellering en die resultate van vorige navorsing oor geotekstielbuis stabiliteit. Die metode het ‘n bykomende voordeel deurdat dit minder begrens is deur beperkings m.b.t. toepassing as die van vorige studies.

Acknowledgements

This thesis was partly supported by the research project: “Development of sustainable as well as environmental-friendly, adaptive and cost-effective technical protection measures for sandy beaches”, funded by the BMBF and the NRF and undertaken in co-operation with the CSIR (Stellenbosch) for which the author is very grateful.

Completing this thesis would not have been possible without the appreciated contributions by others. Thank you to everyone whom I consulted for your valuable time:

Mr G. Toms, Stellenbosch University: Thesis supervisor and head lecturer.

Mr A. Theron and Mr D. Phelp, CSIR: Early help with thesis topic selection and general guide lines.

Prof B. Brinkmann, Leuphana University Lüneburg: Facilitating my stay in Germany.

Ms K. Werth, NAUE: Supplying the geotextile and help with geotextile selection for physical modelling.

Mr D. Dassanayake, Leichtweiss-Institut fur Wasserbau der TU Braunschweig: Hydraulic laboratory visit and thesis discussion.

Dr A. Bezuijen and Mr K. Pilarczyk: Presentation of thesis proposal and discussion of previous geotextile tube breakwater projects.

Mr P. van Steeg, Deltares: Hydraulic laboratory visit in Delft and discussion of the wave reduction factor.

Mr C. Rossouw, RLH: Meeting on physical modelling and general geotextile tube breakwater design and construction.

Mr C. Soltau, WSP Africa Coastal: Discussion of geotextile tube breakwaters.

Hydraulic Laboratory personnel, Mr C. Visser, Mr N. Combrinck, Mr A. Lindoor and Mr E. Wanza: Help with physical model construction, set-up and equipment hire.

Geotextile used in physical modelling was provided free of charge by: *NAUE GmbH & Co. KG. / Bauberatung Geokunststoffe GmbH & Co. KG*

Table of Contents

List of Figures

In Text

In Appendixes

List of Tables

In Text

In Appendixes

List of Appendixes

Nomenclature

α	Angle with horizontal plane
β	Wave incidence angle / wave approach angle.
χ	Effective wave height reduction factor
Δ_t	Relative buoyance density of geotextile tube
η^*	Projected height in Goda method, where $p_2 = 0$
λ	Modification factor, depending on structure type
μ_s	Static friction coefficient
ρ_s	Density of saturated sand
ρ_w	Density of water
ξ_p	Breaker parameter, surf similarity parameter or Iribarren number
a	Vertical distance between the centre of half circles and the crest of the tube
b	Width of geotextile tube
C_t	Coefficient of transmission
d	Water depth
D_x	Particle size from sieving curve of which x% of sample is smaller
E	Energy
f	Filling percentage of geotextile tube
F_G	Gravity force
F_H	Horizontal hydraulic force
g	Acceleration due to gravity; 9.81m/s^2

h	Height of geotextile tube
H_{max}	Maximum wave height in an irregular storm
H_{m0}	Spectral significant wave height
H_s	Significant wave height. $H_{1/3}$
L	Length of geotextile tube
L_0	Deep water wave length
M	Circumference of the half eclipse in the tube cross-section
O	Circumference of geotextile
O_x	Geotextile opening size of which x% of openings is smaller than
p	Pressure
r	Radius of the small half-circles in the tube cross-section
R	Radius of theoretical circle of tube cross-section at 100% filling
R_c	Crest height of structure above SWL.
s_P	Wave steepness
SWL	Still water level
T	Tensile stress
T_p	Peak period.
U	Stochastic variable signifying bias an uncertainty
x	Horizontal displacement for specific test
x_{cum}	Cumulative horizontal displacement from initial measurement

Definitions of Terms

Bulk reflection coefficient: Ratio of the reflected wave height to the incident wave height.

Dilatancy angle: The amount by which a dry amount of sand will expand when it becomes saturated

Filling percentage: A tube's filling percentage can be described by either the percentage of its height to that of the height of the theoretical circle of the tube at 100% filling, f_h, or the percentage of its cross-sectional area to that of the cross-sectional area of the theoretical circle at 100% filling, f_a. Filling percentage, as used in this thesis, always refers to f_a, except when clearly stated otherwise. See Figure 2.3.

Filling port: Opening in geotextile tube by which it is filled.

Geotextile tube/Geotube/Sand tube/Sand sausage: Hydraulically filled geotextile container. Geotube® is a geotextile tube product from TenCate Geosynthetics, but also a common term used for geotextile tubes. In this thesis these elements are also referred to as "tubes".

Geosystem: Any civil engineering application making use of geotextiles

Relative or buoyance density: The relative density of a geotextile tube under water.

Sand tightness: The ability of the geotextile to prevent loss of contained fill through its texture.

Transmission coefficient: The ratio between the transmitted and incident wave height.

Chapter 1 – Introduction

1.1 – General

Coastal structures have become very expensive to build and maintain, largely due to the shortage of natural rock (Pilarczyk 2000). Shorelines are continuously being eroded, and in the light of the expected rise in sea level this problem will only worsen. Consequently the demand for cheaper materials for constructing coastal structures is growing (Oh & Shin 2006).

Geotextiles used for soil and sand containment in various types of containers have been used for the last 35 years. The use of geotextile tube technology is well established for flood and water control, and more recently, for the prevention of beach erosion and shore protection (G. R. Koerner & R. M. Koerner 2006).

The possibilities of geotextile use in coastal engineering are immense. One element impeding its use is the limited knowledge and understanding thereof. Geotextile technology is currently being researched widely for use in coastal applications, and the materials themselves are also continuously being improved. Extensive testing has been done on the hydraulic stability of single geotextile tubes, but very little is known about how a multi-layered structure performs.

A breakwater constructed from sand-filled geotextile tubes could be a viable alternative to more conventional rubble mound breakwaters in cases where temporary protection is required or rock is not obtainable and too difficult to transport to the site. With the expected worsening of coastal erosion as a result of the rise in sea level, a soft, inexpensive solution will be a strong contender to replace a more conventional hard engineering solution as small coastal communities become affected.

The environmental impact of said structure should also be less than that of a rubble mound structure, as the quarrying and transporting of rock are not required and the structure can easily be removed in the case of adverse unforeseen impacts. The ability to use local material and unskilled labour makes construction easier and faster and construction in isolated areas possible.

1.2 – Motivation

Current understanding of hydraulic stability of stacked geotextile tube structures is limited at best and the potential for future application with better understanding is vast. A geotextile tube breakwater could be both an innovative and "low-cost" solution for various coastal projects.

1.3 – Objectives

The objective of this thesis was to:

- Determine the hydraulic stability of multi-layered geotextile tube structures.
- Define critical aspects of this type of structure and hydraulic conditions that will increase and decrease stability.
- Provide a method to calculate the hydraulic stability.
- Evaluate findings against current methods and formulae.

1.4 – Methodology of Research

The objective for this research was achieved by means of:

Firstly, a literature study was done on current application and design practice. Parallel to the literature study consulting firms with current or previous geotextile tube structure design projects were visited and queried on their experience. Hydraulic laboratories that have completed hydraulic testing of geotextiles for coastal applications were visited in South Africa, Germany and the Netherlands. From the literature review it was determined that the best way to determine the hydraulic stability will be a 2D physical model (see Chapter 2).

Secondly a 2D physical model was constructed that could accurately replicate a typical application area for the intended structure. Different structure configurations with varying hydraulic conditions were tested (see Chapter 3 and 4).

Thirdly, comparing the data collected from these tests against current methods and analysing the data to generate a new method for calculating hydraulic stability (see Chapter 5).

Fourthly, using the analysed data to draw conclusions and make recommendations for application and further study (see Chapter 6).

Chapter 2 – Literature Review

2.1 – Overview

The literature study starts with a background to geotextile use in coastal engineering. The materials and properties of different geotextiles are compared and the benefit of their use was studied. The mechanical properties of a geotextile tube structure relevant to its hydraulic stability against wave loading are investigated to give a better understanding of the physical properties and forces involved. Current methods and formulae used to calculate stability and their development were studied and shortcomings were highlighted. Previous applications of geotextiles were studied to better understand possible applications and find limits of their use. The properties of a typical wave climate (at the structure) were investigated to provide an understanding of the nature of wave forces that can be expected. See Figure 2.1 for the intended mode of application studied in this thesis.

Figure 2.1: Geotextile tube breakwater (photo: Geofabrics Australia)

2.2 – Background

Geotextile tubes, sand sausages, sand tubes or geotubes are long, cylindrical hydraulically filled geotextile tubes that are permeable to water but not to sand. They are generally filled with sand, but other granular material is occasionally used. Sizes

range from 0.5 to 4.0m in diameter and from 25 up to 100m in length (CUR 2006). Common applications include: groynes, dune foot protection, underwater reefs, core replacement for conventional rubble mound breakwaters and dykes, breakwaters and to dewater dredged material.

Geosynthetic products are applied in many types of maritime structures. The reasons for replacing classic material, such as gravel, rock and concrete, include the unavailability of common materials, a reduction in the quantities required, improved functionality, simplified execution and a reduction in execution time. All of these advantages could lead to lower construction costs. The maintenance costs of the structure during the service life must also be taken into consideration (PIANC 2011).

The cost benefit of a structure increases with an increase in the isolation of the construction site. Local material and low-skilled labour can be used, rather than transporting all the required construction materials and labour to the construction site. Compared to traditional construction methods the application of geotextile sand filled elements may add considerable operational advantages to the execution of marine works and may offer attractive financial opportunities. The main advantages of geotextile systems when compared with traditional methods, including prefabricated concrete units, are reduction in work, use of local material, equipment and low-skilled labour, and no need for heavy construction machinery (Ergin et al. 2003).

Using geotextile tubes in conjunction with dredging operations has the advantage of reduced environmental impact in the aquatic habitat surrounding the site. Disposing of dredged material by hydraulically filling geotextile tubes greatly reduces the turbidity, siltation and migration of fines to the surrounding area and impacts on the environment (Fowler et al. 2002).

2.3 – Geotextile

The first use of geotextiles dates from circa 1950 and was a product used in the floor covering industry (CUR 2004).

Geosynthetic materials, or geotextiles, are tough, flat sheets typically made of synthetic fibres produced from polymeric materials that are woven, knitted, punched, melted resin treated or simply pressed together. Woven and knitted sheets are termed woven geotextiles , and sheets that are pressed, melted, matted, heat bonded, resin

treated or punched together are termed nonwoven geotextiles (Fowler et al. 1997). Woven geotextiles have high strength with small elongation, but can easily be punctured. Non-woven geotextiles have lower strength with high elongation (see Figure 2.2), but perform well at resisting puncturing. Composite geotextiles are an attempt to incorporate the advantages of both.

Geosynthetics are manufactured from the following main types of polymeric materials: polyester (PET), polypropylene (PP), polyethylene (PE) and polyamide (PA) No geosynthetic product is made of 100% polymer resin. The main resin is mixed or formulated with additives such as antioxidants, screening agents, fillers and/or other materials for a variety of purposes. The total amount of each additive in a given formulation varies widely – from a minimum of 1% to as much as 50%. The additives function as UV light absorbers, antioxidants, thermal stabilisers, etc. (PIANC 2011). See the Table below for comparative properties.

Table 2.1: Comparative properties of geotextiles (after Pilarczyk 2000)

Property		PET	PA	PP	PE
Strength		3	2	1	1
Elastic modulus		3	2	1	1
Strain at failure		2	2	3	3
Creep		1	2	3	3
Unit weight		3	2	1	1
Cost		3	2	1	1
Resistance to:					
UV light	Stabilized	3	2	3	3
	Un-stabilized	3	2	2	1
Alkalis		1	3	3	3
Fungus and pests		2	2	2	3
Fuel		2	2	1	1
Detergents		3	3	3	3

3: High, 1: Low

The main benefits of geosynthetics are:

- Quality-controlled manufacture in a factory environment
- Quick installation in many cases
- Generally replace raw material resources
- Generally replace different designs using soil or other construction materials
- Cost competitive against soils or other construction materials that they replace
- Technical database (both design and testing) is reasonably established

(R. M. Koerner 2005 cited in PIANC 2011)

Geotextile tubes can be constructed from woven, non-woven or composite geotextiles.

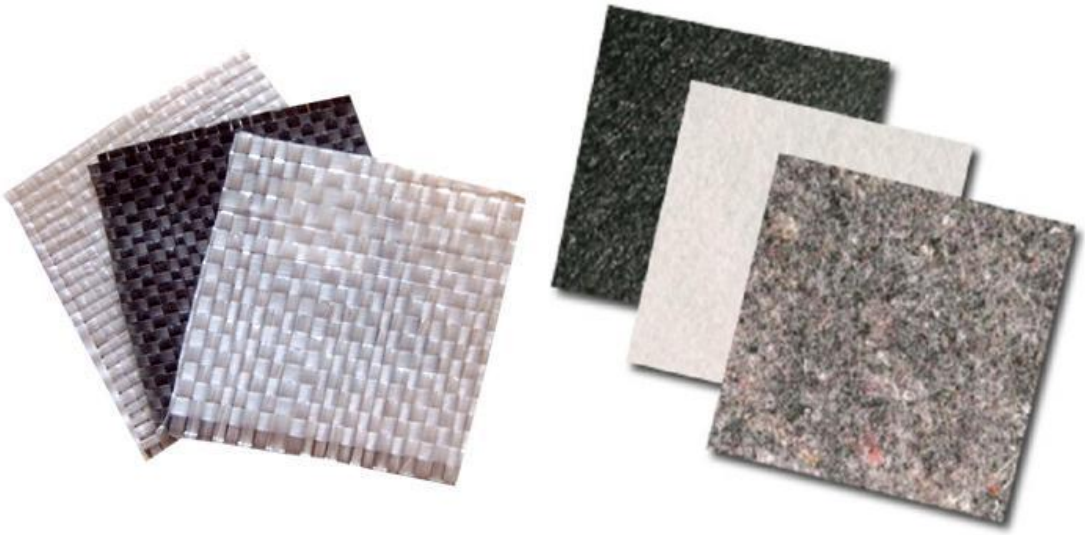

Figure 2.2: Woven geotextiles (left) and non-woven geotextiles (right) (photo: Geosintex)

Geotextiles for coastal application are available in South Africa from the following manufacturers:

Geofabrics, Australia

Kaytech, South Africa (sister company of Geofabrics)

NAUE, Germany

Ten Cate, the Netherlands

The strength and elongation properties of geotextiles depend on the polymer, the production method and the thickness of the geotextile. Tensile strengths of the standard available geotextiles range from as little as 5kN/m to over a 1,200kN/m. (See physical properties of polymer in Table 2.2.)

Table 2.2: Polymer physical properties (after PIANC 2011)

Property	PET	PA	PP	PE
Density (kg/m^3)	1380	1140	900	920
Tensile Strength 20°C (N/mm^2)	800-1200	700-900	400-600	80-600
Elasticity (N/mm^2)	1200-18000	3000-4000	2000-5000	200-6000
Strain at failure (%)	8-15	15-30	10-40	10-80
Melting Point (°C)	250	220	160	110-135

Sewn seams are regarded as the most reliable way to bind geotextile sheets (CUR 2004). Seam strength is given as a percentage of the geotextile strength. Depending on the type of seam used, an efficiency of more than 70% can be reached (CUR 2006).

2.4 – Mechanical Properties Relative to Hydraulic and Structural Stability

2.4.1 – General

There are several causes for the structural failure of geotextile tube structures.

The key failure mechanisms are:

- sliding
- overturning
- overall stability (slip circle)
- bearing capacity failure in the subsoil
- movement of the elements
- internal migration of sand in the tube, resulting in large deformations
- scour in front of the structure
- geotextile skin rupture

Aspects that influence the stability of the structure are:

- size of the element
- location of the element in the structure
- friction between the elements
- layout of the structure
    - slopes of the structure
    - overall stability of the structure
    - scour in front of the structure

The stability characteristics depend on:

- wave-induced forces on the tubes, which are determined by:
    - wave height and currents
    - angle under which the waves and current reach the tubes
- wave induced pressure differences in the tube, which are influenced by:
    - internal movement of sand in the tubes
    - filling percentage
    - sand characteristics
    - tube dimensions
- other processes leading to the deformations and displacement of the tubes are influenced by:

- fixation between the tubes
- friction coefficient between the tubes

(PIANC 2011)

An aspect of the stability that is easily overlooked, but should be taken into account is the instability of the geotextile tube during filling. The geotextile tube does not have any torsion stiffness during this procedure and cannot provide any resistance to currents or wave action. It therefore should be fixed horizontally until filling is complete (CUR 2004, see Figure 2.19). The placement of geosystems in general requires calm conditions (Bezuijen & Vastenburg 2008).

2.4.2 – Tube Shape

The design of hydraulically filled geotextile tubes is theoretically based on the surface tension of a water drop lying on a smooth surface. The original methods of calculation were developed to design membrane containers for the storage and transport of fluids (Cantré & Saathoff 2011).

Field experience has demonstrated that it is possible to fill geotextile tubes to 80% of the theoretical maximum circular area. The dredged material used to fill geotextile tubes can be any material capable of being transported hydraulically (Oh & Shin 2006).

To predict the shape of a tube filled with coarse-grained material is easier than one filled with fine-grained material, due to the immediate settling and effective free drainage of coarse-grained material. In the case of fine-grained material, the consolidation process is more complicated due to suspended fine particles, the clogging of the geotextile, nonhomogeneous slurry, and the staged filling process (Oh & Shin 2006).

Numerical methods used to determine the shape of the tube are based on Timoshenko's method (CUR 2006). Timoshenko's method assumes that the tensile stress in the geotextile is constant over the circumference of the tube with the exception of the length that is in contact with the bottom surface, that the material does not have any bending stiffness or weight, and that the filling material is a fluid and therefore that no hydrostatic state of stresses exists in the tube. No shear stresses develop between the tube and the slurry (CUR 2006).

The nonlinear differential equation used to determine the shape of the tube has no closed-form solution, meaning that it needs to be solved numerically (D. Leshchinsky et al. 1996). Due to its complexity, numerical models like the commercially available computer software GeoCoPS (Leschinsky 2007) are used to solve it. The CUR 217 (2006) gives simplified methods for calculating tube forces and shapes that correspond well to solutions given by computer software. Table 2.3 provides a summary of tube cross-sections for certain filling percentage. (See Figure 2.3 for r, b and h.) R is the theoretical radius of the tube at 100% filling.

Table 2.3: Tube shape at different filling percentages, after CUR 217 (2006)

Filling %	r	b	h
100	1.000R	2.000R	2.000R
95	0.700R	2.279R	1.593R
90	0.584R	2.396R	1.421R
85	0.499R	2.485R	1.287R
80	0.430R	2.561R	1.172R
75	0.371R	2.627R	1.069R
70	0.320R	2.686R	0.976R
65	0.275R	2.740R	0.889R
60	0.235R	2.790R	0.807R

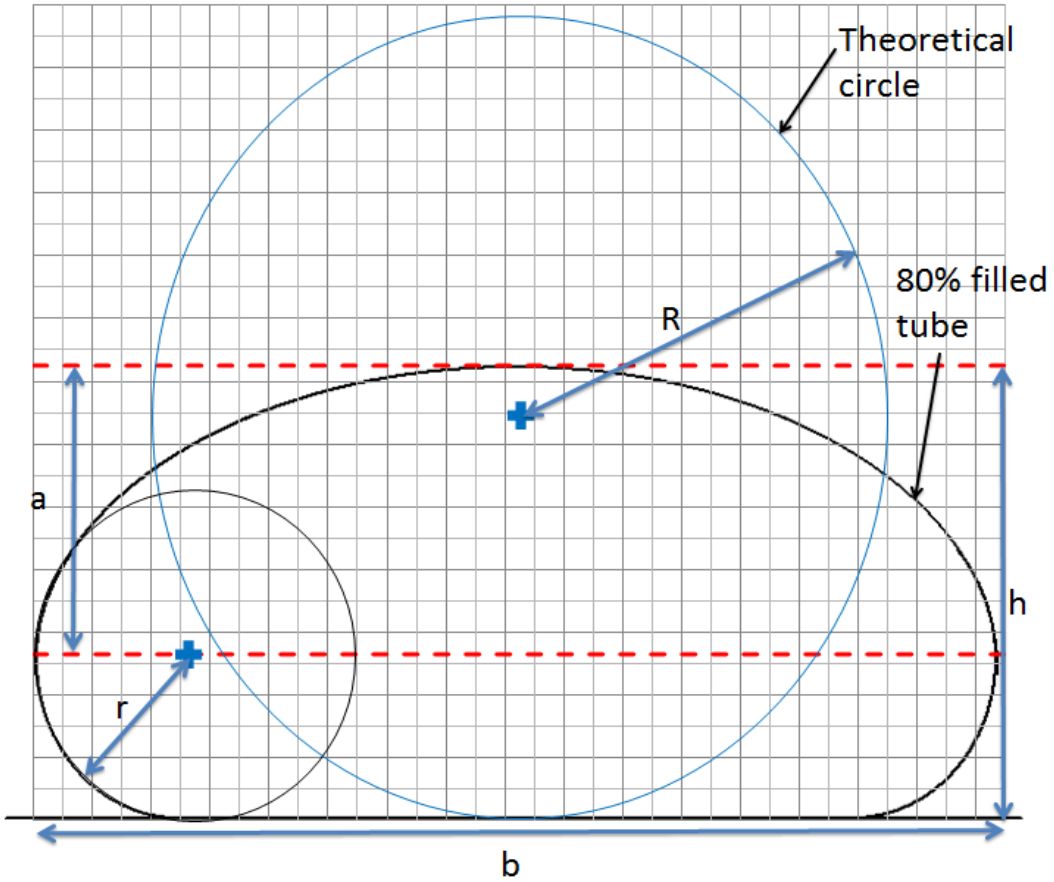

Figure 2.3: Tube filled to 80% and theoretical circle at 100% filling

To calculate the circumference of a geotextile tube cross-section given the measurements in Figure 2.3 the formulae below can be used.

$$O = (2\alpha^2 + \pi - 2)r + M = 2\pi R$$

with:

O = circumference

$$\alpha = \frac{a}{r}$$

Circumference of half an eclipse, M:

$$M = \pi\alpha^2 r \frac{\sqrt{1 + \frac{35}{72}m^2 + \frac{2}{15}m^4}}{1 + m}$$

with:

$$m = \frac{\alpha - 1}{\alpha + 1}$$

R = radius of circle at 100% filling

To calculate the area of the cross-section of a tube given the measurements in Figure 2.3, use the formulae below.

$$A = \frac{1}{2}\pi\alpha^3 r^2 + 2\alpha^2 r^2 + \left(\frac{1}{2}\pi - 2\right)r^2$$

$$A \approx f R^2 \pi$$

f = fill percentage (area)

To calculate the height and breadth of the tube, Table 2.3 or the equations below can be used.

$h = (1 + \alpha)r$ (*height*)

$b = 2\alpha^2 r$ (*breadth*)

In relation to the stability of the geotextile tubes, shape and deformation play a significant role. A flat tube (tube with low filling percentage) will resist rolling and sliding better than a roundish one, due to a reduced area interacting with horizontal wave forces and an increased distance between the pivot point and the mass centre of the tube. The shear stress in the geotextile is also less in a flat tube. Using tubes with lower filling percentages would increase the amount of tubes required to reach the

design height of the structure, while simultaneously increasing the base width of the structure. Reduced fill percentages also lead to sand migration in the tubes, causing deformation. The reduced fill percentage could also lead to possible mechanical wear of the geotextile due to wave loading dislodging and mobilising the material inside the tube. This will reduce the lifetime of the geotextile, i.e. the structure. Higher filling percentages also reduce the occurrence of internal sand migration from wave loading that leads to the deformation of geotextile tubes (Van Steeg & Vastenburg 2010). An optimal fill percentage and geotextile tube size therefore is necessary. An 80% fill percentage by the cross-sectional area of the tube is considered to be close to the practical maximum to which a geotextile tube can be filled under prototype conditions.

2.4.3 – Deformation, Filling Percentage and Sand Tightness

The retention of fill of a dredged material-filled tube is provided by the geotextile envelope. Geotextile selection is based on the geotextile's opening characteristics, which must match the fill particle size and permeability. A composite fabric shell is sometimes used, since it incorporates both the nonwoven fabric for filtration and a woven fabric for strength.

With a multi-layered structure, the bottom layer of tubes will receive loading from the tubes above it (see Figure 2.4). This loading causes deformation of the bottom tube, which depends on the characteristics of the fill material and the sand tightness.

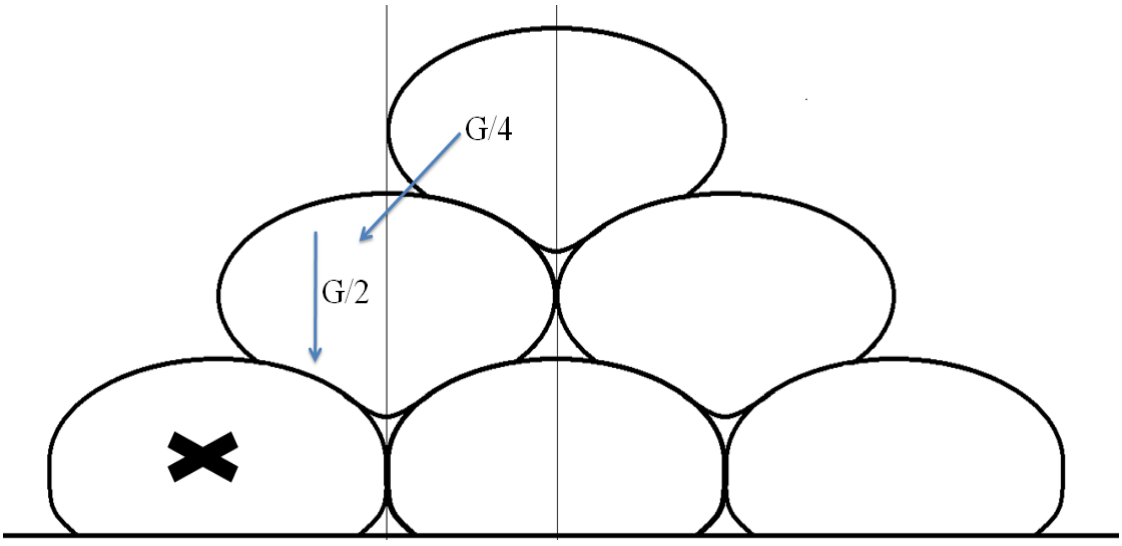

Figure 2.4: Loading on bottom tube from weight of tubes above it. G = weight of one tube (after Cantré 2002)

The deformation of the tubes is less at a higher fill percentage. Deformation occurs as a loss of height in the geotextile tube. A formula calculating this height loss for fill percentages from 41% to 74% has been derived by Van Steeg and Vastenburg (2010)

$$S_{tube} = -0.41 p_{h.b} + 0.323$$

$$S_{tube} = \frac{D_{deformed} - D_{initial}}{D_{initial}}$$

with:

p_{hb} = *filling percentage based on height*

$D_{deformed}$ = *deformed height*

$D_{initial}$ = *initial height after filling*

In single geotextile tube structures the deformation should make the structure more stable due to the decrease in height. In a multi-layered structure, deformation could have negative effects on the stability as higher tubes might roll off the lower layer of deformed tubes more easily as a result of unequal settling or deformation.

The sand transport in the tube is highly dependent on the filling percentage. A low filling percentage enables the sand to move within the geotextile element resulting in deformation. Tubes with high filling percentages show very little erosion or sand migration inside the tube. In most cases a geotextile tube will be filled to its (practical) maximum. This will lead to high degrees of filling (80% on basis of area). Therefore, it is unlikely that internal sand migration within a geotextile tube will be a realistic failure mechanism for a structure consisting of geotextile tubes with high filling percentages. (Van Steeg & Vastenburg 2010)

When filling a geotextile tube with granular sands or gravels, as in shoreline protection, the process of draining the slurry water through the fabric is quite rapid. Inversely, when filling a geotextile tube with fine grained soil or silts, as in dewatering for water purification, the process of draining water is very slow. This is due to the build-up of a filter cake of fine sediment on the inside surface of the fabric. Depending on the permeability of the filter cake, higher filling pressures and/or repeated sequences of filling become necessary. Fundamentally, the fabric must act

successfully as a filter, allowing water to pass but retaining the contained soil particles. In order to optimize water drainage from the filling material, the opening size of the fabric being considered is important. If too open, soil particles will be lost. Conversely, if too tight, excessive pressure might be required that could exceed the fabric or seam strength and result in a failure (G. R. Koerner & R. M. Koerner 2006).

To ensure sand tightness, the following formula needs to be used (CUR 2006):

$$O_{90} \leq D_{90}$$

$$O_{90} < 1.5 D_{10} C_u^{1/2}$$

O_{90} = the opening size which corresponds to the D_{90} of the soil passing through the geotextile

with:

D_x = *sieve size of the rectangular openings of the theoretical sieve where x% of the grains of sand pass through*

C_u = uniformity coefficient (D_{60}/D_{10})

2.4.4 – Forces in Geotextiles

The structural integrity of a dredged material-filled tube is provided by the geotextile envelope. The strength of the geotextile and the seam strength are the major design considerations in order to resist pressures during filling.

The tension in the geotextile is constant over its circumference. This tension can be expressed as $T = p.r.$, where p is the hydraulic pressure in the fill-material and r is the radius at a random location in the cross-section. The basic principle to calculate the force in the geotextile is based on Timoshenko's method (CUR 2006). This method does have an analytical solution, but due to its complexity, numerical models like GeoCoPS (Leschinsky 2007) are used to calculate it. This solution can also be solved graphically, although an approximate error of about 10% is normally made and this method should only be used for quick estimates (see Figure 2.5).

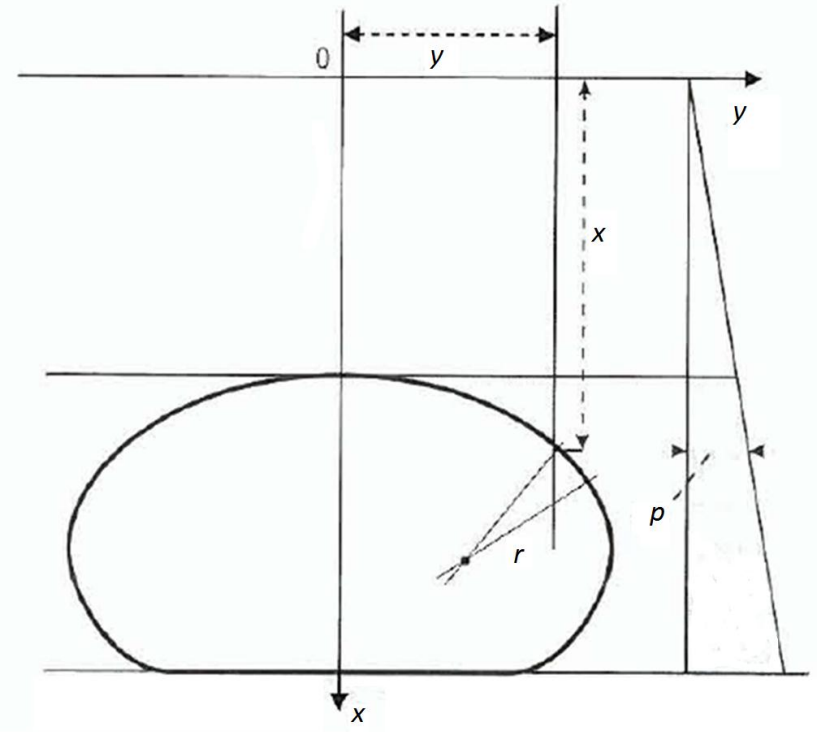

Figure 2.5: Graphical presentation of Timoshenko's method to calculate tensile stress in the geotextile (CUR 2006)

When calculating shear stress in the geotextile according to CUR 214 (2004), three forces need to be taken in to account:

1. Pumping pressure (PP). Constant over circumference
2. Pressure from fill material. (PM)
3. Pressure from water (PW) – only for submerged tubes

Figure 2.6 provides the force diagram and the equations below are used to calculate the reaction forces.

$$R_A = \left(\frac{P_P - P_{WB}}{2}\right) h + \left(\frac{P_M - P_{WO}}{6}\right) h$$ Shear stress in top part of tube

$$R_A = \left(\frac{P_P - P_{WB}}{2}\right) h + \left(\frac{P_M - P_{WO}}{3}\right) h$$ Shear stress in bottom part of tube

P_{WB} = *water pressure at top*

P_{WO} = *water pressure at bottom*

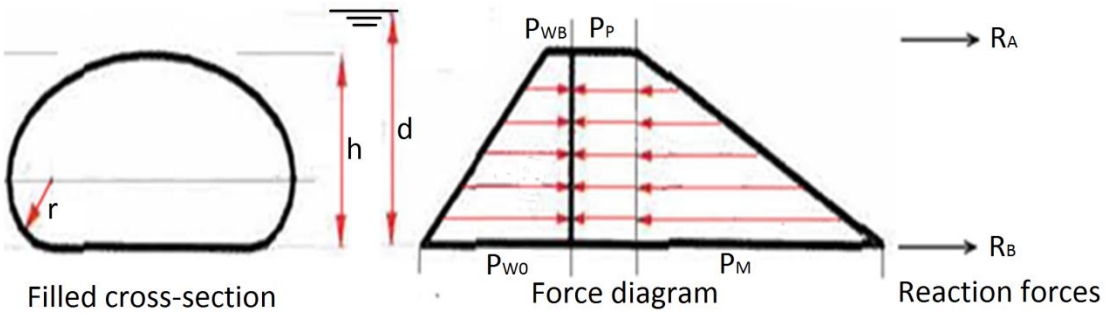

Figure 2.6: Geotextile force diagram (after CUR 2004)

Figure 2.7 shows the results of a numerical calculation for a geotextile tube with a circumference of 12m under different fill percentages. Note the sharp increase in the shear stress with higher fill percentages.

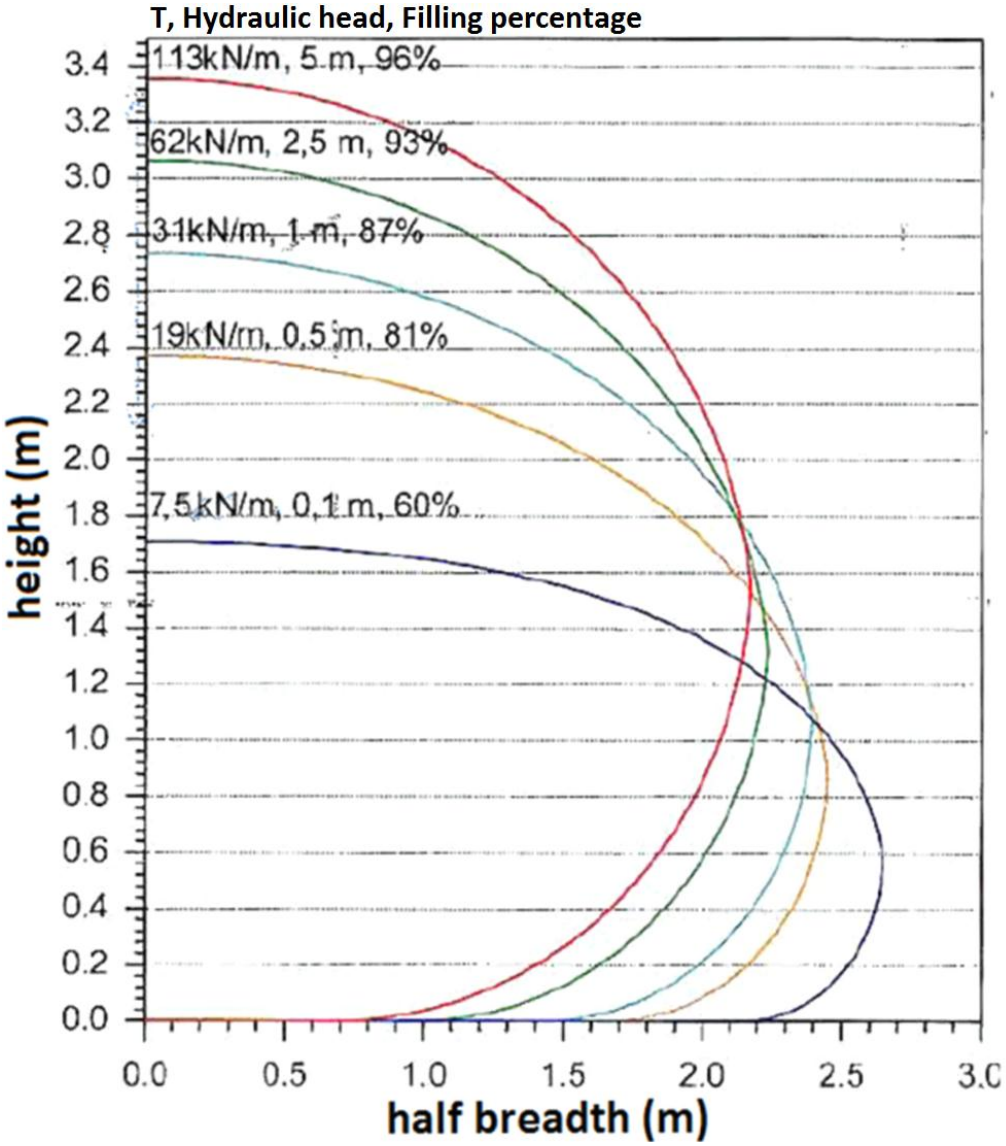

Figure 2.7: Tensile stress, hydraulic head and filling percentage corresponding to different shapes of a tube with a circumference of 12m (CUR 2006)

Typically the circumferential force will be much larger than the axial force. If a geosynthetic with isotopic strength is used, which is common, the axial force is not needed in the design. (D. Leshchinsky et al. 1996) Tension in the geotextile needs to be taken in account at three different locations (see Figure 2.8). Circumferential and axial tension as discussed earlier in this chapter and tension around the filling port connection. The port connection tensions are a function of filling pressure and filling height. With high filling percentages the tension at the filling port can be very high.

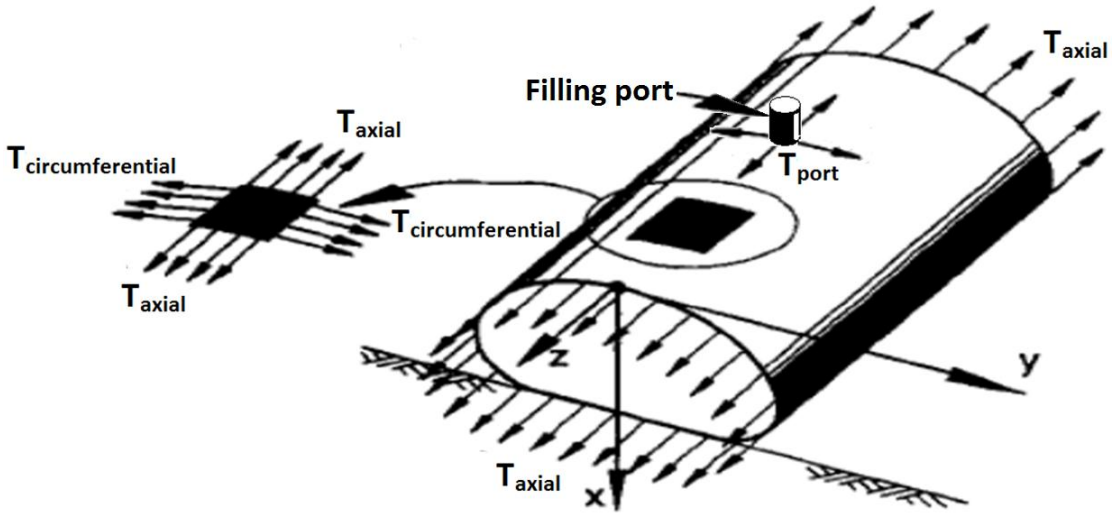

Figure 2.8: Tensile stress in geotextile (after D. Leshchinsky & O. Leshchinsky 1996)

2.4.5 – Friction

Interface friction between geotextile-sand and geotextile-geotextile is of the utmost importance and has a big impact on the hydraulic stability of the structure against sliding and the fixation of the tubes in the structure.

For explanation of interface friction and tests, see Appendix H. Interface friction is also included in most of the stability formulae discussed in Chapter 2.6.

2.4.6 – Permeability

Juan Recio (2008) concluded in his PhD thesis that the permeability of a geotextile sand-container structure is governed by the gaps between the geotextile sand containers. The way the geotextile tubes will be stacked in the flume will not create any gaps between the tubes on the face receiving wave loading. In the study done by Van Steeg and Vastenburg (2010) on geotextile tube stability it was concluded that

the water flow through the fabric and fill of the geotextile tubes themselves is so little that it can be neglected in respect of scaling rules.

The importance of the permeability comes into play when considering the stability formulae and the schematisation of the forces in them. The permeability of a geotextile tube structure would not only exert vertical uplift forces on the upper tubes in a structure, but will also increase sand transport inside the tubes if the tubes themselves are permeable.

2.4.7 – Toe Scour

As with a conventional breakwater, scour at the toe of the structure needs to be prevented.

With the use of single geotextile tubes for shore protection it was found that wave action on the tube itself rarely causes the tube to fail. Rather the wave-induced scour around the tube leads to failure. The failure of a tube that is parallel to the shore usually occurs when the tube becomes displaced differentially along its length. Observations suggest that the displacement is most often seaward as the tubes become undermined when the beach scour propagates landward under the tube. The beach slope steepens locally until the tube falls seaward into the scour hole (Weggel 2005). See Figure 2.9.

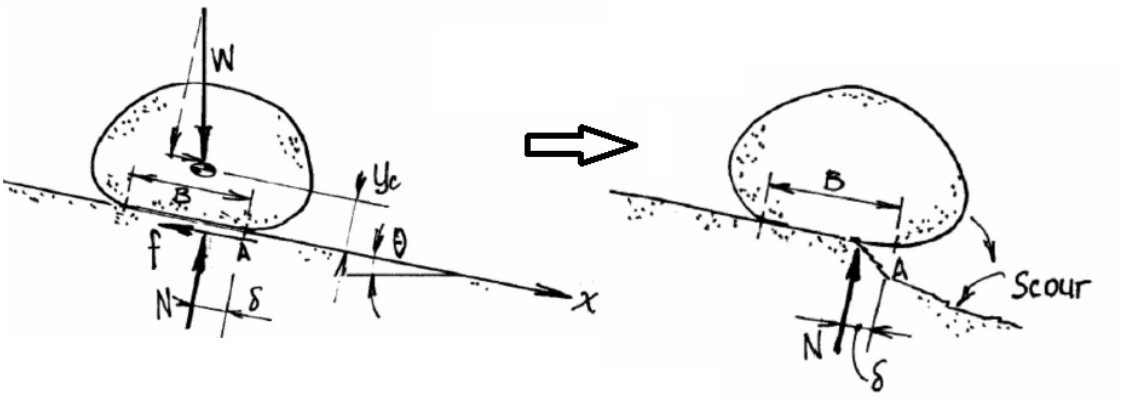

Figure 2.9: Scour propagating under geotextile tube (Weggel 2005)

From the above schematisation of forces the following equation describing the moments of the forces is given by:

$$\delta = \frac{B}{2} - y_c tan\theta$$

with:

Θ = *beach slope angle*

B = *base contact width*

y_c = *height of the tube's centre of mass above the base*

δ = *distance landward of point A where the normal restoring force, N, acts*

Assuming that friction is sufficient to prevent sliding of the tube seaward, overturning failure will occur when δ reaches 0. This distance depends only on the beach slope and the ratio of the height of the tube's cross-sectional centroid to its base width.

Solutions to prevent the toe scour problem include:

- Outrigger or anchor tubes, connected to the main tube by a geotextile mat in order to prevent the landward movement of the scour hole (see Figure 2.10 and Figure 2.31). As the scour progresses, the outrigger tube settles into the hole and prevents or slows the scour process (Weggel 2005);
- Additional geotextile tubes at the toe of the structure;
- A pre-dredged trench into which the bottom layer of tubes of the structure fits.

Figure 2.10: Geotextile tube as shore protection in Grand Isle, Louisiana. (Photo: TenCate Geosynthetics)

2.5 – Wave Climate

2.5.1 – Wave Height Distribution

Due to the shallow foreshore conditions that would be present in a typical application, shoaling and depth limiting of waves need to be considered. The deep-water relation of the significant wave height to the maximum wave height is no longer valid in the breaker zone and wave periods shorten. Using an incident offshore H_s in the stability calculation could be problematic. The method of Battjes and Groenendijk (2000) can be used to calculate the wave height distribution from the spectral significant wave height, H_{m0}.

2.5.2 – Breaker Parameter

The breaker parameter is also referred to as the surf similarity parameter or Iribarren number, $\xi_P = tan\alpha/\sqrt{s_0}$. The combination of foreshore slope and wave steepness will result in a certain type of wave breaking. As wave breaking will already occur on the foreshore for a common application of the structure, the foreshore slope, α, is used to determine the breaker type. Breaker types can be categorised according to the Iribarren number (Pullen et al. 2007):

- Spilling: 0.2 < ξ_P
- Collapsing: ξ_P ± 2-3
- Plunging: 0.2 < ξ_P < 2-3
- Surging: ξ_P > 2-3

Waves plunging perfectly onto a structure result in impact loading of the structure. These impact forces are considerably larger than those created by non-breaking waves, but last only for a few hundredths of a second (U.S. Army Corps of Engineers 2006). The structure will experience more damage as a result of impact loading than as a result of pulsating loading.

2.6 – Current Methods to Calculate Stability

Design methods have been published based on the results of many reduced scale tests. However, the failure mechanisms that lead to the instability of the tubes are complicated and have not yet led to a generic approved design method, (PIANC 2011). All stability formulae used are for geotextile tubes lying perpendicular to the wave direction.

2.6.1 – Pilarczyk (2000)

A theoretical derivation of the stability of a stacked geotextile tube with the crest at the SWL was done on the results obtained from a study undertaken on the stability of sand- and mortar- filled geotubes and geocontainers for Nicolon by Delft Hydraulics (1994). It was concluded that the critical wave height was equal to the theoretical diameter of the tube (see Chapter 2.4.2 - Tube Shape). A reduction of the wave period, flattening of the tube and reducing the water level were found to have a positive effect on the stability. See Figure 2.11 for schematization of forces.

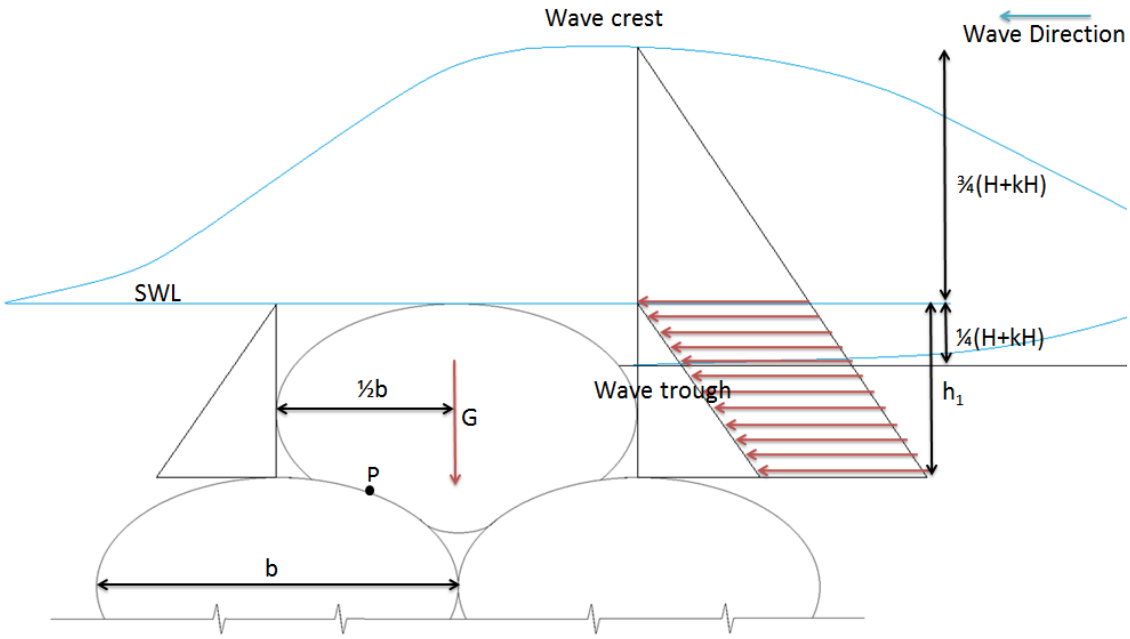

Figure 2.11: Schematization of forces acting on crest tube (after Pilarczyk 2000)

According to Pilarczyk (2000):

Overturning moment around point P: $M_O = \frac{3}{4}(1+k)H\frac{1}{2}h_1^2\rho_w g$ *per m length*

Restoring moment around point P: $M_R = A(\rho_s - \rho_w)g\frac{1}{2}b$ *per m length*

with:

k = *Reflection coefficient (≈ 0.45)*

H = *Wave height*

h_1 = *Height of tube*

ρ_w = *Density of water*

g = *Acceleration by gravity*

A = *Area of tube cross-section*

ρ_s = *Density of saturated sand*

b = *Tube width*

For stability against overturning:

$$H < \frac{4}{3} Ab \frac{\Delta_t}{h_1^2(1+k)}$$

with:

Δ_t = $(\frac{\rho_s - \rho_w}{\rho_w})$ *relative weight of tube*

The above equation can be simplified for tubes lying parallel to the axis of a breakwater with their crests below or at SWL to produce the dimensionless stability relation:

$$\frac{H_s}{\Delta_t b} < 1$$

Filling percentage is not included in the formula, but from the height and width measurements of the geotextile tubes used in the physical modelling, which were used to determine the above stability formula it is calculated that the tubes were filled to approximately 90%.

2.6.2 – CUR 217 (CUR 2006)

CUR 217 (CUR 2006) recommends using a very similar formula for calculating the limiting significant wave height to that prescribed by Pilarczyk (2000). It is more cautious, however, as it replaces the width with that of the height of the geotextile tube. This has a significant effect on the allowed wave height as the width of an average tube is nearly twice that of its height.

CUR (2006) states that the tube that receives the heaviest loading is the tube at the crest of the structure. A formula for a limiting significant wave height for the stability of a geotextile tube on the crest of a breakwater is given.

$$\frac{H_s}{\Delta_t D_k} \leq 1$$

with:

H_s = *significant wave height*

D_k = *height of geotextile tube (with tube perpendicular to wave direction)*

= *length of geotextile tube (with tube parallel to wave direction)*

Δ_t = *relative weight of tube or relative buoyant weight of tube*

Note that filling percentage is not specified or used in this formula.

Using the above formula gives an estimated H_s equal to the height of the tube ($\Delta_t \approx 1$)

The wave height from the above formula is the wave height at which the geotextile tube is expected to start moving.

2.6.3 – Deltares (Van Steeg & Vastenburg 2010)

Before the study done by Van Steeg and Vastenburg (2010), the behaviour of geotextile tubes under wave loading was uncertain as no large scale modelling of geotextile tubes had been done. This severely limited the use and incentive to use the tubes as coastal protection structures.

To test the stability of sand-filled geotextile tubes under wave attack, large-scale physical models were tested in the Delta Flume of Deltares, with an approximate scale of 1:2 to 1:4 (see Figure 2.12 for the different configurations tested). All failure resulted from sliding. Sand migration in tubes filled to less than 70% decrease stability, but is minimal in tubes with high filling percentages (Van Steeg & Vastenburg 2010).

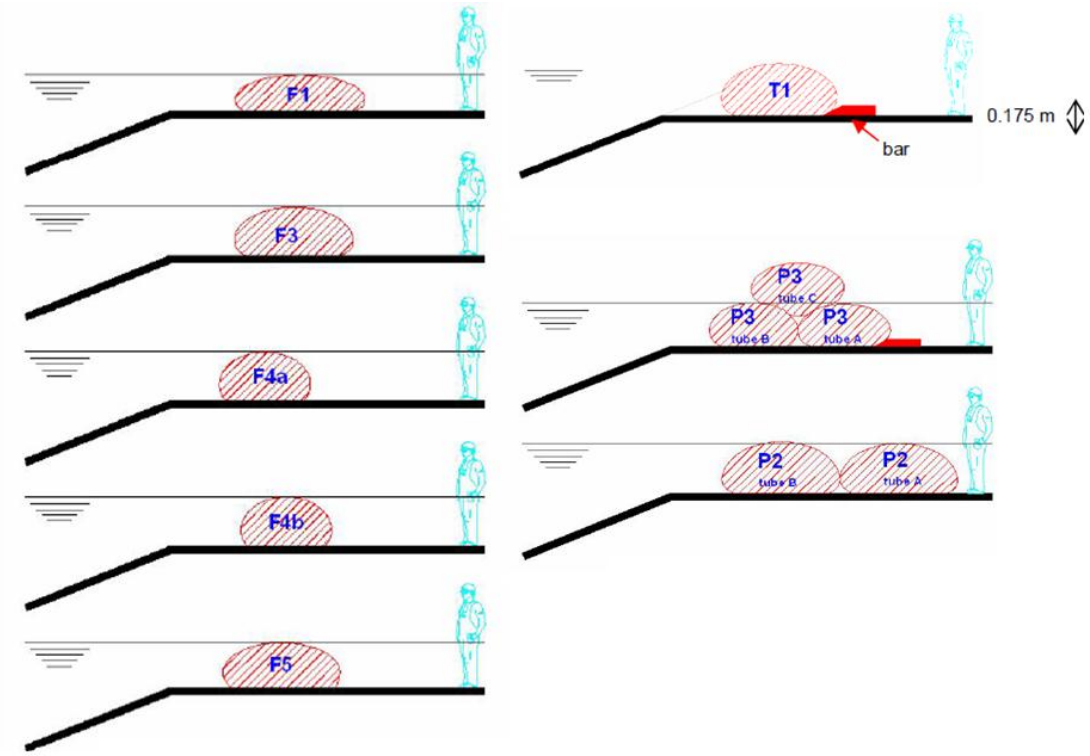

Figure 2.12: Different configurations tested (Van Steeg & Vastenburg 2010)

As previous stability formulae are not clear on all the different possible input factors a new dimensionless stability relation was suggested that incorporates factors relative to hydraulic stability. The new derived stability relation for a single placed geotextile tube is:

$$\frac{\chi H_s}{\Delta_t \sqrt{BD}(f\cos\alpha + \sin\alpha)} \leq 0.65$$

with:

H_s = *significant wave height at limit of stability*

Δ_t = *relative density of geotextile tube*

B = *width of geotextile tube*

D = *height of geotextile tube structure*

f = *friction coefficient of the geotextile and supporting structure interface*

α = *slope of the supporting structure*

χ = *reduction factor for lost energy due to overtopping (see Figure 2.13). SWL assumed at crest of structure.*

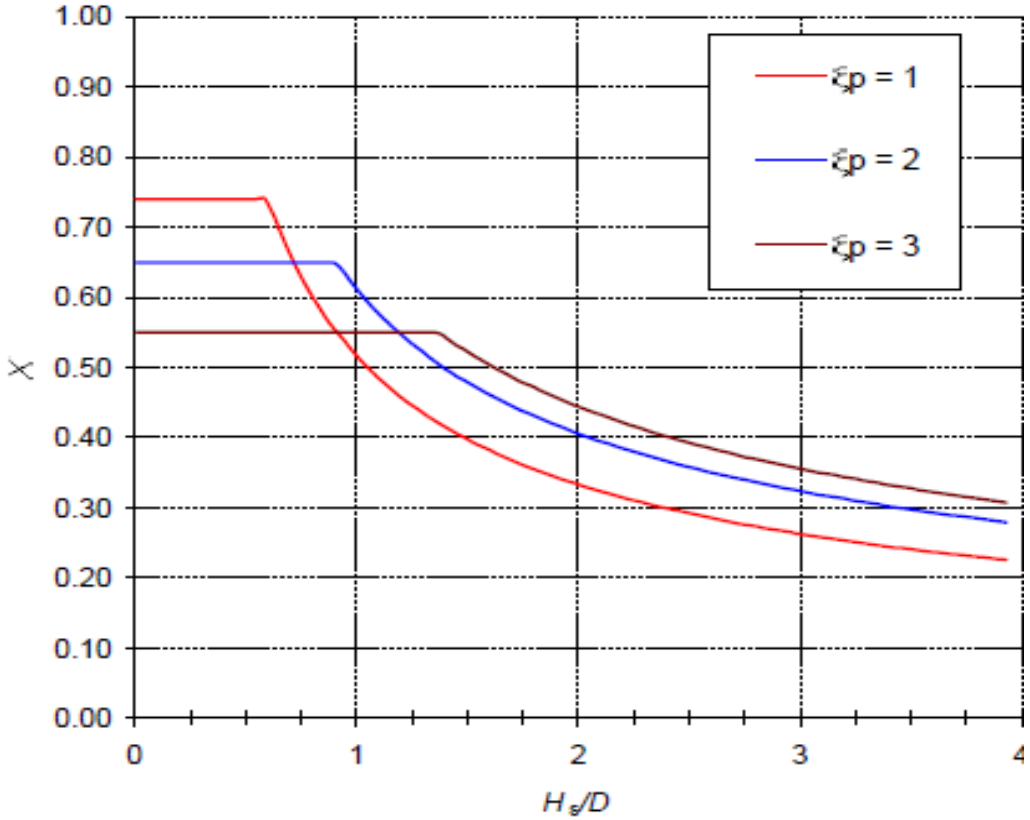

Figure 2.13: Reduction factor χ (Van Steeg & Vastenburg 2010)

ξ_p = *breaker parameter*

See Appendix B for an explanation of the above graph and the reduction factor.

Van Steeg & Vastenburg (2010) stated that the maximum displacement of the geotextile tube should be less than 5% of its width during a storm consisting of approximately 1,000 waves to be accepted as hydraulically stable. Wave conditions resulting in a displacement of more than 5% of the width of the tube had much larger final displacements.

Placing two geotextile tubes behind each other did not increase the hydraulic stability. The reason for this was ascribed to the hydrostatic pressure caused by the water entrapped between the two tubes and the hydrodynamic water pressures caused by the wave action, which caused the land-side tube to shift. It is recommended that the same formula be used as for a singly placed geotextile tube.

It is possible that slip-circle failure of the structure will occur before failure due to the sliding of the crest tube in heavy wave loading. This problem was found by Van Steeg and Vastenburg (2010) in their physical modelling, which had a friction coefficient of 0.5 between the geotextile and the supporting structure. Support to keep the bottom layer of geotextile tubes from sliding outward is important. The support can be provided by additional tubes on the bottom layer or a pre-dredged trench for retaining the bottom layer of tubes.

2.6.4 – Oh and Shin (2006)

Oh and Shin (2006) conducted experiments on geotextile tubes to prevent shore erosion on the east coast of South Korea East. In contrast to previous stability formulae calculating limiting significant wave heights using dimensionless stability relations, they used established methods to calculate wave forces on the geotextile tubes to determine hydraulic stability.

In order to assess the stability of the filled geotextile tube structure, wave forces were estimated using well-established methods. In their paper, the theoretical stability analysis employed was a 2-D hydraulic stability analysis, based on linear wave theory and geotechnical stability analysis. Oh and Shin (2006) reviewed several methods to address wave loading, including:

Hiroi's empirical equation (Hiroi 1920 as cited in Oh & Shin 2006)

$P_w = 1.5\, \rho_w\, H_{1/3}$,

with

P_w = *hydrodynamic pulsating load*

ρ_w = *density of sea water*

$H_{1/3}$ = *significant wave height*

A modified Minikin method as outlined in the US Army Corps of Engineers' SPM (1984) was used to calculate impact loading on an offshore geotextile tube breakwater for shore protection at Young-Jin beach on the South Korean coast. An equivalent rectangle was used instead of the more complex geotextile tube cross-section (see

Figure 2.14). It was found that a double-lined geotextile tube offshore breakwater was the most stable and effective for wave absorption.

The factor of safety against sliding can be expressed by the formula below.

$$SF_{sliding} = \frac{F}{P_h} = \frac{P_v \times tan\emptyset'}{P_w \times h_{GT}}$$

with:

P_h = *horizontal force*

F = *vertical force*

P_v = *overburden pressure and gravity weight of geotextile tube,*

P_w = *hydraulic pulsating load*

h_{GT} = *effective height (height exposed to horizontal wave loading)*

$Ø'$ = *interface friction angle between geotextile and base sand.*

The factor of safety against overturning about the toe of an equivalent rectangular tube can be expressed by the formulae below.

$$SF_{overturning} = \frac{M_R}{M_O} = \frac{P_v \times \frac{B'}{2}}{P_w \times \frac{h_{GT}}{2}}$$

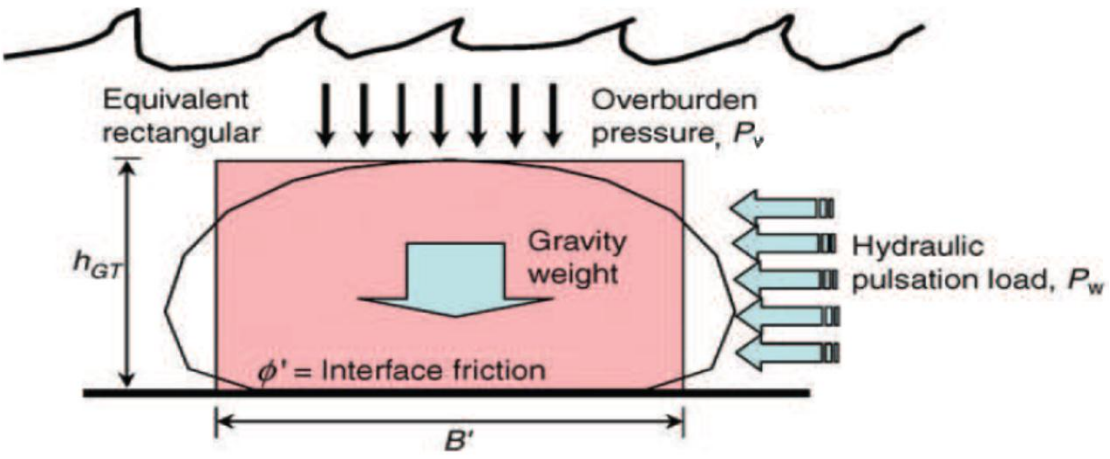

Figure 2.14: Schematization of forces used with an equivalent rectangle. (Oh & Shin 2006)

2.7 – Case Studies

2.7.1 – General

Of the five case studies mentioned in this thesis, Limeburners breakwater in Australia is the only application of geotextile tubes that is illustrative of the mode of application covered in this study. The other case studies were included to illustrate the advantages of using geotextiles, specifically geotextile tubes, in various modes.

2.7.2 – Amwaj Islands

Location: Muharraq Island, Bahrain

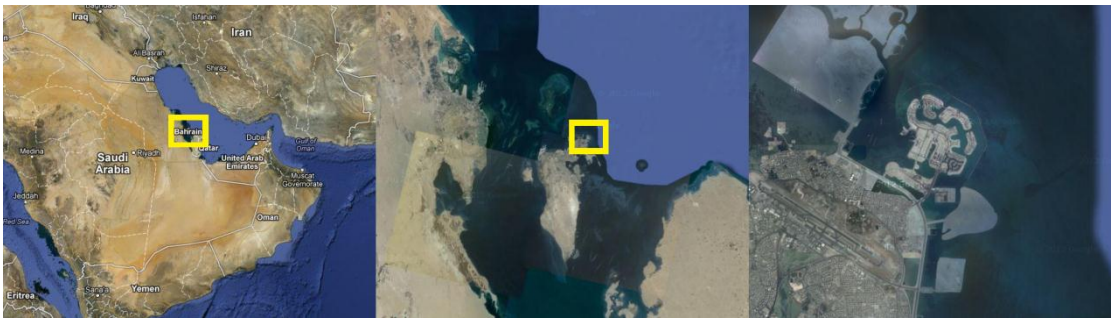

Figure 2.15: Location of Amwaj Islands (Google Earth)

Description: Venice style resort. Geotubes® were used for the containment of 12 million cubic meters of dredged sand and for core replacement in the surrounding breakwaters.

Figure 2.16: Aerial view of Amwaj Islands (photo: Ten Cate Geosynthetics)

The Amwaj Islands project involved the development of a new island off the north-eastern shore of Muharraq Island in Bahrain. The key element in the successful design,

construction and completion of the Amwaj Islands development project was the use of sand filled geotextile tubes. The tubes were stacked two high to form the island perimeter for the containment of 12 million cubic metres of dredged sand that formed the basic platform for the development project and were used as a single layer in protective offshore breakwaters with geotextile tubes as cores (see Figure 2.17 and Figure 2.18).

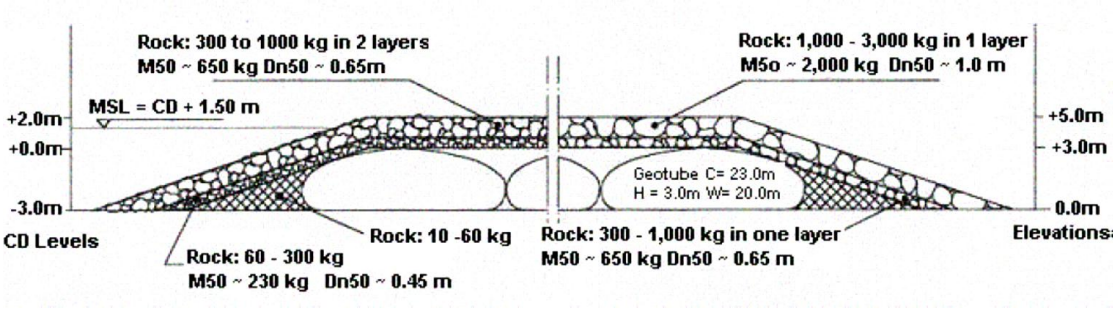

Figure 2.17: Cross-section of offshore breakwater (Fowler et al, 2002)

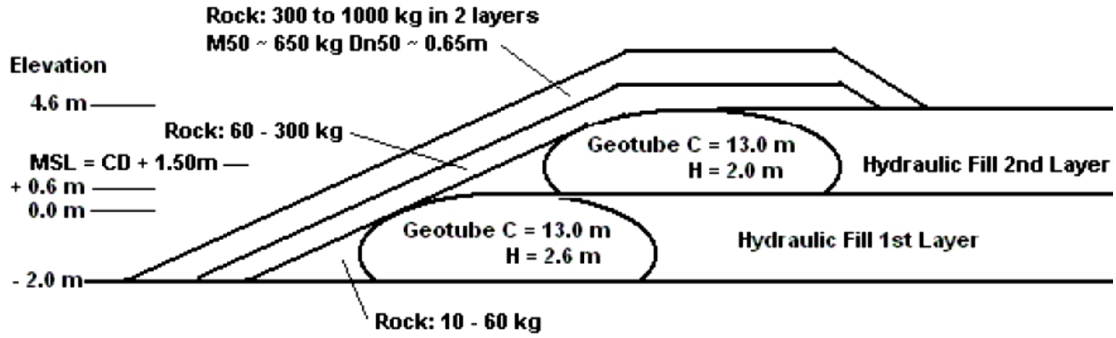

Figure 2.18: Geotube placement at Island perimeter (Fowler et al. 2002)

The island was constructed to a height of over 3 m above mean sea level. Work proceeded faster than anticipated and the islands shoreline was created in just five months.

The tidal range is 1.5m with a 1 in 50 year storm surge of 1.5m. The wave height is severely limited by the shallow water depth around the island. A 1 in 50 year storm event for the island has a water depth of 3.4m, with a maximum wave height of 2.7m.

According to Mario Santiago (cited in Fowler et al. 2002), project manager for the Amwaj Islands project, the selection of the geotube method has proven to be 50% more economical than the original quotation for the construction of the containment using traditional methods of rock bund construction.

See Figure 2.19 and Figure 2.20 for before and after photos of the filling process.

Figure 2.19: Geotube® placement before filling started. Note the fixing of the tube against horizontal movement (Fowler et al, 2002).

Figure 2.20: Geotube® filled to approximate design height of 2.6m (Fowler et al, 2002)

2.7.3 – Kirra Groyne

Location: North Kirra Beach, Queensland, Australia

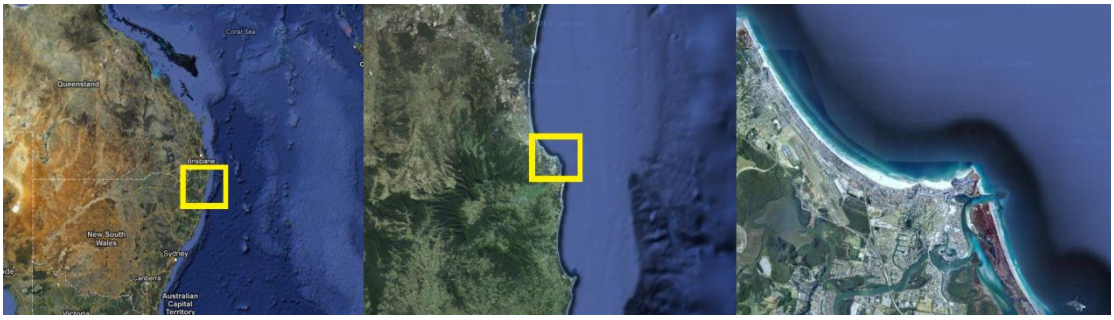

Figure 2.21: Location of Kirra Groyne (Google earth)

Description: Groyne to retain sand nourishment. 120m long x 5m high sand-filled groin made from geotextile tubes

Figure 2.22: Kirra Groyne (Restall et al. 2002)

A temporary structure was needed to retain nourishment to restore the eroded beach while long-term solutions were found. The structure had a design life of five years. The structure reached an age of 15 years before it was completely covered by sand from the nourishment system.

The structure was to be built in an active surf zone. Offshore wave heights exceeded 12m during extreme events. The tidal range is approx. 1.5m.

Conventional armour units were not an option due to their cost and the difficulty of the eventual removal of the rock and/or concrete units. Another prerequisite was that the structure should be safe for swimmers and surfers, who regularly use the area.

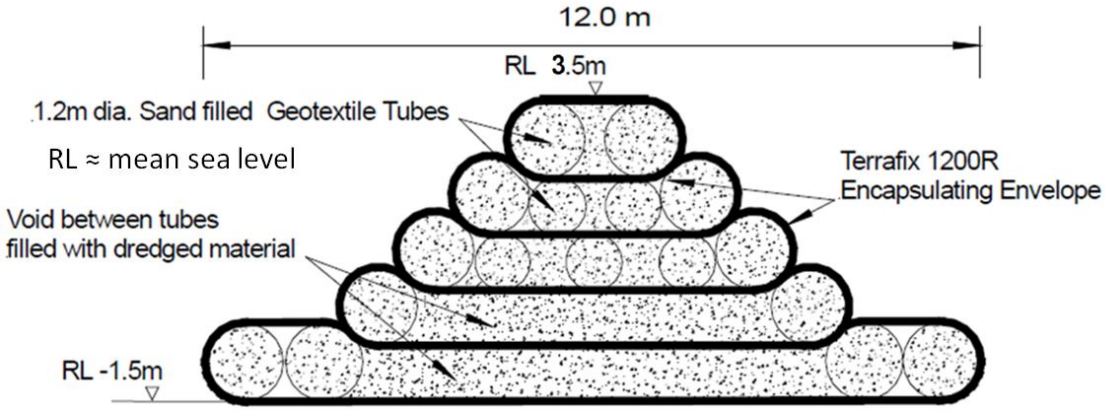

Figure 2.23: Groyne cross-section (Restall et al 2002)

The experience with vandalism suffered by this project led to trials with coatings such as bitumen and early patching techniques.

The use of geotextile tubes translated into an estimated saving of approximately 40% compared to a rock alternative (Restall et al. 2002).

2.7.4 – Limeburners Breakwater

Location: Limeburners Point Harbour, Geelong, Australia

Figure 2.24: Location of Limeburners breakwater (Google Earth)

Description: 250m^3 to 420m^3 geotextile tubes incorporating vandal deterrent panels stacked in a 3-2-1 layout.

Figure 2.25: Limeburners breakwater (photo: Geofabrics Australia) (Google Earth)

Wave propagation through the entrance of the Limeburners Point boat harbour necessitated the construction of an emergent offshore breakwater across the entrance. A number of alternative materials were investigated to construct the 80m long by 5.5m high breakwater in order to obtain the most cost effective solution to the problem. The use of large 250m^3 to 420m^3 geotextile sand containers incorporating vandal deterrent panels was considered the preferred option with the funds available and in relation to the long-term plans for the harbour. The containers were filled in-situ and the operation required considerable input from the client, the contractors and the supplier to ensure that the project proceeded according to plan.

The tidal range is approximately 1m. The long fetch across Port Phillip Bay during northerly to westerly winds greater than 20 knots resulted in a wind generated swell of 400 to 500mm (H_{max}) entering the harbour and riding up the boat ramp. This caused

considerable damage to the floating pontoons and made the launching/retrieving of recreational vessels difficult and dangerous. The harbour was recognised as unsafe and in need of an immediate solution to the primary regional launch and retrieval facility in central Geelong.

The structure was constructed in September 2004. See Figure 2.26 for the plan and cross-section of the breakwater. It poses only a limited threat to the small craft using the harbour, and, in the unlikely event that they should collide with the breakwater the damage to the small craft is expected to be far less than if they were to impact with a rock/concrete structure.

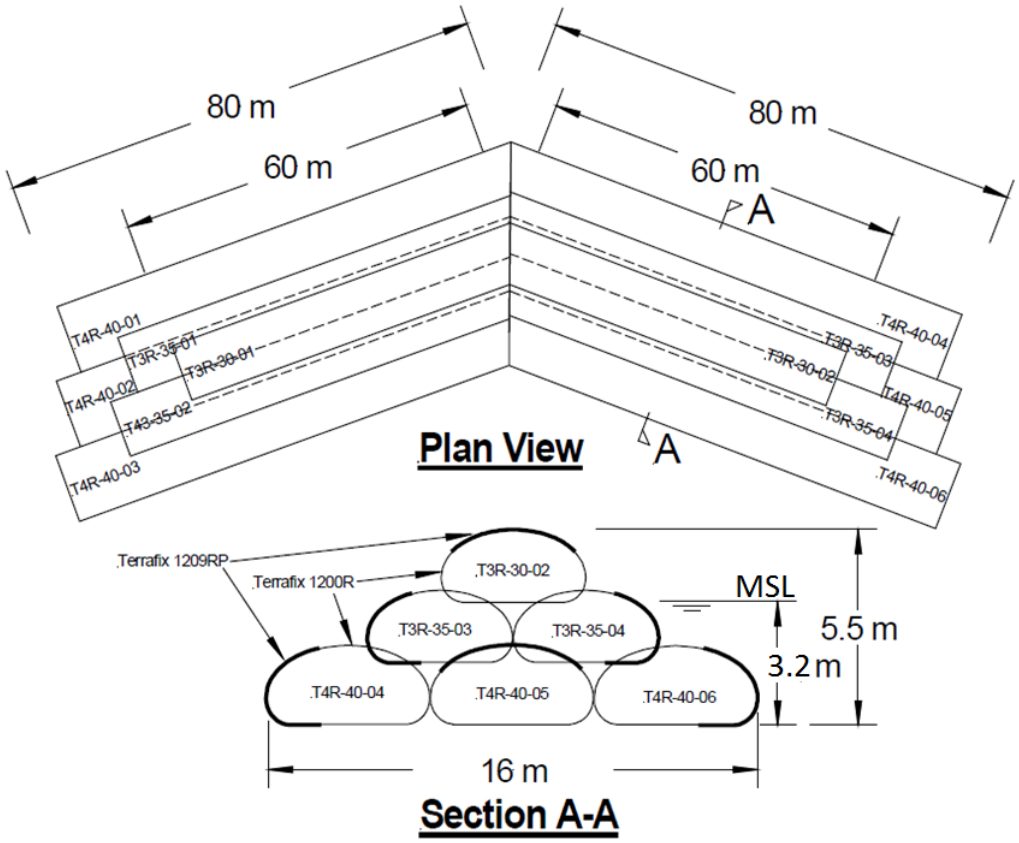

Figure 2.26: Plan and cross-section of the Limeburners breakwater (W. Hornsey & Jackman 2005)

The decision to proceed with the geotextile tube breakwater was based on the following (Hornsey & Jackman 2005):

1. Lower cost of construction

2. Minimal construction timeframe

3. Innovation

4. Flexibility for long term use

5. Safer in the event of accidental impact

The final design consisted of a 3-2-1 layout of the containers, as seen in Figure 2.26. The base layer consisted of three containers, each with a circumference of 14m, with a theoretical height of 2.3m, and a length of 40m. The middle and top layers made use of containers with a circumference of 12m, a theoretical height of 2.1m, and a length of 35m and 30m respectively. The overall dimensions of the detached breakwater are 80m long and 16m wide at the base, with a crest length of 60m and 5m wide, creating an approximate volume of 4,500m^3.

The containers were manufactured from Terrafix® nonwoven stable fibre geotextiles. Terrafix® 1209RP composite (vandal deterrent) geotextile was used on the exposed surfaces of the containers to minimise the possibility of damage to the containers whether from vandalism or incidental damage. Features such as the high-strength seam configuration (80% seam efficiency) and the double seal filling and filling ports, developed for the standard containers, were incorporated into the fabrication methodology.

2.7.5 – Narrowneck Reef

Location: Gold Coast, Queensland, Australia

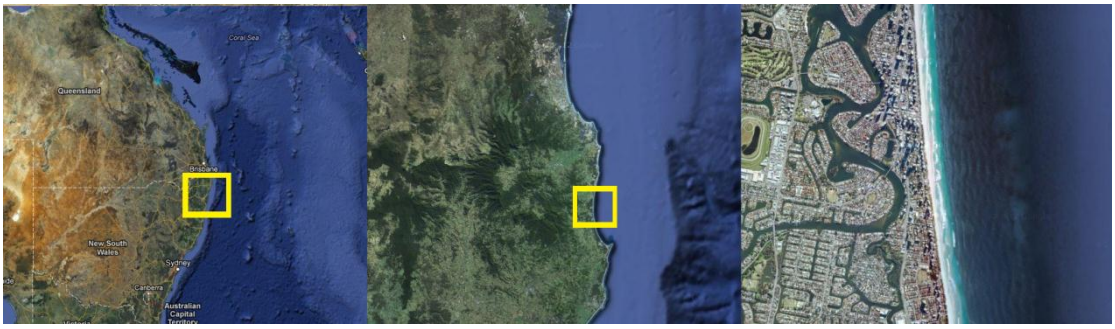

Figure 2.27: Location of Narrowneck Reef (Google Earth)

Description: 400m x 200m submerged reef

Figure 2.28: Aerial view of Narrowneck reef (Jackson & Hornsey 2003)

The Narrowneck Artificial Reef is a large submerged structure constructed from 1999 to 2001. The reef is located at Narrowneck at the northern end of Surfers Paradise, on Australia's Gold Coast. The Gold Coast is the major coastal holiday destination in Australia and the economy of the region is dependent on the tourism industry. In order to continue to attract tourist, a dual purpose reef was constructed from geotextile tubes. The submerged structure both protects the beach and creates favourable surfing conditions.

The water depth at the structure varies between 11 and 3m with a tidal range of approximately 1.5m. Large storm events can have offshore significant wave heights of more than 3.2m.

A number of alternative construction materials, including rock and concrete, were investigated, but it was decided to construct the reef using Geosynthetic sand-filled containers for the following reasons:

• Cost: The Geosynthetic structure was approximately half the cost of a similar rock structure.

• Safety/public liability: As the structure would be used by surfers it was important that any risk of injury to surfers be minimised. Also, using sand from the ocean on site for construction meant that the truck traffic hauling rock or concrete units would not cause a hazard to road or beach users.

• Environmental: The transporting of 45,000m^3 of rock from quarries along busy city roads would increase road traffic emissions into the air as well increase the need for road maintenance.

• Ease of removal: As the use of a submerged reef was untested and in effect a full scale model, approval conditions required that the structure be able to be removed or modified should there be any unforeseen adverse impacts created by the structure. Rock and concrete would have been expensive if not impossible to remove.

(Jackson & Hornsey 2003)

2.7.6 – Young-Jin Beach

Location: Young-Jin Beach, South Korea

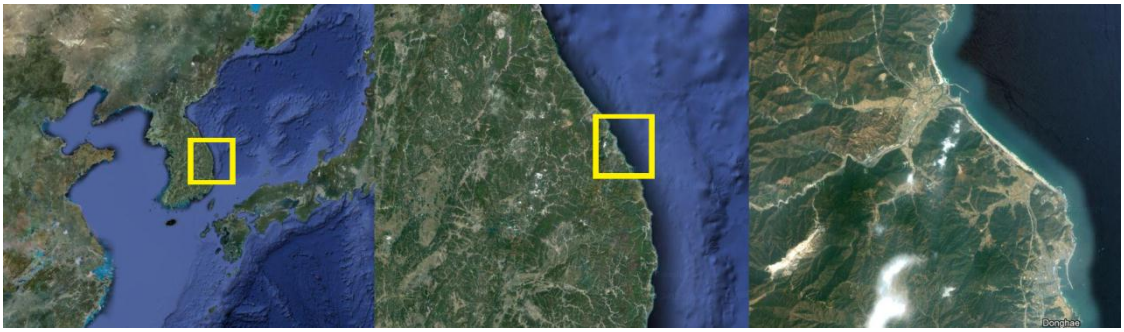

Figure 2.29: Location Young-Jin beach (Google Earth)

Description: Two-line submerged geotextile tube breakwater.

Figure 2.30: Seaweed covered submerged geotextile tube at Young-Jin beach (Oh & Shin 2006)

Shore erosion was causing severe damage to scenic shoreline views and to public property along the east coast of South Korea. Alternative solutions were considered to find an inexpensive and environmentally sustainable solution.

The area has a very small tidal range of approx. 0.6m. Winter storms produce offshore significant wave heights of up to 4m.

The benefits of the geotextile tube technology at Young-Jin beach included: in-situ filling with local material by hydraulic pumping, lower costs and faster construction compared to other technologies. The lower price and easier installation of the geotextile tube system makes it a good alternative for hydraulic and coastal structures (Oh & Shin 2006).

The geotextile tubes were designed as two tubes, side by side, serving as detached breakwaters, and had to be installed in about 3.0 m of water, 90 to 100 m from the shoreline.

Dimension of geotextile tube: 9.5m circumference (diameter: 3.5m),
50m length
1.8m effective height
4.2m width (approx. 77% filling)

The breakwaters covered 240 m of near shore along the shoreline of Young-Jin beach. The cross section of the structure is shown in Figure 2.31. The apron mat was installed as a fabric blanket to protect against scour. The edge of the fabric was folded back 0.5 m and sewn together forming a small anchor tube that was filled with sand. This small tube keeps the scour apron in place during wave action.

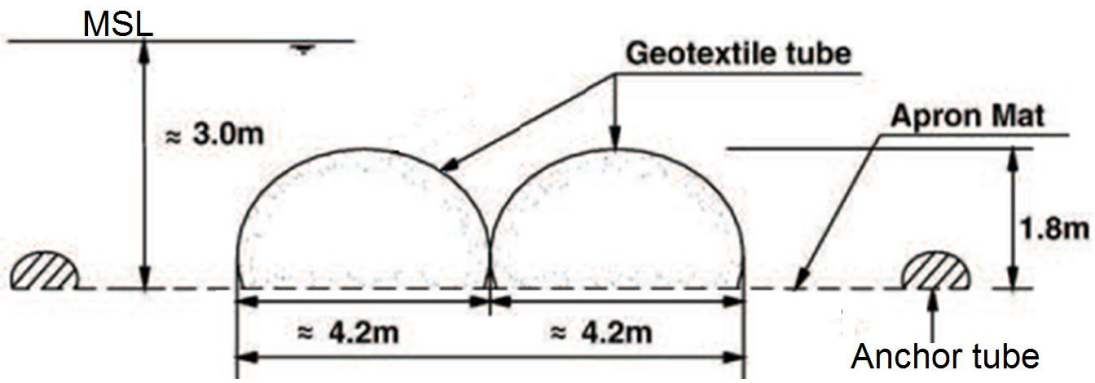

Figure 2.31: Cross-section of submerged breakwater (Oh & Shin 2006)

2.7.7– Upham Beach

Location: Upham Beach, West of Florida, United States of America

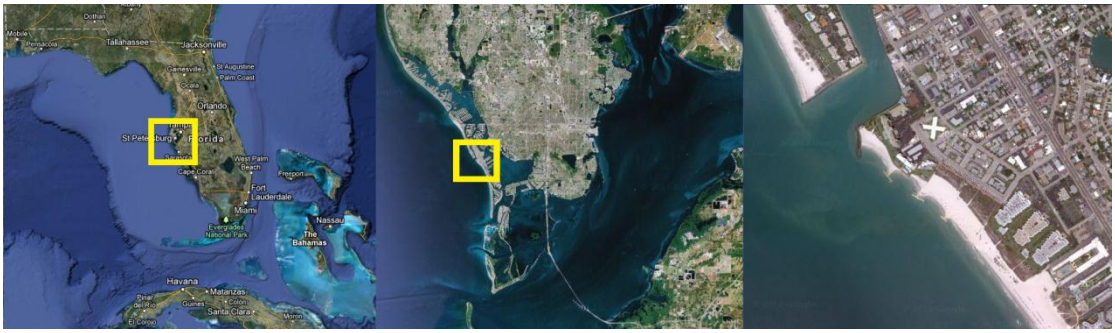

Figure 2.32: Location of Upham beach T-groynes (Google Earth)

Description: T-groynes to reduce post beach nourishment erosion rates

Figure 2.33: Aerial view of two of the T-groynes (Google Earth)

Figure 2.34: Construction of T-groins (Elko & Mann 2007)

The US Army Corps of Engineers had maintained Upham Beach in Pinellas County for over 30 years before the geotextile tube solution was installed. The construction of five geotextile tube T-groins along the beach has greatly reduced the required frequency of beach nourishment. Special T-head groynes 61m long and 58m wide were constructed to prevent waves and cross-shore currents from eroding the beach and to have sand accumulate behind them.

The tidal range for the area is relatively small at approximately 0.8m.

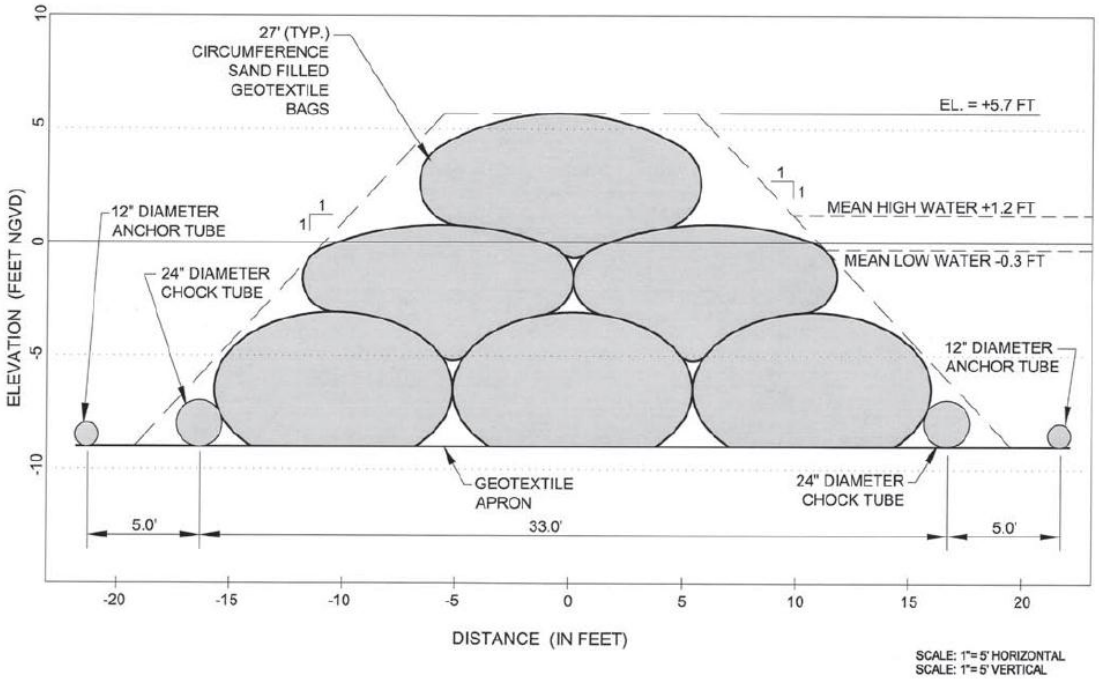

Figure 2.35: Cross-section of T-groyne head (Elko & Mann 2007)

Note the "chock" tube in Figure 2.35. The small tube is used as a wedge to prevent possible slip circle failure. The anchor tube keeps the scour apron in place during wave action.

The crest tubes are above the mean sea level and are vulnerable to the elements and vandalism. The crest tubes were covered with a polyuria coating to enhance their durability and protect the geotextile from damage caused ultraviolet radiation.

2.8 – Geotextile Tube Application

Geotextile tubes are filled on site. As with most geosystems the installation thereof requires calm conditions. This requirement can limit the application areas or limit construction intervals, which could extend construction times past acceptable levels.

Geotextile tubes are easily removable compared to conventional structures and therefore they are ideal for use as temporary structures.

Cautious use and design of geotextile tube structures needs to be applied as the durability and lifetime of the structure is uncertain.

Due to the characteristics of geotextiles, the locations for a geotextile tube breakwater will be limited to shallow sandy or silty sea beds. This, in turn, will affect the wave climate that could interact with the structure due to a foreshore with a relatively small slope.

Unlike conventional rubble mound breakwaters the crest of the structure closely follows the profile of the seabed. The structure therefore needs to have flexible height and alignment requirements.

In the case studies, numerous different applications for geotextile tubes were explored and discussed. In addition the possibilities for application of a geotextile tube breakwater could include:

Construction: A geotextile tube breakwater could provide temporary protection for construction projects until more permanent structures are in place or could provide protection from wave action for the duration of a project in a secluded location and be removed easily once the project is completed.

Salvage: A temporary breakwater could provide protection from wave action during delicate salvage operations and could then easily be removed when the operations are completed.

Mining: A geotextile tube breakwater could be used for mining on beaches. The breakwater could be used for containment and could easily be removed after mining has been completed in that area. The re-use of material could be possible.

Short term: Numerous projects for which short-term protection is required.

2.9 – Projected Lifetime of Structure

The marine and coastal environment is an extremely harsh environment in which to use what is a relatively thin light weight material. Geotextiles used in the coastal and marine environment should be able to withstand conditions that are far more aggressive than the original intended construction applications. The maximum service lifetime of the geotextile is the time in which the geotextile strength reduces by 10%, (PIANC 2011).

There are many factors influencing lifetime in the marine environment, including mechanical wear from wave action, abrasion from marine sediment, UV damage from sunlight, marine growths, waterborne debris and possible vandalism. Vandalism is a big problem facing exposed geotextile structures as one person with a sharp object could quickly endanger the structural integrity of an entire structure. A structure constructed from large geotextile tubes will fail with the failure with a single element and is therefore extra sensitive to vandalism.

Predictions for the lifetime of the structures for their intended use vary widely, from as short as five years up to 30 years. Many different procedures are recommended to extend the lifetime of the structure, including: extra geotextile and covering for the structure; designing the structure with expected perishing of the tubes getting the most loading; planned refurbishment during structure lifetime and regular inspection of the structure with on-hand repair kits.

Current structures are still young and more prototype data is required to make accurate predictions of design lifetime.

2.10 – Europe visit Report

Being part of the research project: “Development of sustainable as well as environmental-friendly, adaptive and cost-effective technical protection measures for sandy beaches”, funded by the BMBF and NRF and in co-operation with CSIR (Stellenbosch), provided the author with the opportunity to visit Germany and the Netherlands.

Various sites on the German North Sea coast were visited to see geotextiles in coastal applications. Applications mainly made use of geotextile bags used for shore and beach protection in conjunction with nourishment schemes.

A meeting at the Leichtweiss-Institut fur Wasserbau der TU Braunschweig was held with Mr D. Dassanayake, at the time one of Prof H. Oumeraci's PhD students, where an overview of their current and past research was given and included a tour of the hydraulic laboratory. The Leichtweiss Institute focuses heavily on the hydraulic stability of smaller geotextile sand containers (bags) and complementary construction aspects, due to the added robustness of the structure. (Whole structure does not fail with the failure of a single element)

The author also then visited the NAUE factory where modern production process and quality control methods used in the manufacture of their geotextiles were observed.

A meeting was held with Dr A. Bezuijen and Mr K Pilarczyk in Delft where good insights and understanding of the current deficiencies and limitations of a geotextile tube breakwater were received. Points of concern emerging from the meeting were: uncertainty of the behaviour of the geotextile tube structure under wave attack, durability (ageing, sunlight, vandalism etc.) and construction (lack of experience).

Finally a meeting at the Deltares hydraulic laboratory was undertaken including a quick tour of the hydraulic laboratory and discussion with Mr P. van Steeg on 2D physical modelling of geotextile tubes and the wave reduction factor.

The insights received from these visits for this thesis were invaluable. Various good research papers on the use of geotextiles for coastal protection were recommended.

2.11 – Summary of Literature Review

Geotextiles are available in various mixtures of polymers and additives in a large range of strengths. Non-woven and woven geotextiles have different benefits and can be used together in composite form. Forces in the geotextile can be calculated by simplified methods or using commercially available computer software.

Factors relevant to hydraulic stability include tube shape, friction between the geotextile and the supporting base and the geotextile-geotextile interface, deformation, wave climate and fill material density.

Failure mechanisms that lead to instability are complex and no generic approved design method is yet available. The hydraulic stability formula that was originally derived by Delft Hydraulics (1994) has evolved to include more of the factors relevant

to hydraulic stability. The geotextile tube on the crest of the structure is the critical tube for hydraulic stability against wave attack, provided that the bottom layer of tubes is secured against sliding. If the bottom layer of tubes is not secured against sliding the whole structure could displace. Quantifying the structural damage from wave attack is done by measuring the displacement of the tubes. Most stability formulae are vague on what constitutes a hydraulically stable structure. The CUR (2006) gives the start of movement as being unstable, while Van Steeg and Vastenburg (2010) recommend that a single tube should move less than 5% of its width in a 1,000-wave storm. Calculating hydraulic stability against wave attack has also been done using established methods to calculate wave forces.

Previous applications of geotextile tubes are in areas with a relatively low tidal range, shallow slopes and calm to moderate wave climates. Locally available materials that can be used as fill and a seabed profile and material that do not pose possible hazards to the geotextile are also required.

Apparently conflicting proposals for the stability of two tubes behind each other by Van Steeg and Vastenburg (2010) and Oh and Shin (2006) can be explained by the fact that in the Korean example, the geotextile tubes would be submerged constantly, whereas the Deltares set-up created conditions where the tube on the landward side would start to shift due to hydrostatic pressure caused by the water entrapped between the two tubes and the hydrodynamic water pressures from the wave action at the landward side of the tubes.

From the Upham beach T-groynes and Young-Jin beach submerged breakwater case studies it is clear that erosion at the foot of the structure can be a problem and is negated by installing a scour apron. The apron consists out of a geotextile sheet that is held in position by a smaller anchor geotextile tube at the seaward foot of the structure.

Encapsulation of the tubes as done in the Kirra groyne case study should increase the overall stability of the structure and significantly increase the durability of the structure.

Chapter 3 – Methodology

A detailed explanation of the methodology applied and the set-up for the hydraulic model tests is given in this chapter.

3.1 – General

From the information on previous research on the hydraulic stability of geotextile tubes provided in the literature study it was decided that a 2D physical model would be best suited to investigate the stability of a multi-layered structure against wave loading.

The expected application of a multi-layered geotextile tube structure is in areas with sandy seabeds with shallow foreshore slopes and relatively small tidal ranges. A 1 in 20 slope angle was selected to be on the steeper end of the expected foreshore conditions. Water levels at the structure varied from the crest to the base of the tube at the crest of the structure in accordance with the findings from the literature study where it was found that this provides critical stability limits.

The original wave conditions selected corresponded to those of a continental East African tropical cyclone, due to a possible future application in this area. The wave conditions had very long peak periods, which were found to be outside the generation capacity of the hinged paddle, regardless of the relatively small significant wave heights. The peak periods of the waves were shortened to fit inside the generation capacity of the wavemaker. With the shortened periods the wave conditions could still be described as swell conditions, but were no longer representative of a continental East African tropical cyclone. The lack of a true representative prototype wave condition for the cyclone should not affect the results obtained from the applied waves, however. Later in the test series a second set of wave conditions representative of wind-driven conditions was also used to study the effect of different period waves on the structure, as the current stability formulae used to calculate the limiting significant wave height did not include wave period.

After establishing the largest wave condition within the capacity of the wave generator, a smaller wave condition was selected and used in the stability formulae prescribed by the CUR (2006) and Van Steeg and Vastenburg (2008) for single

geotextile tubes. The geotextile tube size predicted by the stability formulae was estimated to be a good indication of the tube size to be used in the physical model.

3.2 – Test Set-up

3.2.1 – General

A fixed-bed, 2D model was used to analyse hydraulic stability against wave attack.

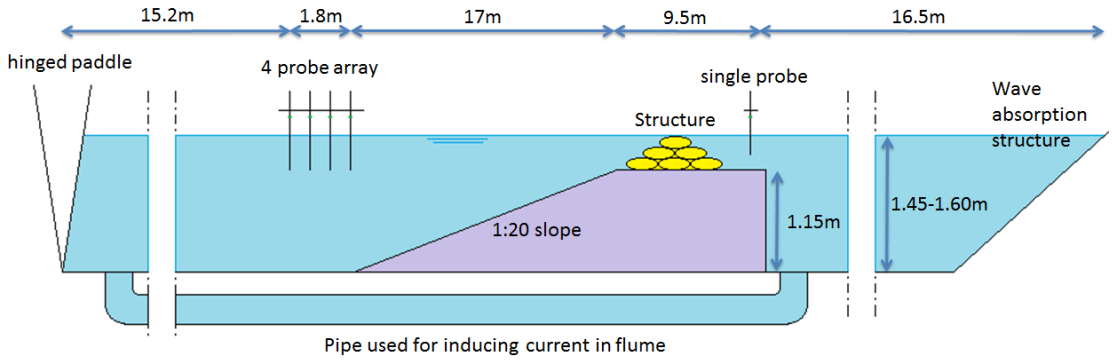

Figure 3.1: Representation of test set-up (not to scale)

With the relatively low crest height of the structure, excessive overtopping was expected in most of the tests. To keep the water level seaward and leeward of the structure constant, the pipe below the flume (used to induce current in the flume) was opened. This did not have any measurable effect on the wave conditions and visual inspection during testing confirmed that it was working (see Figure 3.1).

The recommended water depth in the flume is 1.5m. The height of the supporting structure was made as high as possible to ensure that tests were run close to this water level and to ensure water depths as deep as possible for offshore conditions. The position of the supporting structure in the flume was selected to coincide with that of the supporting structure from a prior study done in the flume to minimise construction time and the fill material required.

At the back of the flume there was a hollow, stepped structure filled with old nets with a bulk reflection coefficient of 0.1 to 0.2, depending on the wave conditions. The bulk reflection coefficient was determined from runs without the structure in place.

3.2.2 – Facility

The Stellenbosch University large wave and current flume is situated in the hydraulics laboratory of the Department of Civil Engineering of the University.

Of the facilities available, this facility could produce the largest wave conditions, i.e. the largest possible scale could be used. The hinged paddle provides active wave absorption, which allows the testing of structures with high reflection coefficients. Modern software from HR Wallingford (Wavemaker and HR DAQ) for wave generation and data acquisition were used.

See Appendix A for a full description of the facility and the generation curves.

3.2.3 – Bathymetry

A 1 in 20 slope was built out of compacted sand with a cement mortar topping to resemble the slope of a steep sandy beach. The fixed bed boundary was modelled with light cement and finished using a smooth steel float. This method of construction assumes a uniform bottom roughness over a large area. The wavemaker is at the offshore deep water side of the basin.

3.2.4 – Stacked Geotextile Tube Construction

Hydraulic filling of the geotextile tubes was achieved by pumping a sand and water mixture from a $2m^3$ container into the tubes. The container was continuously filled using a secondary pump to maintain the water level and also to help suspend the sand particles. Geotextile tubes at the bottom of the structure were placed between large bricks to help with the positioning and to prevent unwanted movement during the filling process. The bricks were removed with the completion of the bottom layer. As the tubes were completed they were sewn shut and the excess material that formed the filling port connections was tucked in underneath the tubes and sewn fast. This was done to prevent flapping during testing and to reduce possible extra drag forces on the filling port connections. See Appendix E for photos of the construction procedure.

3.3 – Hydraulic Conditions

Experiments were conducted with irregular waves. It has been demonstrated by several authors that the use of regular waves, with a height and period equal to that of the significant wave, can give inconsistent or inaccurate results in the analysis of wave transformation and wave action (Goda 2000)

There is no specific prototype condition that was modelled, but rather a selection of conditions to encompass as wide an array of as possible. Eight different wave

conditions were tested. These can be divided into two groups: steep short-crested waves with short periods relative to wind-driven sea conditions and long-crested waves with longer periods relative to swell conditions. Both result in plunging breakers on the structure (see Appendix D for wave conditions). For all the wave data collected during testing, see the "Physical modelling" folder on the DVD supplied with this thesis.

The tests started with small wave heights which were increased incrementally after each test. Irregular waves with a JONSWAP spectrum with a peak enhancement factor (γ) of 3.3 were used in all the tests. The tests consisted of approximately 1,000 waves each.

HR Wallingford's Wavemaker software was used for wave generation. The software is a signal generation program. The signal from the computer is sent to the remote control unit. The remote control unit (RCU) controls the hinged paddle, monitors the various signals from the wavemaker and controls dynamic wave absorption. The dynamic wave absorption prevents waves reflected back from a model being re-reflected from the paddle.

The water depth given is the water depth at the toe of the structure. Deep-water wave steepness, s_p, and breaker parameter, ξ_p, were calculated with the equations below. For the slope angle α, the foreshore slope was used instead of the slope of the structure, as the largest waves will break on the foreshore.

$$s_p = \frac{H_s}{L_0}$$

$$\xi_p = \frac{tan\alpha}{\sqrt{s_{0p}}}$$

with:

H_s = significant wave height

$L_0 = \frac{gT_p^2}{2\pi}$, deep-water wavelength

α = slope angle

For each wave condition, data is available for the incident wave and the conditions at the selected location of the toe of the structure without the structure in place. Wave data on the leeward side of the structure is also available from Test Series 7 due to the availability of additional instrumentation. The leeward data were used in the derivation of the wave transmission coefficients and the wave reduction factors (See p.78, 79 and Appendix B).

Wave conditions for Test Series 10 and 11 were the largest wave conditions from the short- and long-period waves, scaled down appropriately and increased incrementally until the critical failure of the structure was reached.

3.4 – Scaling

3.4.1 – General

The model was built as big as the available facilities would allow. The model is a geometrically undistorted model. A geotextile tube size that was expected to fail on the basis of the largest wave condition in the flume was calculated using the stability formulae from the CUR (2006) and Van Steeg & Vastenburg (2010). From the size of the geotextile tube used in the physical modelling, the scale of the model tests could be taken as being between 1:10 to 1:20.

3.4.2 – Froude Similarity

The size of the model was selected to be as big as possible to ensure that gravity and inertial forces would dominate and that viscous and surface tension effects would be insignificant and could be neglected, i.e. Froude similarity could be used.

The Froude criteria for similarity can be used to upscale the tests. Thus the Froude number is the same in the model as in the prototype, (Hughes 1993). Being an undistorted model with inertial and gravity forces dominating, the breaking process is properly simulated, which means that viscous and surface tension effects are negligible. (See Appendix I for Froude scaling laws.)

3.4.3 – Sand

Sand can normally not be down-scaled, due to the range of permeability and cohesive properties that need to be considered and that change the normal soil characteristics. This is often a problem with the use of sand in model tests.

No sand scaling was done. This kept the friction angle and dilatancy angle the same as in the prototype and circumnavigated issues that might arise concerning the sand tightness of the geotextile. The permeability appears to play a very small role in the physical modelling, provided that the geotextile tubes are hydraulically filled to a good fill percentage (approximately 80%). See Appendix F for the characteristics of the sand used.

3.4.4 – Geotextile

The down-scaling of geotextiles under consideration of porosity is not possible. As hardly any flow was expected through the geotextile tubes due to the high filling percentage, scaling rules regarding permeability could be neglected.

The static friction parameter is based mainly on the surface properties and the confining stress created in the geotextile tube. The friction was expected to be the same in smaller scale.

Down scaling the geotextile in respect of tensile strength is not possible, as this would result in an extremely thin, non-existent geotextile.

For model tests the geotextile is normally reduced by mass per area. However, it should however be noted that 150g/m^2 is the smallest possible and that a slightly thicker geotextile was selected to ensure sand tightness and to prevent rupture during the hydraulic filling of the tubes.

The geotextile selected is not to scale, as a geotextile simulating all the above properties does not exist. The effect this would have on the hydraulic stability of the geotextile tubes was considered to be negligible. The geotextile tubes were made of a nonwoven, needle-punched polypropylene material. (See Appendix G for geotextile specifications.)

3.5 – Measurements

3.5.1 – Wave Measurements

The waves in the model were measured with resistance probes coupled to a data acquisition box. The probes were calibrated by taking measurements at three different water levels. A calibration constant was then derived for the entire length of the probe.

As the water level varies around the probes, so does the resistance reading. The resistance readings are coupled to the corresponding water level. By analysing the probe output, the resistance data is converted to a time-series of the variation in the water surface elevation, from which the wave parameters were calculated.

Four probes initially were available. These probes where placed at 0.6m spacing 15.8m from the paddle. With the known spacing between the 4 probes, reflection analysis could be done with HR Wallingford's HR DAQ software, using a least squares method of Mansard and Funke (1980) to calculate incident and reflected wave spectra. The software uses the zero up-crossing technique to determine wave statistics: H_s, $H_{10\%}$, $H_{2\%}$ and H_{max} and wave spectrum analysis to determine T_p and H_{mo}.

A fifth probe and an additional acquisition box became available for use half-way through the testing. This probe was used to measure waves on the leeward side of the structure to give an indication of energy overtopping the structure. Resistance probes are sensitive to conductivity changes in the water and therefore calibration of the probes was done twice a day or after every time that water was added or removed from the flume. With gain tuning of the flume before placement of the structure, wave measurements were also taken at the position of the seaward toe of the structure. Full wave spectra for all tests that were completed can be found in the "Physical modelling" folder on the DVD supplied with this thesis.

Figure 3.2: Data acquisition boxes (left) and four probe array (right)

3.5.2 – Structure Measurements

The structure was manually measured on three different cross-sections perpendicular to the length of the structure. The location of the cross-section can be identified by a black cross at the centre of the crest tube (see Figure 3.3). Measurements were taken before and after every test. See Figure 3.4 for an indication of where the

measurements were taken on a typical cross-section. Structures with dual tube crests also had a measurement taken between the centres of the two crest tubes.

A digital camera was set-up to take photos of the structure before and after each test for the purpose of documentation and analysis. These photos can be viewed on the DVD attached to this thesis in the "Physical modelling" folder.

The displacements of the tubes after each test are given in Chapter 4. In the test series, the displacement of the tubes is given after every test, as is the cumulative displacement from the initial measurements before testing started. These displacements are the averages measured from three cross-sections. For all measurements, see the "Physical modelling" folder on the DVD attached to this thesis.

Figure 3.3: Positions of measured cross-sections

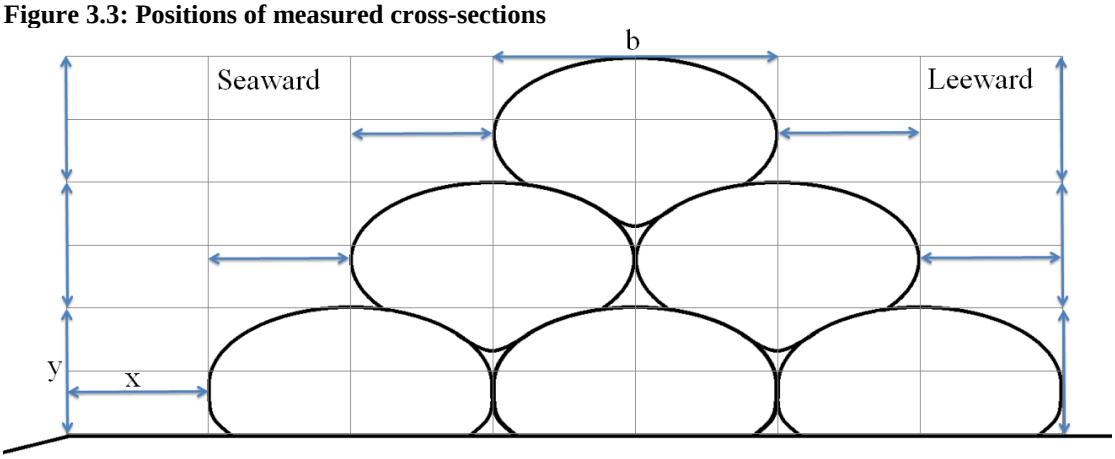

Figure 3.4: Indication of measurements taken before and after each test

3.5.3 – Deformation

Although measurable deformation of specific tube shapes was not expected based on the deformation formula of Van Steeg and Vastenburg (2010) and the small scale, visual observation was used for the possible deformation and settling of individual tubes.

3.6 – Structure Configurations

Different structure configurations with respect to stacking arrangement and water level were tested to investigate any possible effects these set-ups might have on hydraulic stability. See Table 4.1 for the different structural configurations tested.

3.7 – Physical Model Limitations

There are inherent shortcomings in a 2D model. Unidirectional waves are generated to approximate directional waves. However it provides a reasonable approximation for the intended simulation.

Additional three dimensional (3D) drag forces that an offshore stacked geotextile tube breakwater would experience on its edges are not modelled in this 2D configuration. The walls of the flume contain the tubes, but due to the very small friction coefficient between the walls and the geotextile it is considered insignificant.

A fixed seabed was simulated in the flume. Scour at the foundation of the structure, bearing stability and foundation settlement cannot be simulated.

The scale used prevented the geotextile and sand from being scaled properly. This meant that geotextile rupture/tear, and loss of fill through the geotextile could not be simulated properly.

Despite all these limitations of the physical model, it was expected that the model would give valid qualitative answers with respect to hydraulic stability against normal wave attack, as the important processes were scaled correctly.

Chapter 4 – Tests and Results

The various test series and the results obtained from these tests are summarised in this chapter.

4.1 – Overview

The physical modelling included 65 tests spread over eight different structural configurations with varying water depths and wave conditions. An overview of the test series is provided in Table 4.1 below.

Table 4.1: Overview of test series

Series	Cross-section	Series	Cross-section
0	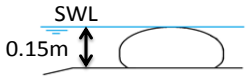 Structure Code: 1	6	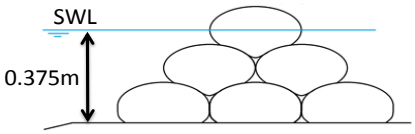 Structure Code: 3-2-1
1	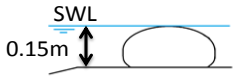 Structure Code: 1	7	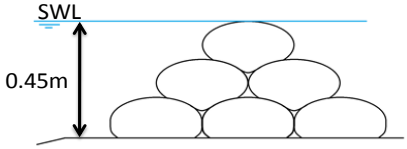 Structure Code: 3-2-1
2	 Structure Code: 2-1	8	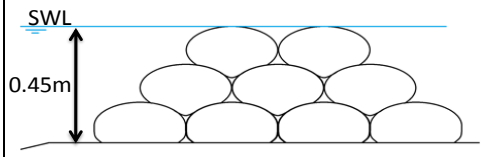 Structure Code: 4-3-2
3	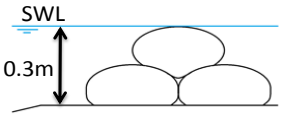 Structure Code: 2-1	9	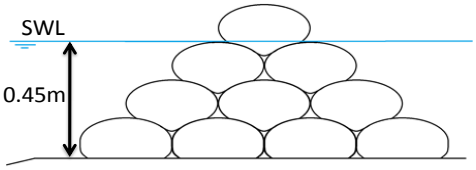 Structure Code: 4-3-2-1
4	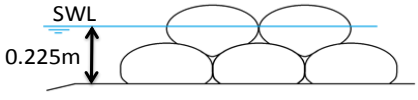 Structure Code: 3-2	10	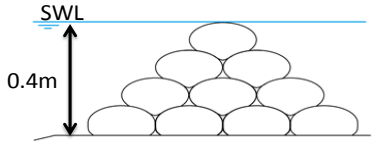 Structure Code: 4-3-2-1
5	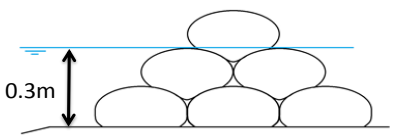 Structure Code: 3-2-1	11	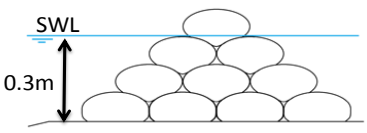 Structure Code: 4-3-2-1

The structure code describes the structure by assigning numbers to the amount of tubes per layer starting at the base layer.

All geotextile tubes, with the exception of the tube in test series 0, were filled to approximately 80% to simulate a practical maximum filling percentage achievable in prototype application. All tests were approximately 1,000 waves long (a duration of $1{,}000T_p$) to simulate an average storm duration and is typically used in this type of study.

Before the high friction coefficient between the flume bed and geotextile became apparent test series 2 to 5 were done with wedges restraining the bottom layer of tubes to ensure that overall or slip circle failure did not occur from outwards sliding of the bottom layer of tubes, as experienced in the physical modelling done by Van Steeg and Vastenburg (2010). Test 5-4 was re-done without the wedges, which resulted in the same results as with the wedges. Therefore subsequent tests were done without the wedges.

Test series 1 to 5 were done further up the slope on a specially constructed extra piece of slope, which was broken out for test series 6 to 11. This was done to keep the water depth in the flume as close to 1.5m as possible.

For test series 0 to 9, the theoretical tube size was 0.15m high and 0.328m wide. Tubes were filled until the required height was reached. The width of the tubes varied slightly, as the strain characteristics also varied slightly over the geotextile sheet. Width measurements varied from 0.313 to 0.335m. This variance could sometimes be found in different cross-sections of the same tube. All the tubes were measured, but only a few were weighed.

The construction method is provided in Appendix E and the sand characteristics are given in Appendix F. The structures in test series 2 to 5 were built by adding tubes to the previously existing structure. Test series 6 was created with new geotextile tubes, and structures for the test series thereafter by adding additional tubes.

Test series 0 to 9

Tube measurements	Theoretical	Actual
Height:	0.15m	ranged from 0.145 to 0.155m
Width:	0.328mm	ranged from 0.313 to 0.335m
Length:	2m	2m

Volume:	0.0825m^3	not measured
Submerged weight:	85.8kg	ranged from 84 to 88kg
Saturated weight:	168.3kg	ranged from 168 to 176kg

Test series 10 and 11 are the structural configuration from test series 9 scaled down to two-thirds of its original size. Working on a slightly smaller scale provided the opportunity to simulate a larger wave condition and, higher water level and to compare the results with the larger scale to see whether there are any unforeseen scale effects. Tube filling and construction were similar to that of test series 0 to 9.

Test series 10 and 11

Tube measurements	Theoretical	Actual
Height:	0.10m	ranged from 0.098 to 0.105m
Width:	0.219mm	ranged from 0.205 to 0.225m
Length:	2m	2m
Volume:	0.0367m^3	not measured
Submerged weight:	38.17kg	ranged from 37 to 39.4kg
Saturated weight:	74.87kg	ranged from 72.5 to 77.2kg

Measurements, wave data and photos for all test series and selective video footage of certain tests can be found in the "Physical modelling" folder on the DVD supplied with this thesis. Measurements shown in this chapter are the averages from the three measured cross-sections. The two measurements displayed are x and x_{cum}.

x: the horizontal movement measured from a specific test

x_{cum}: the cumulative horizontal movement after the specified test from the initial measurements taken before initial testing started.

To be able to compare the different size tubes with each other, the relative displacement, x_{cum}/b, which is a fraction of the width of the tubes (b), is used in the graphs.

All wave spectra for the tests are not presented in the thesis, but can be found in the "Physical modelling" folder on the DVD supplied with the thesis.

Figure 4.1 illustrates the wave spectra from test series 9 as an example of typical wave spectra measured in the test series.

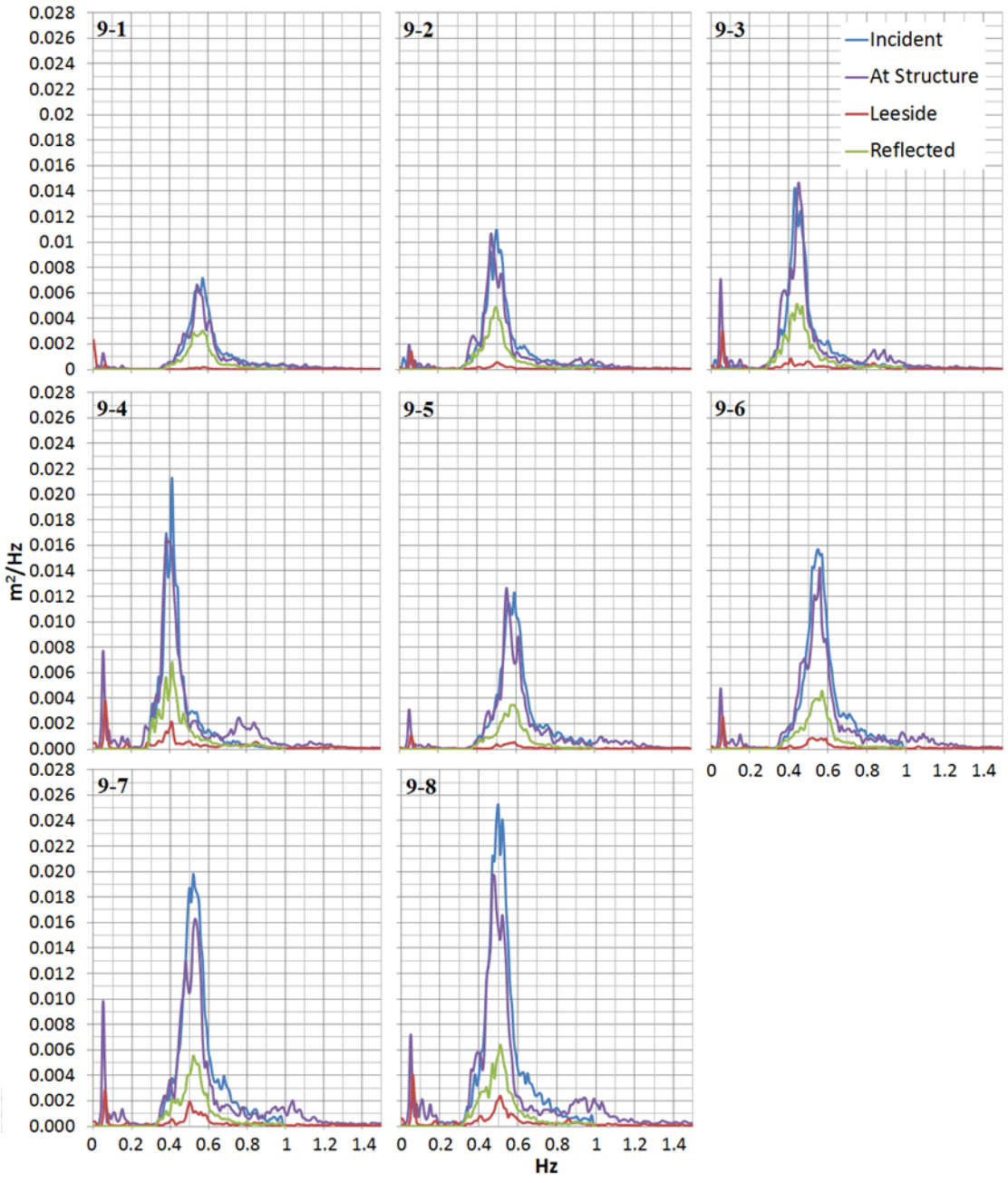

Figure 4.1: Wave Spectra from test series 9

Note the long wave (low frequency) energy on the wave spectra from Figure 4.1 at the structure. The energy occurs at a frequency of approximately. 0.55, which translates to an 18s wave period in model scale. This long wave is characteristic of the phenomenon of wave basin seiching. Wave seiching is the formation of standing

waves in a water body from incoming wave conditions and subsequent reflections from the ends of the basin.

Calculating the long wave length:

$C = L/T$

with:

C = wave celerity (speed)

L = wave length

T = wave period

$C = \sqrt{gd}$ for shallow water conditions

with:

d = depth of flume

g = acceleration by gravity (9.81m/s^2)

Combining the above two formulas

$L/T = \sqrt{gd}$

∴ L ≈ 71m

The length of the flume from the paddle to the structure is 35m. This is about half of the wave length of the long wave in the basin and corresponds to a seiching wave in the basin with a modal number (number of points with no change in elevation - nodes) of 1. See Figure 4.2. This mode of seiching also explains why the additional energy is hardly noticeable on the measurements taken by the offshore 4 probe array, as the location of the array is close to the point not experiencing change in water elevation (17m from wave generator paddle).

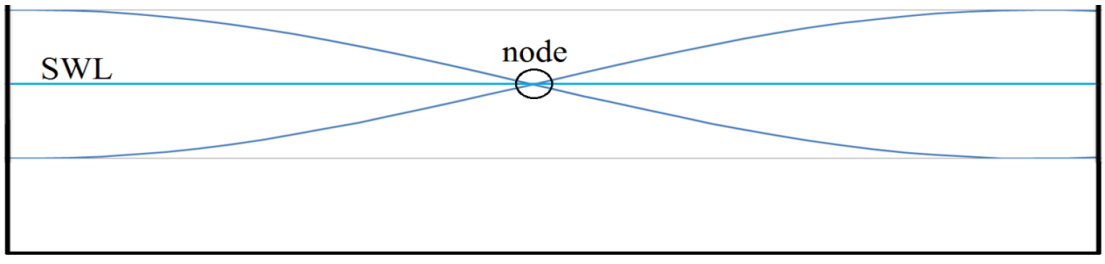

Figure 4.2: Seiching in a basin with a modal number of 1. (not to scale)

This phenomenon was present in all the test series and could not be removed. The long wave should have very little effect on the stability of the tubes and would only raise or lower the water level slightly at the structure.

4.2 – Test Series 0

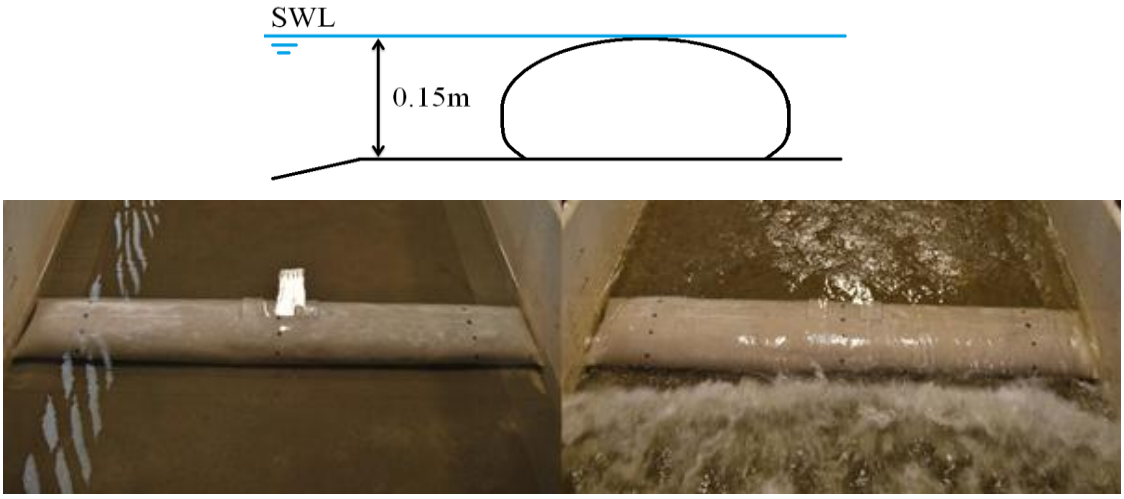

Figure 4.3: Test series 0

Structure 1: ($f \approx 75\%$) with the SWL at its crest (0.15m depth at structure)

Due to the expansion of the geotextile with the pumping pressure a tube larger than planned was constructed. Filling was stopped when the tube reached the intended height of 0.15m, but its width (0.37m) exceeded the planned width and subsequently more closely represented a larger tube that was approximately 75% filled. Testing on this configuration continued whilst changes were made to the dimensions of the geotextile for the tubes of all future tests.

No movement was measured during this test series, as the structure built was inherently more stable than the planned structure and because of the depth limitation on the waves at the structure.

Wave conditions were the same as those of tests 1.

All tests experienced severe overtopping, but showed a significant visual reduction in wave energy on the leeside of the structure. There was no visual movement/rocking of the geotextile tube in any of the tests. A significant reduction in wave energy due to depth induced breaking was noted in the larger wave tests and high visual reflection was noted in all tests

4.3 – Test Series 1

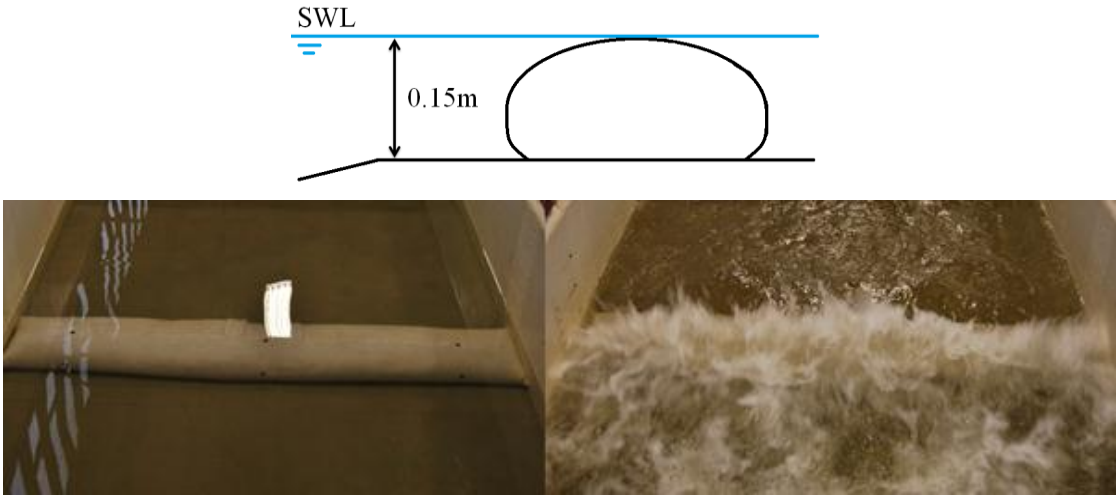

Figure 4.4: Test series 1

Structure 1: with the SWL at its crest (0.15m depth at structure)

Four irregular wave conditions were tested in this series (see Table 4.2 below and Appendix D for full wave characteristics). No movement was measured during this Test Series due to the depth limited waves at the structure and the unanticipated high friction coefficient between the geotextile and the flume surface. Due to the lack of any movement in this test series, planned testing of a double geotextile tube structure was cancelled.

Table 4.2: Wave conditions for test series 1

Test no.	Wave condition	Incident			At structure		
		H_s (m)	T_p (s)	H_{max} (m)	H_s (m)	T_p (s)	H_{max} (m)
1-1	1	0.13	1.79	0.242	0.125	1.79	0.184
1-2	2	0.15	2.01	0.279	0.14	2.17	0.208
1-3	3	0.16	2.24	0.298	0.148	2.27	0.235
1-4	4	0.18	2.46	0.335	0.150	2.63	0.239

All tests experienced severe overtopping, but showed a significant visual reduction in wave energy on the leeside of the structure. There was no visual movement/rocking of the geotextile tube in any of the tests. A significant reduction in wave energy due to depth induced breaking was noted in the larger wave tests and visual reflection was noted in all tests.

4.4 – Test Series 2

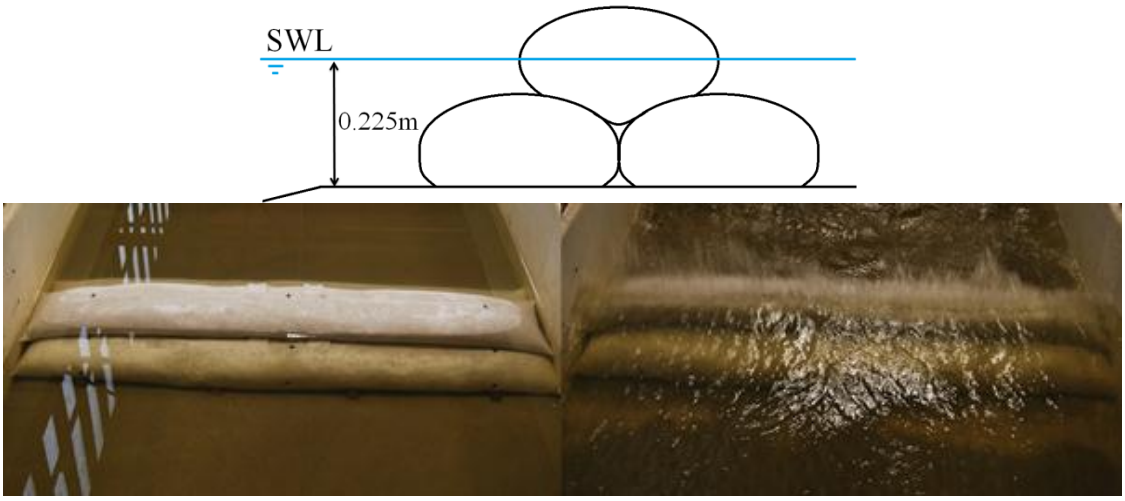

Figure 4.5: Test series 2

Structure 2-1: with the SWL at half the height of the crest tube, (0.225m depth at structure).

Four irregular wave conditions were tested in this series (see Table 4.3 below and Appendix D for full wave characteristics).Visual rocking of the top tube with impact loading from the largest waves breaking onto the structure was noted in test 2-1 to test 2-4. There was high visual reflection off the structure in all tests. Visual shoaling and energy loss due to depth induced breaking were found in on tests 2-2 to 2-4.

Table 4.3: Wave conditions for test series 2

Test no.	Wave condition	Incident			At structure		
		H_s (m)	T_p (s)	H_{max} (m)	H_s (m)	T_p (s)	H_{max} (m)
2-1	1	0.13	1.79	0.242	0.145	1.75	0.249
2-2	2	0.15	2.01	0.279	0.174	2	0.263
2-3	3	0.16	2.24	0.298	0.190	2.38	0.29
2-4	4	0.18	2.46	0.335	0.208	2.44	0.304

Measurements were taken before and after every test. Only the crest tube showed any measurable movement during tests. See Figure 4.6 below for H_{max} at the structure vs. the relative cumulative horizontal displacement. The x- and y-axis of the figures showing the horizontal cumulative displacements are kept constant for easier visual comparisson.

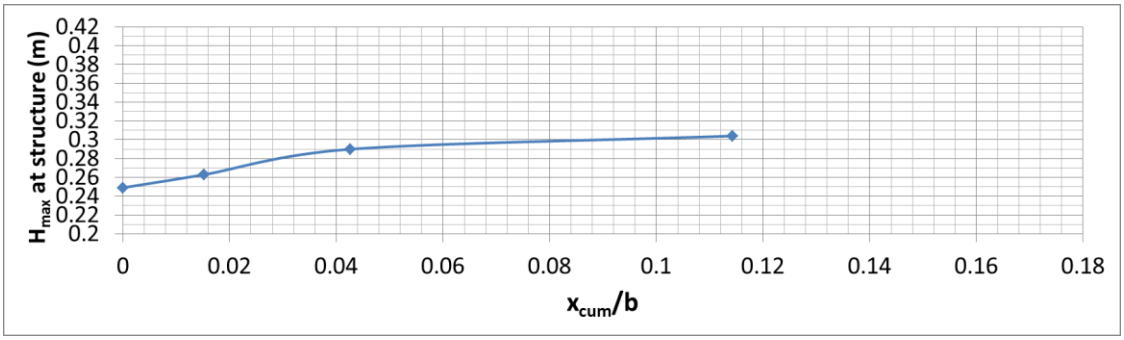

Figure 4.6: Test series 2 – H_{max} vs. relative cumulative horizontal displacement for crest tube

4.5 – Test Series 3

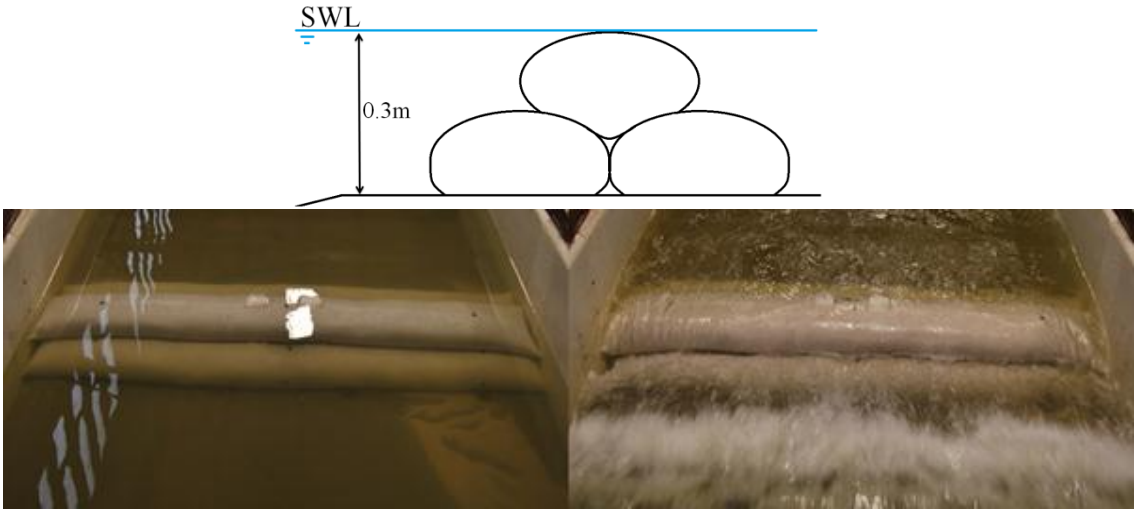

Figure 4.7: Test series 3

Structure 2-1: with the SWL at the crest of the top tube, (0.3m depth at structure).

Four irregular wave conditions were tested in this series (see Table 4.4 below and Appendix D for the full wave characteristics).Visual rocking of the crest tube with impact loading from the largest waves breaking onto the structure from test 3-2 to test 3-4 was noted. There was high overtopping and energy transfer to the leeside of the structure in all the tests.

Table 4.4: Wave conditions for Test Series 3

Test no.	Wave condition	Incident			At structure		
		H_s (m)	T_p (s)	H_{max} (m)	H_s (m)	T_p (s)	H_{max} (m)
3-1	1	0.13	1.79	0.242	0.13	1.75	0.21
3-2	2	0.15	2.01	0.279	0.164	2.13	0.289
3-3	3	0.16	2.24	0.298	0.204	2.22	0.339
3-4	4	0.18	2.46	0.335	0.231	2.38	0.382

Measurements were taken before and after every test. Only the top tube showed any measurable movement after the tests. There was no measurable movement for Test 3-1. Figure 4.8 below illustrates the H_{max} at the structure vs. the relative cumulative horizontal displacement.

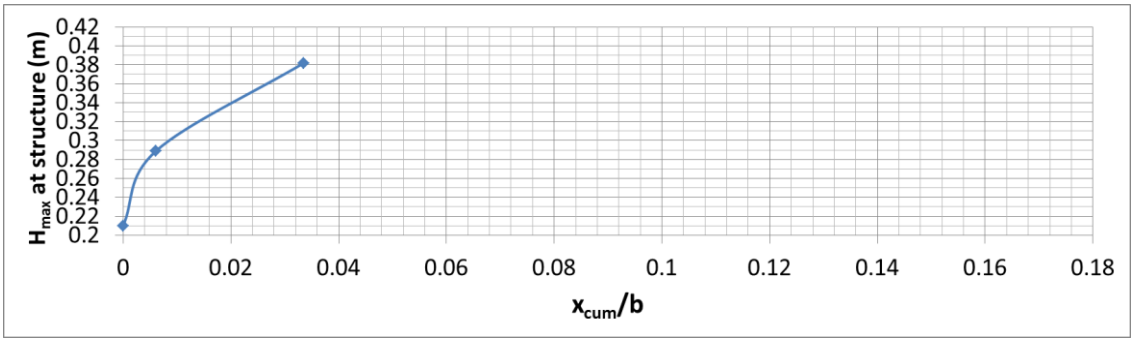

Figure 4.8: Test series 3 - H_{max} vs. relative cumulative horizontal displacement for crest tube

4.6 – Test Series 4

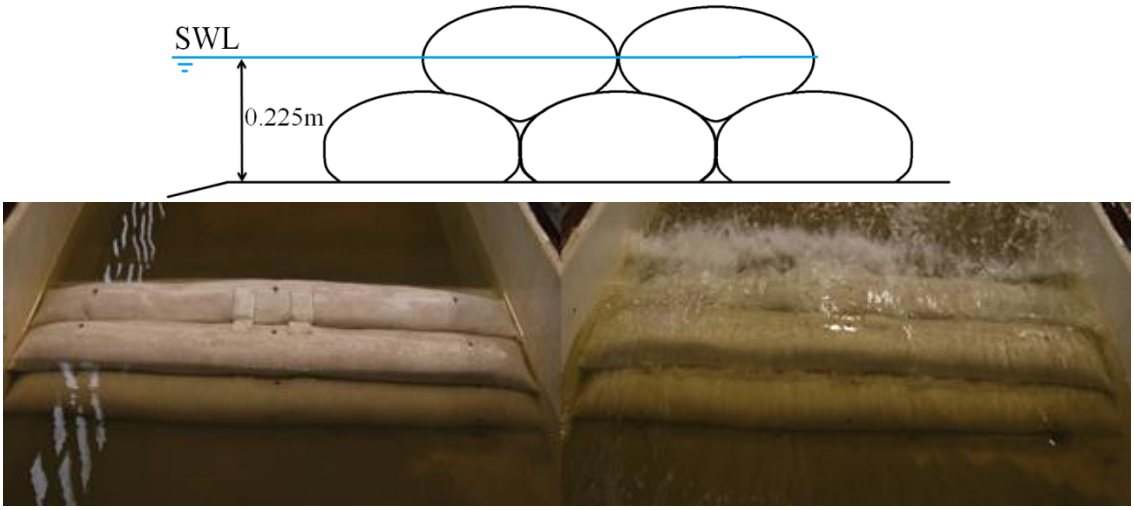

Figure 4.9: Test series 4

Structure 3-2: with the SWL at half the height of the crest tube, (0.225m depth at structure).

Two irregular wave conditions were tested in this set-up (see Table 4.5 below and Appendix D for the full wave characteristics).Visual rocking of the crest tube with impact loading from the largest waves breaking onto the structure from test 4-1 to test 4-2 was noted. There was high visual reflection off the structure in all the tests. Visual shoaling and energy loss due to depth induced breaking occurred in test 2-2 to 2-4.

Table 4.5: Wave conditions for test series 4

Test no.	Wave condition	Incident			At structure		
		H_s (m)	T_p (s)	H_{max} (m)	H_s (m)	T_p (s)	H_{max} (m)
4-1	3	0.16	2.24	0.298	0.19	2.38	0.29
4-2	4	0.18	2.46	0.335	0.208	2.44	0.304

Measurements were taken initially and after every test. Only the top layer of the tubes showed any measurable movement after the tests. Figure 4.10 below show the H_{max} at structure vs. the relative cumulative horizontal displacement of the two crest tubes.

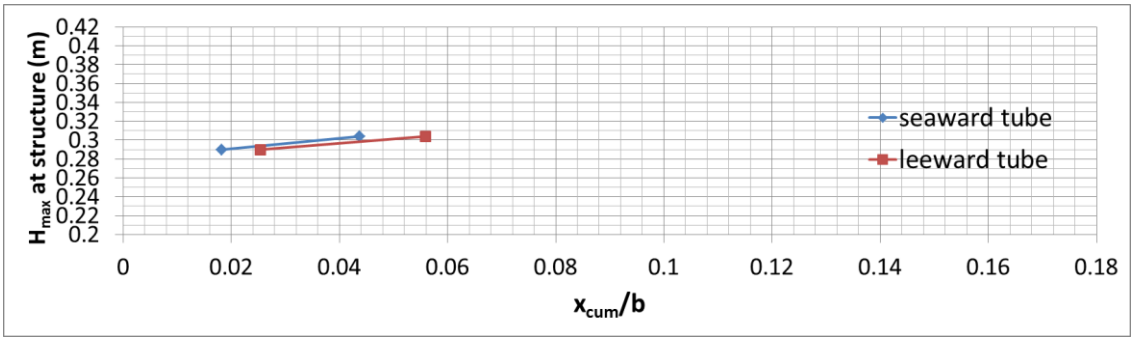

Figure 4.10: Test series 4 - H_{max} vs. relative cumulative horizontal displacement of the two crest tubes

4.7 – Test Series 5

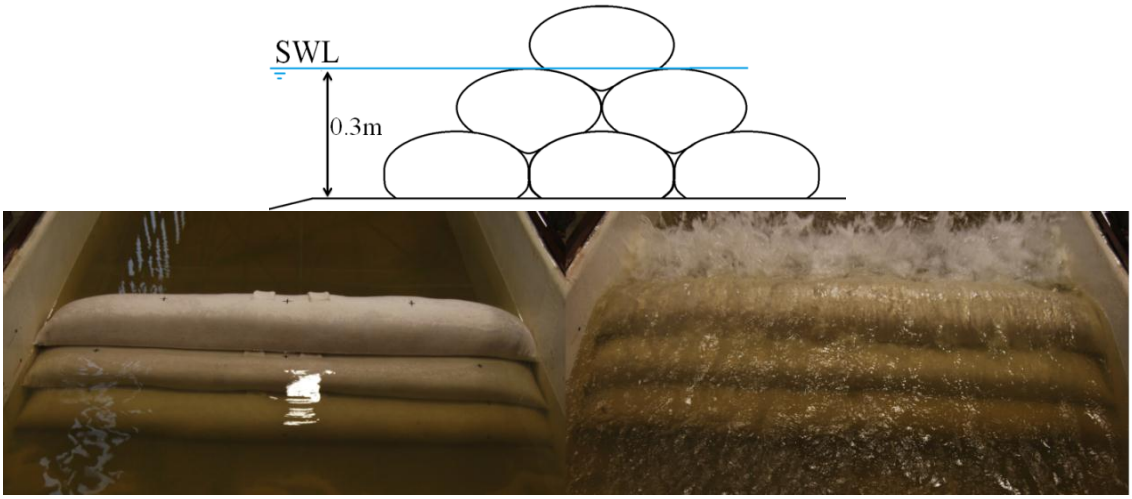

Figure 4.11: Test series 5

Structure 3-2-1: with the SWL at the crests of the second layer of tubes. (0.3m depth at structure)

Four irregular wave conditions were tested in this set-up (see Table 4.6 below and Appendix D for full wave characteristics).Visual rocking of the crest tube with impact

loading from the largest waves breaking on the structure from test 5-1 to test 5-4 was noted. There was high visual reflection off the structure on all tests.

Table 4.6: Wave conditions for test series 5

Test no.	Wave condition	Incident			At structure		
		H_s (m)	T_p (s)	H_{max} (m)	H_s (m)	T_p (s)	H_{max} (m)
5-1	1	0.13	1.79	0.242	0.13	1.75	0.21
5-2	2	0.15	2.01	0.279	0.164	2.13	0.289
5-3	3	0.16	2.24	0.298	0.204	2.22	0.339
5-4*	4	0.18	2.46	0.335	0.231	2.38	0.382

*Test was run a second time after the wedges securing the bottom layer of tubes were removed to see if the bottom layer of tubes will slide outward and additional displacement of the crest tube will occur. The bottom layer remained secured and additional displacement of the crest tube was negligible.

Measurements were taken initially and after every test. Only the crest tube showed any measurable movement after tests. There was no measurable movement after test 5-1. Figure 4.12 below illustrates the H_{max} at the structure vs. the relative cumulative horizontal displacement.

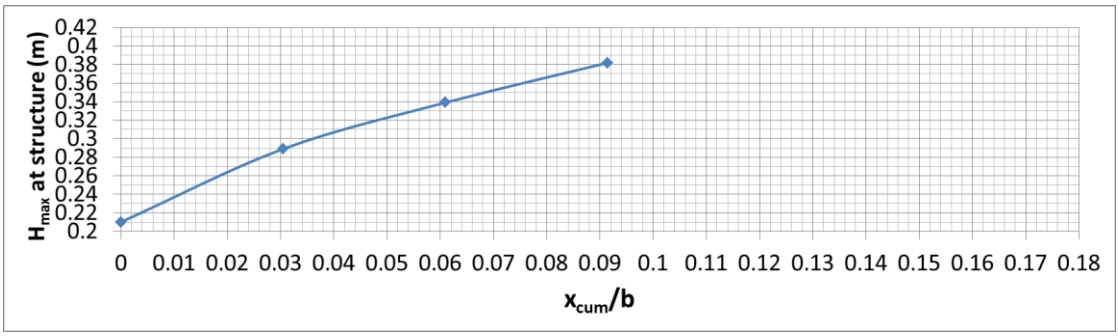

Figure 4.12: Test series 5 - H_{max} vs. relative cumulative horizontal displacement of the crest tube

4.8 – Test Series 6

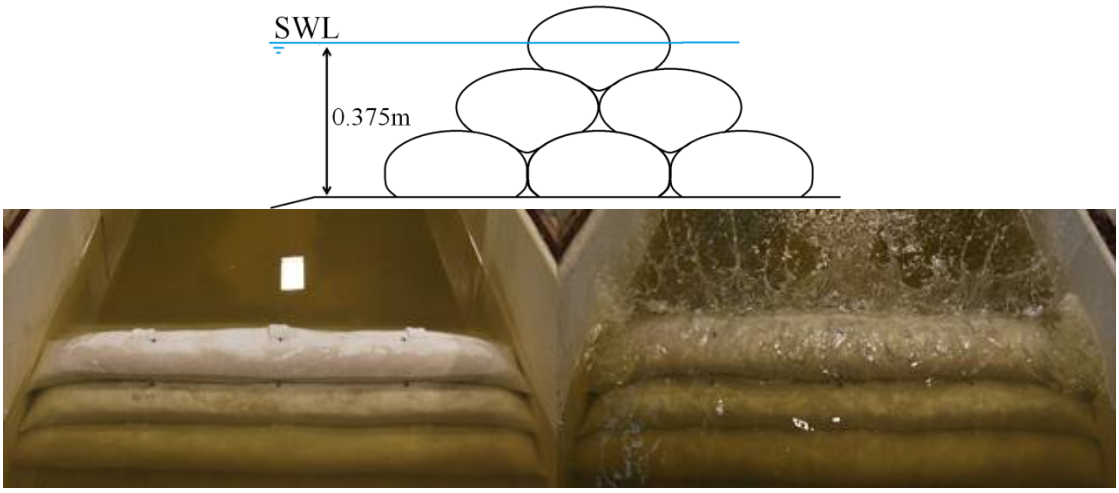

Figure 4.13: Test series 6

Structure 3-2-1: with the SWL at half the height of the crest tube, (0.375m depth at structure).

Three irregular wave conditions were tested on this set-up (see Table 4.7 below and Appendix D for full wave characteristics). Wave condition 4 was outside the flume capacity for the specific waterlevel. Visual rocking of the crest tube with impact loading from the largest waves breaking onto the structure was noted in test 6-1 to test 6-3.

Table 4.7: Wave conditions for test series 6

Test no.	Wave Condition	Incident			At structure		
		H_s (m)	T_p (s)	H_{max} (m)	H_s (m)	T_p (s)	H_{max} (m)
6-1	1	0.13	1.79	0.242	0.133	1.75	0.25
6-2	2	0.15	2.01	0.279	0.171	2.13	0.305
6-3	3	0.16	2.24	0.298	0.197	2.27	0.364

Measurements were taken initially and after every test. Only the crest tube showed any measurable movement after the tests. There was no measurable movement after test 6-1. Figure 4.14 below gives the H_{max} at the structure vs. the relative cumulative horizontal displacement.

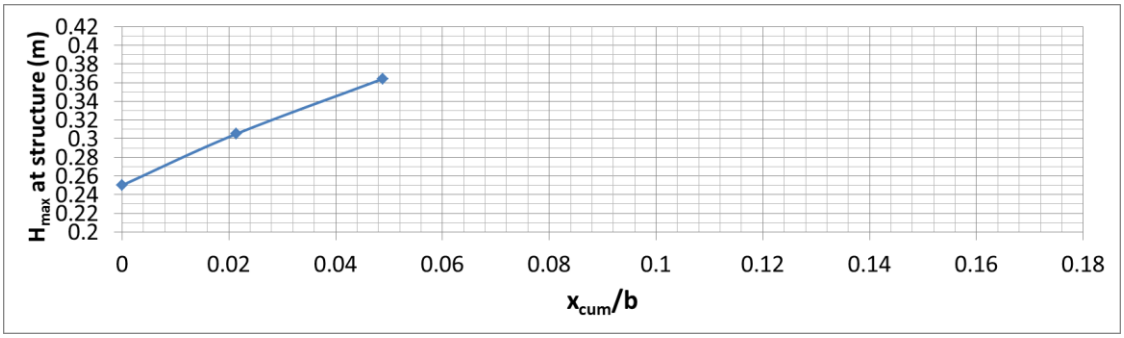

Figure 4.14: Test series 6 - H_{max} vs. relative cumulative horizontal displacement of the crest tube

4.9 – Test Series 7

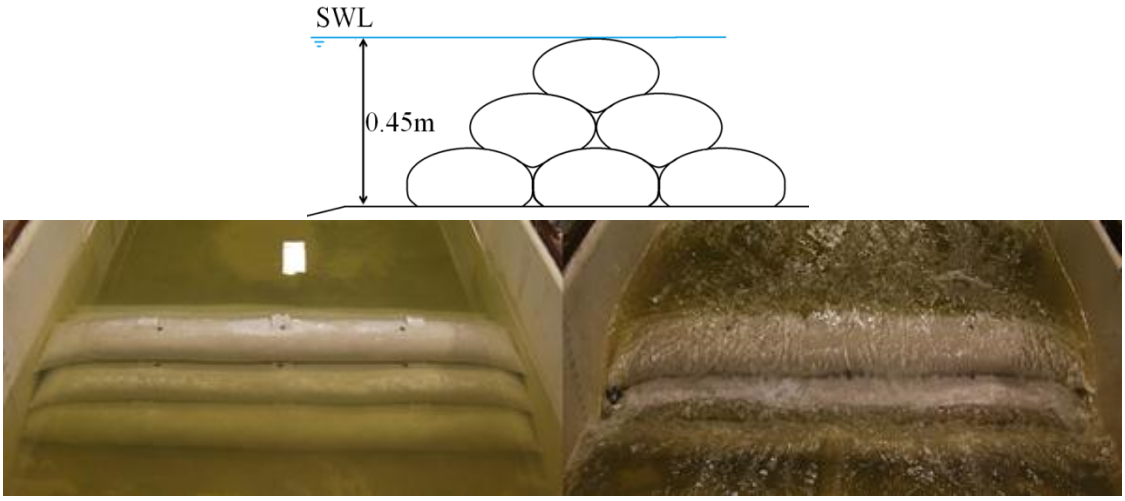

Figure 4.15: Test series 7

Structure 3-2-1: Geotextile tube structure with the SWL at the crest of the top tube, (0.45m depth at structure).

Eight irregular wave conditions were tested in this set-up (see Table 4.8 below and Appendix D for full wave characteristics). Visual rocking of the crest tube with impact loading from the largest waves breaking onto the structure from Test 7-2 to Test 7-8 was noted.

Table 4.8: Wave conditions for test series 7

Test no.	Wave condition	Incident			At structure		
		H_s (m)	T_p (s)	H_{max} (m)	H_s (m)	T_p (s)	H_{max} (m)
7-1	1	0.13	1.79	0.242	0.13	1.85	0.259
7-2	2	0.15	2.01	0.279	0.161	2.13	0.29
7-3	3	0.16	2.24	0.298	0.189	2.22	0.349
7-4	4	0.18	2.46	0.335	0.225	2.33	0.409
7-5	5	0.18	1.73	0.335	0.177	1.82	0.328
7-6	6	0.2	1.82	0.372	0.205	1.79	0.349
7-7	7	0.22	1.91	0.409	0.229	1.89	0.353
7-8	8	0.24	1.99	0.446	0.25	2.13	0.397

Measurements were taken initially and after every test. Only the crest tube showed any measurable movement during the tests. Figure 4.16 illustrates the H_{max} at the structure vs. the relative cumulative horizontal displacement.

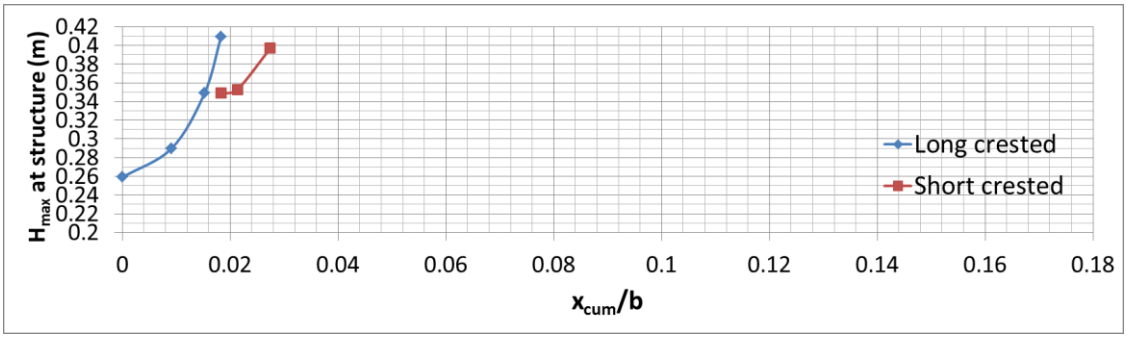

Figure 4.16: Test series 7 - H_{max} vs. relative cumulative horizontal displacement for the crest tube

4.10 – Test Series 8

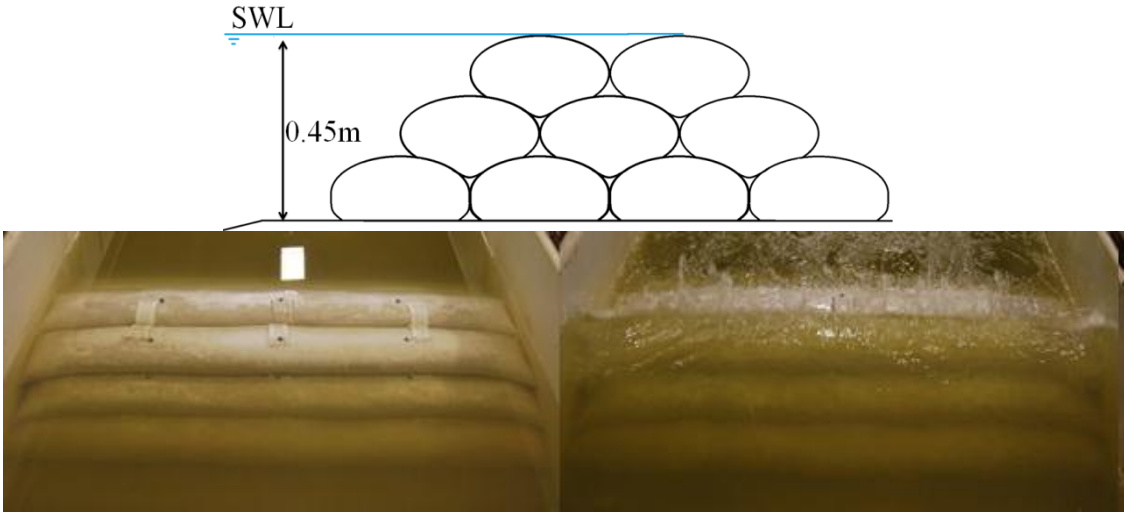

Figure 4.17: Test series 8

Structure 4-3-2: with the SWL at the crest of the top tube. (0.45m depth at structure)

Six irregular wave conditions were tested in this set-up (see Table 4.9 below and Appendix D for full wave characteristics). Visual rocking of the crest seaward tube with impact loading from the largest waves breaking onto the structure was noted from test 9-2 to test 9-8.

Table 4.9: Wave conditions for test series 8

Test no.	Wave condition	Incident			At structure		
		H_s (m)	T_p (s)	H_{max} (m)	H_s (m)	T_p (s)	H_{max} (m)
8-1	3	0.16	2.24	0.298	0.189	2.22	0.349
8-2	4	0.18	2.46	0.335	0.225	2.33	0.409
8-3	5	0.18	1.73	0.335	0.177	1.82	0.328
8-4	6	0.2	1.82	0.372	0.205	1.79	0.349
8-5	7	0.22	1.91	0.409	0.229	1.89	0.353
8-6	8	0.24	1.99	0.446	0.25	2.13	0.397

Measurements were taken initially and after every test. Most movement was measured on the leeward crest tube with minimal movement of the seaward tube, which eventually started edging seaward slightly during test 8-6. Figure 4.18, depicting the H_{max} at the structure vs. the cumulative relative displacement, is for the leeward tube only.

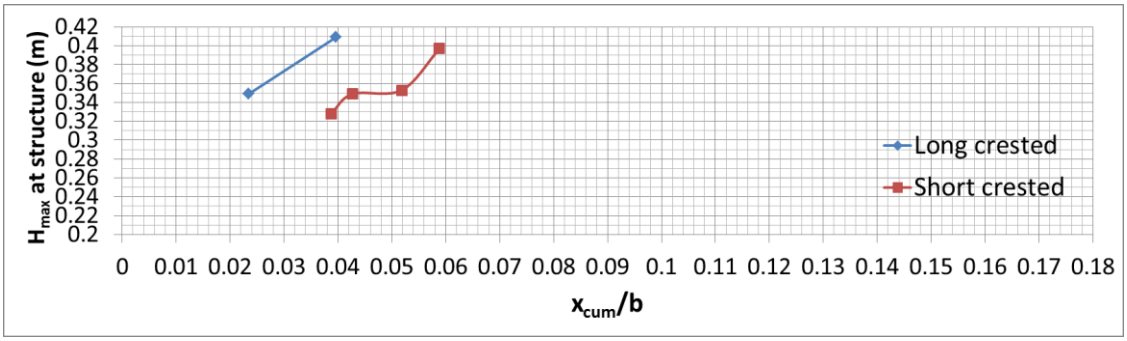

Figure 4.18: Test series 8 - H_{max} vs. relative cumulative horizontal displacement of the leeward crest tube

4.11 – Test Series 9

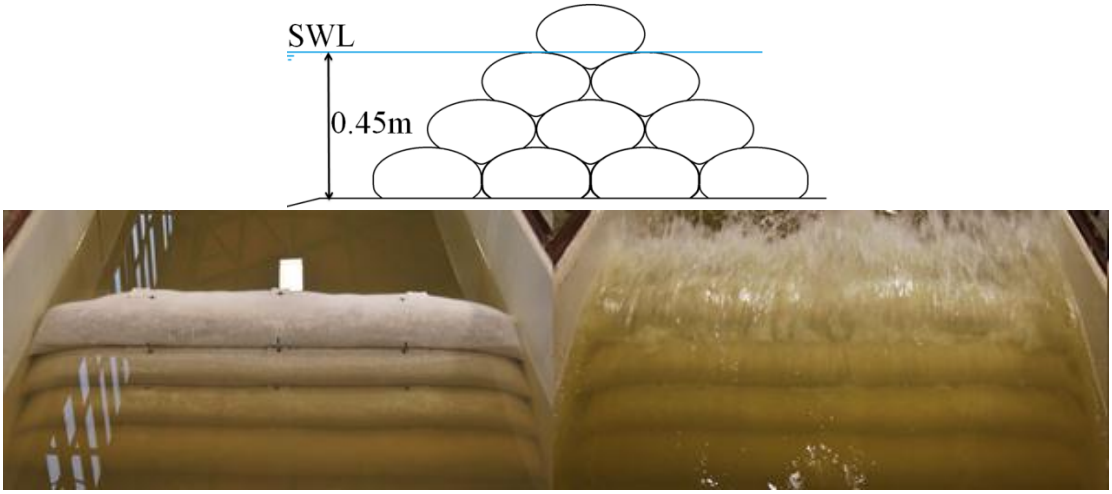

Figure 4.19: Test Series 9

Structure 4-3-2-1: with the SWL at the crest of the third layer of tubes. (0.45m depth at structure)

Eight irregular wave conditions were tested in this set-up (see Table 4.10 and Appendix D for full wave characteristics). Visual rocking of the crest tube with impact loading from the largest waves was noted from test 9-2 to test 9-8.

Table 4.10: Wave conditions for test series 9

Test no.	Wave condition	Incident			At structure		
		H_s (m)	T_p (s)	H_{max} (m)	H_s (m)	T_p (s)	H_{max} (m)
9-1	1	0.13	1.79	0.242	0.13	1.85	0.259
9-2	2	0.15	2.01	0.279	0.161	2.13	0.29
9-3	3	0.16	2.24	0.298	0.189	2.22	0.349
9-4	4	0.18	2.46	0.335	0.225	2.33	0.409
9-5	5	0.18	1.73	0.335	0.177	1.82	0.328
9-6	6	0.2	1.82	0.372	0.205	1.79	0.349
9-7	7	0.22	1.91	0.409	0.229	1.89	0.353
9-8*	8	0.24	1.99	0.446	0.25	2.13	0.397

*Test was run twice to see if additional displacement of the crest tube would occur. Additional displacement of the crest tube was negligible.

Measurements were taken initially and after every test. Only the crest tube showed any measurable movement during the tests. Figure 4.20 below shows the H_{max} at the structure vs. the relative cumulative horizontal displacement.

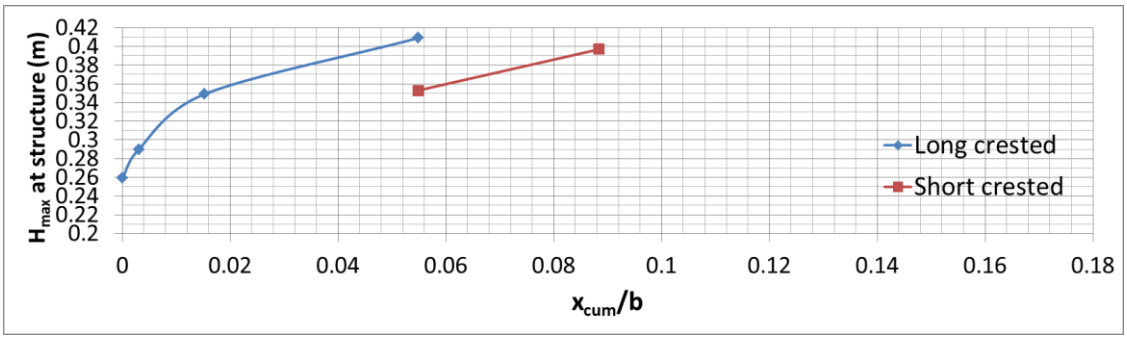

Figure 4.20: Test series 9 - H_{max} vs. relative cumulative horizontal displacement of the crest tube

4.12 – Test Series 10

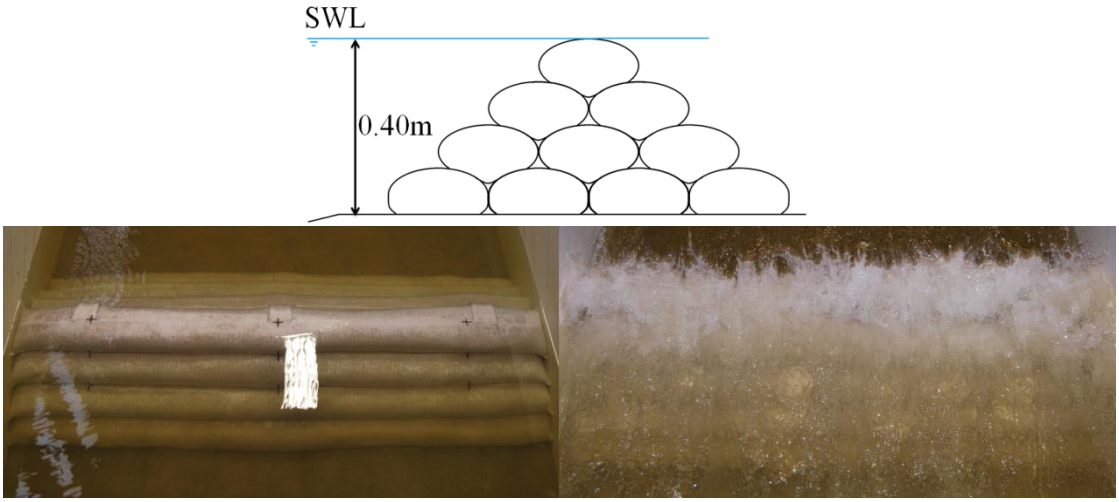

Figure 4.21: Test series 10

Test series 10 and 11 were conducted with smaller geotextile tubes. In test series 1 to 9, the movement of the crest geotextile tube was substantial, but no critical failure of the structure was achieved. As the maximum wave height the facility could produce had already been reached, it was decided to conduct an additional two test series on a slightly smaller scale. The wave conditions for this test series are the maximum wave height of the previous tests scaled down appropriately and increased incrementally to achieve critical structure failure.

Table 4.11: Wave conditions for test series 10

Test no.	Wave condition	Incident			At structure		
		H_s (m)	T_p (s)	H_{max} (m)	H_s (m)	T_p (s)	H_{max} (m)
10-1	S1	0.16	1.63	0.298	0.152	1.61	0.251
10-2	L1	0.12	2.01	0.223	0.134	1.89	0.25
10-3	S2	0.19	1.77	0.353	0.19	1.85	0.298
10-4	L2	0.14	2.17	0.26	0.158	2.13	0.298
10-5	S3	0.22	1.91	0.409	0.223	1.89	0.339
10-6	L3	0.16	2.32	0.298	0.204	2.27	0.359
10-7	S4	0.24	1.99	0.446	0.24	2.13	0.342
10-8	L4	0.18	2.46	0.335	0.233	2.63	0.368

Measurements were taken initially and after every test. Only the crest tube showed any measurable movement during the tests. Figure 4.22 illustrated the H_{max} at the structure vs. the relative cumulative horizontal displacement.

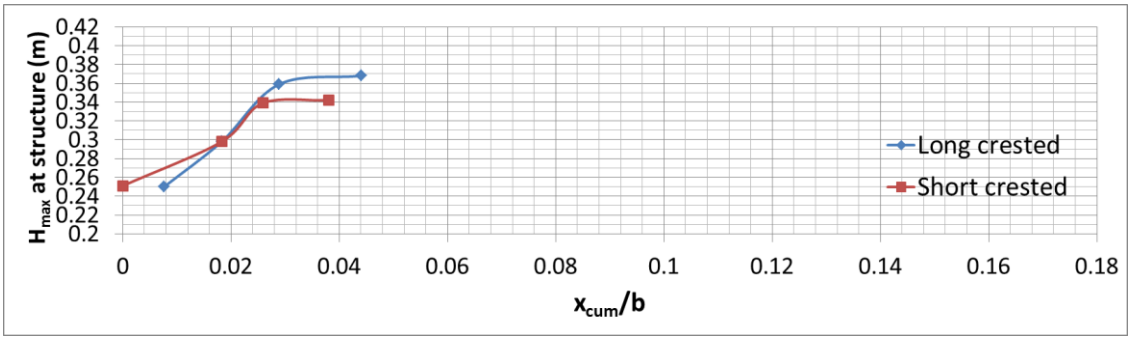

Figure 4.22: Test series 10- H_{max} vs. relative horizontal displacement of the crest tube

4.13 – Test Series 11

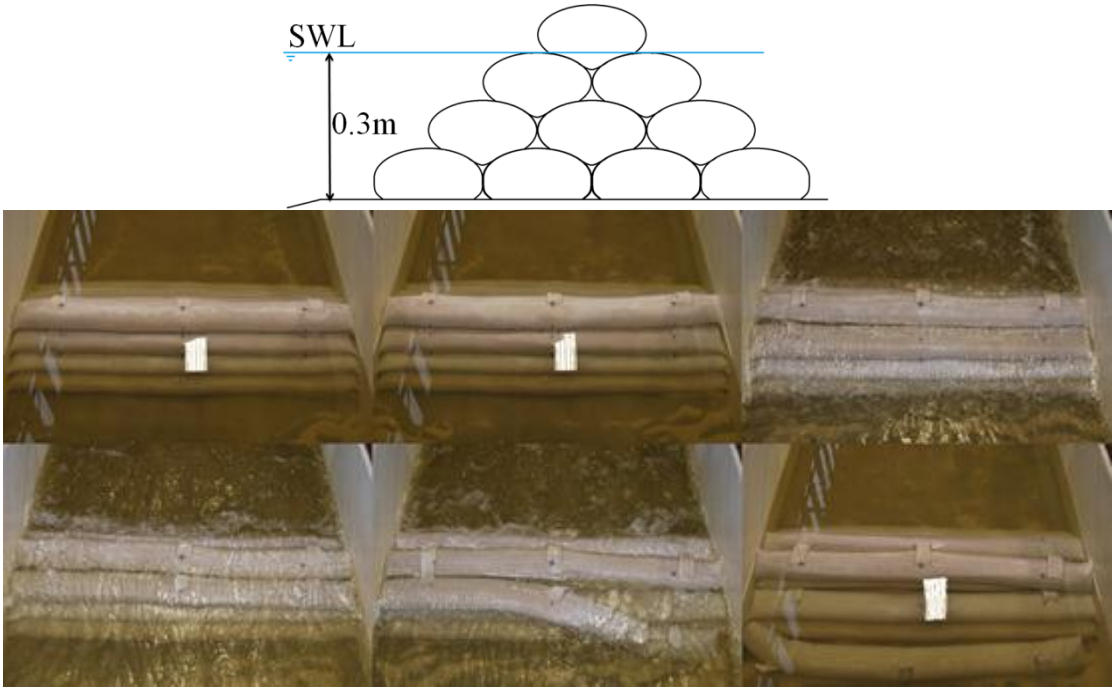

Figure 4.23: Test series 11

Test series 10 and 11 were conducted with smaller geotextile tubes. This test series used the same configuration as that of test series 9, but scaled down. The scale was: 1:1.5 of test series 9.

X_{cum} for test series 11 after test L1 was 12mm. This is exactly 2/3^{rds} of the 18mm x_{cum} experienced in test series 9 after test 9-4, of which test L1 was the scaled down version. The wave reduction factor for the two tests were also very similar, at 0.684 for L1, 0.658 for 9-4, 0.654 for S1 and 0.645 for 9-8.

The observed failure mechanism for this test series was horizontal sliding. Figure 4.23 and Figure 4.24 display the failure mode of the structure. The crest tube moved leeward until its weight was removed from the seaward tube below it. The crest tube

and leeward tube below it moved slightly leeward together, while the seaward tube moved seaward. This seaward movement can be explained by the hydrostatic pressure between the two tubes and the hydrodynamic pressure created by the waves, and it was also observed in test series 8. The crest tube fell in between the two tubes originally supporting it, with the seaward tube finally rolling off the seaward side of the structure. On reflection it can be said that the structure already failed after test L3, due to the large displacement experienced by the crest tube, although the final critical failure occurred during test S4.

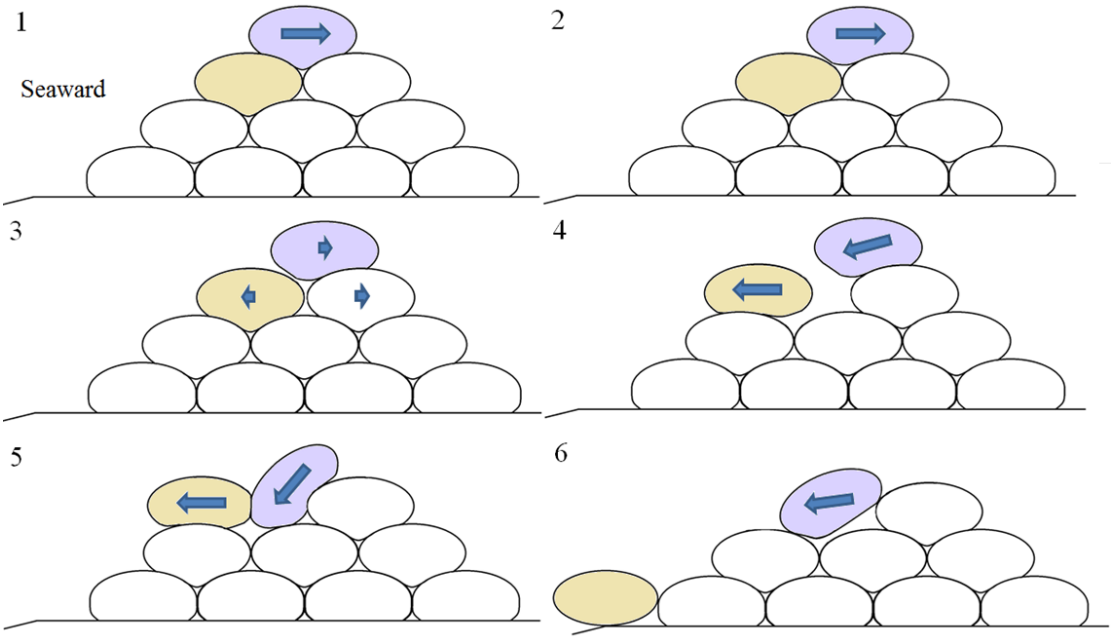

Figure 4.24: Failure mode as experienced in test series 11

The wave conditions for this test series were the maximum wave height of the previous tests scaled down appropriately and increased incrementally to achieve critical structure failure. Wave conditions for test 11-8 was the maximum wave conditions the flume could generate for the specific water depth and ran for approximately 200 waves before the capacity of the wavemaker was exceeded.

Table 4.12: Wave conditions for Test Series 11

Test no.	Wave condition	Incident			At structure		
		H_s (m)	T_p (s)	H_{max} (m)	H_s (m)	T_p (s)	H_{max} (m)
11-1	S1	0.16	1.63	0.298	0.163	1.72	0.251
11-2	L1	0.12	2.01	0.223	0.139	2	0.239
11-3	S2	0.19	1.77	0.353	0.182	1.72	0.271
11-4	L2	0.14	2.17	0.26	0.17	2.08	0.272
11-5	S3	0.22	1.91	0.409	0.203	2.04	0.284
11-6	L3	0.16	2.32	0.298	0.196	2.38	0.292
11-7	S4	0.24	1.99	0.446	0.212	1.96	0.301
11-8	L4	0.18	2.46	0.335	*	*	*

**Wavemaker capacity exceeded*

Measurements were taken initially and after every test. Only the crest tube showed any measurable movement up to test 11-5. After test 11-6 some movement of the leeward tube ,below the crest tube, was measured. Figure 4.25 below illustrates the H_{max} at the structure vs. the relative cumulative horizontal displacement of the crest tube.

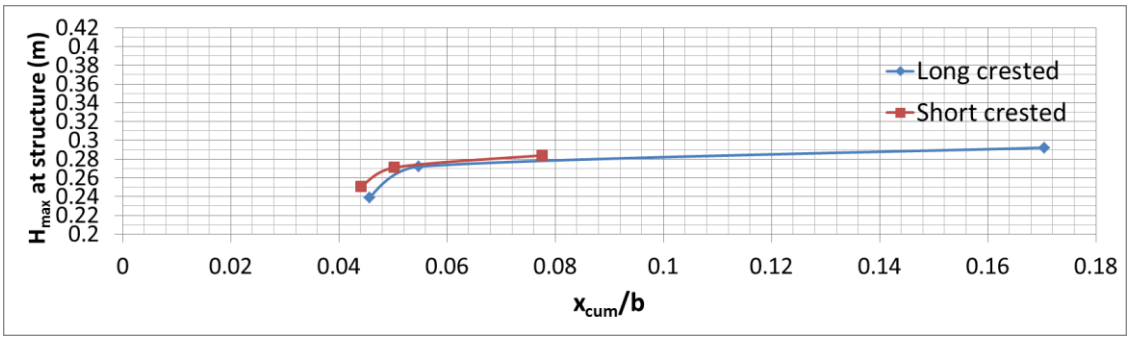

Figure 4.25: Test series 11- H_{max} vs. relative cumulative horizontal displacement of the crest tube

4.14 – Summary

Visual observations of the test series indicate that only impact loading caused damage to the structure. Broken and unbroken waves propagating onto the structure did not produce sufficient force to move the geotextile tubes. Waves breaking onto the structure, encapsulating air in the ridge between the crest tube and the tube just below it, resulted in visible movement or rocking of the crest tube. The term "breaking waves" refers to the waves breaking due to the depth limitation of the foreshore impacting on the seaward side of the structure. The structure became more stable after the initial displacement against the same wave condition. This was observed in the

negligible additional displacement experienced when the same wave condition was re-run in test series 5 and 9.

The high friction coefficient between the geotextile and the flume bed will not be present in prototype applications and it should be noted that entire structure collapse before failure caused by horizontal displacement of the crest tube is possible in cases where the base layer of tubes are not properly secured against outward sliding.

Chapter 5 – Analysis

Analysis of the test results from Chapter 4.

5.1 – Test Overview

From the test results and visual observations it was determined that:

- The tube at the crest of the structure is the most likely to move.
- The key failure mechanism is sliding.
- When the crest tube is dislodged it will be most likely to do so when the incident wave breaks at the toe of the structure causing impact loading and the water level is between the base and crest of the crest tube of the structure.
- Broken and normal waves propagating into and over the structure have far less impact on stability.
- After the initial displacement the structure becomes more stable against the same wave condition.
- Critical failure of the structure occurs at much higher wave energy than initial movement and is progressive from the initial displacement.
- The wave transmission coefficient of the structure has a big effect on the stability thereof, as displayed in test series 10 and 11.
- A double tube crested structure with its crest at the SWL, is negligibly more stable than a single crested tube structure, but it reduces the energy transmitted to the leeside of the structure, as revealed by visual observation in test series 4 and measured in test series 8.

5.2 – Failure Mechanism

Sliding is the key failure mechanism for a stacked geotextile tube structure, constructed from tubes filled to 80% with sand.

Displacement of the tubes is a gradual process that incrementally increases the cumulative displacement until critical failure occurs. The initial movement of the crest tube occurs at relatively low wave energy, but becomes more stable as it gets displaced leeward. Critical failure of the structure occurs at much higher wave energy than the initial movement of the structure. Critical failure of the structure in test series

11 occurred after the crest tube had been displaced sufficiently leeward to remove its weight from the seaward tube just below it. When that occurred the hydrodynamic force of the waves and the static water pressure of water between the two tubes forced the seaward tube with its crest at the SWL forward until the crest tube collapsed in between the two tubes initially supporting it. The seaward tube, with its crest at the SWL, eventually rolled off the seaward side of the structure (see Figure 4.23 and Figure 4.24).

5.3 – Wave Transmission

It was assumed that test series 10 would be the most unstable configuration due to the biggest wave condition occurring at the toe of the structure. Surprisingly test series 11 was the most unstable, with the only occurring critical failure. On closer inspection it was noticed that when comparing the leeside energy spectrum from test series 10 and 11 with each other, substantially more energy was being absorbed and reflected by the structure in test series 11 than that of test series 10.

In their study, Van Steeg & Vastenburg (2010) found that a reduction factor, χ, was required to calculate the hydraulic stability of singly placed geotextile tube. The reduction factor changed the wave height to an effective wave height to accommodate energy lost due to overtopping. The reduction factor used in the study by Van Steeg and Vastenburg (2010) was derived from a study done by Van der Meer et al. (2004) to measure wave overtopping on low crested structures. Figure 5.1 below depicts χ vs. relative crest height, R_c/H_s, with the values as measured in the physical model and used in this report.

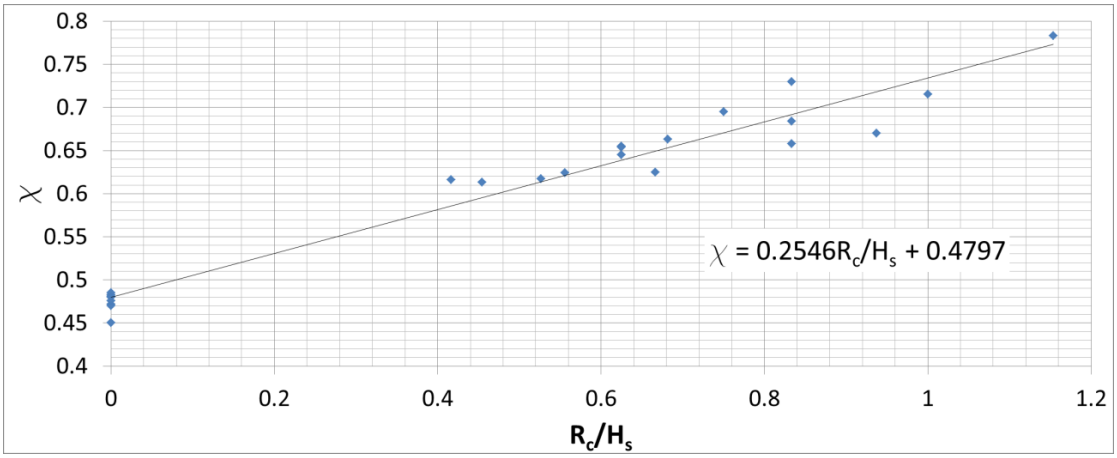

Figure 5.1: Reduction factor vs. relative crest height, from data collected from physical modelling

In test series 11 the crest height was 0.1m above the SWL and the energy transfer to its leeside was much less than that of test series 10. Calculating the effective wave heights at the structures resulted in a higher effective wave height for test series 11 than that of test series 10. Appendix B provides an explanation of the effective wave height, transfer coefficients and the wave reduction factor, χ.

5.4 – Buoyancy Force and Relative Weight

The saturated weight of the geotextile tubes is considerably more than their relative weight, $\Delta_t = (\frac{\rho_s - \rho_w}{\rho_w}) = 1.04$. The tube at the crest of the structure, however, did not display an increase in stability, regardless of whether it was above or below the SWL.

With wave impact the seaward side of the crest tube is submerged regardless of the initial water level.

From this observation the vertical gravity force of the self-weight of the tubes should be used as the relative submerged weight or buoyant weight in calculations of hydraulic stability against wave attack, but the saturated weight should be used for overall stability against slip-circle failure and bearing capacity failure.

5.5 – Reflection

The bulk reflection coefficient calculated at the offshore probe array was the bulk reflection coefficient of the entire set-up and not that of the structure. For instance, in most tests, significant energy loss occurred due to depth induced breaking long before the structure was reached and most of the tests experienced significant energy transfer to their leeside via overtopping. However, there were a few tests with no offshore breaking and minimal overtopping. From these it can be calculated that the bulk reflection coefficient for a non-overtopped multi-layered tube structure is approximately 0.65. The bulk reflection coefficient for a structure with its crest at the SWL was found to be approximately 0.45.

5.6 – Impact loading

5.6.1 – General

From visual observation it was concluded that impact loading is the main cause for the displacement of the geotextile tube on the crest. One of the objectives of this

thesis was to provide a method to calculate hydraulic stability against wave loading. It was decided that the modification of existing formulae to apply to a specific application was preferable to producing a new formula.

There are several methods that can be used to calculate impact loading prescribed by Hiroi (1920), Minikin (1963), Sainflou (1928), Honma & Horikawa (1965) and Goda (1974). The Goda method is the most recent of these methods and has been validated against prototype performance.

5.6.2 – Goda Method

Many of the variables of the physical modelling that affect hydraulic stability are already incorporated in Goda's (1974) formulae to calculate impact loading and the potential of these formulae to easily work in safety factors when designing a structure make Goda's formulae the preferred choice.

The wave pressure formulae of Goda can be applied to the whole range of wave action from nonbreaking to post-breaking waves with smooth transition between them.

Through calibration Goda established that his formulae provide answers that are more accurate than those of previous formulae (Goda 1974).

5.6.3 – Modified Goda Method

The more complex cross-section of the geotextile tube is replaced by that of an equivalent rectangle as done by Oh and Shin (2006). This simplifies the force schematisation and the force calculations significantly.

Energy loss due to overtopping of low crest heights was assumed to have no effect on the wave pressure in Goda's method for simplicity (Goda 1974) and therefore a wave reduction factor is required. On the basis of the observations and data from test series 10 and 11, a wave reduction factor, χ, similar to that used by Van Steeg and Vastenburg (2010), is added to the modified Goda method to calculate wave pressures. When H_s or H_{design} is used to calculate lengths or distances, no reduction factor is needed; when used to calculate forces, the reduction factor must be used.

Due to the flexibility of the Goda technique it is possible to extrapolate the force on a multi-layered structure to a single geotextile tube. The technique can also be applied to single tube structures.

The SWL at the structure can easily be adjusted and is not limited to the crest of the structure. Figure 5.2 to Figure 5.4 shows the schematisation of forces from impact loading on the crest tube with different SWL at the structure.

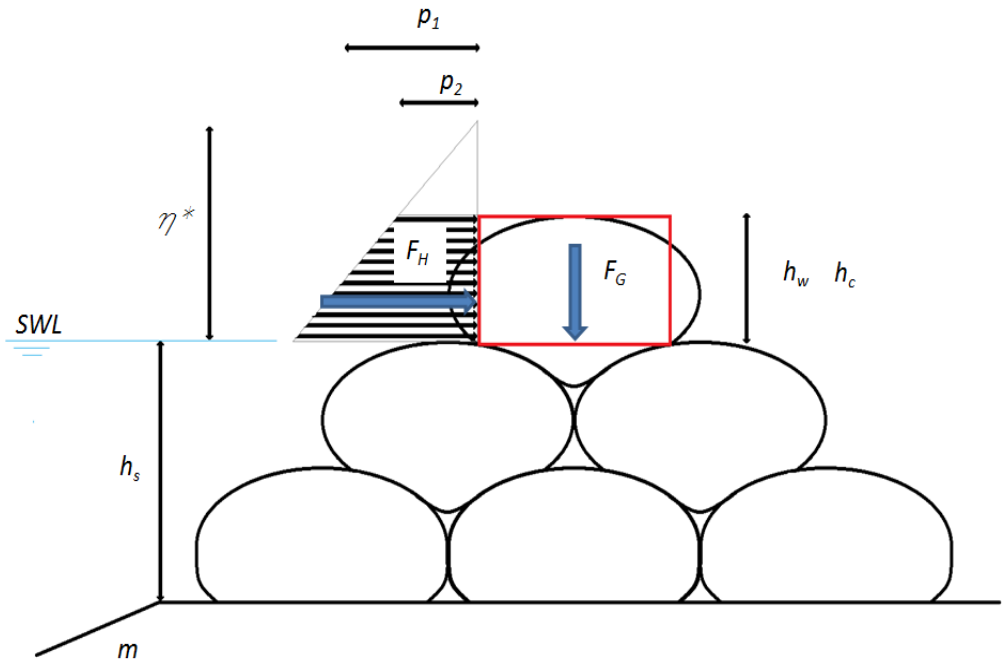

Figure 5.2: Schematisation of forces on the crest tube with the SWL at the base of the crest tube

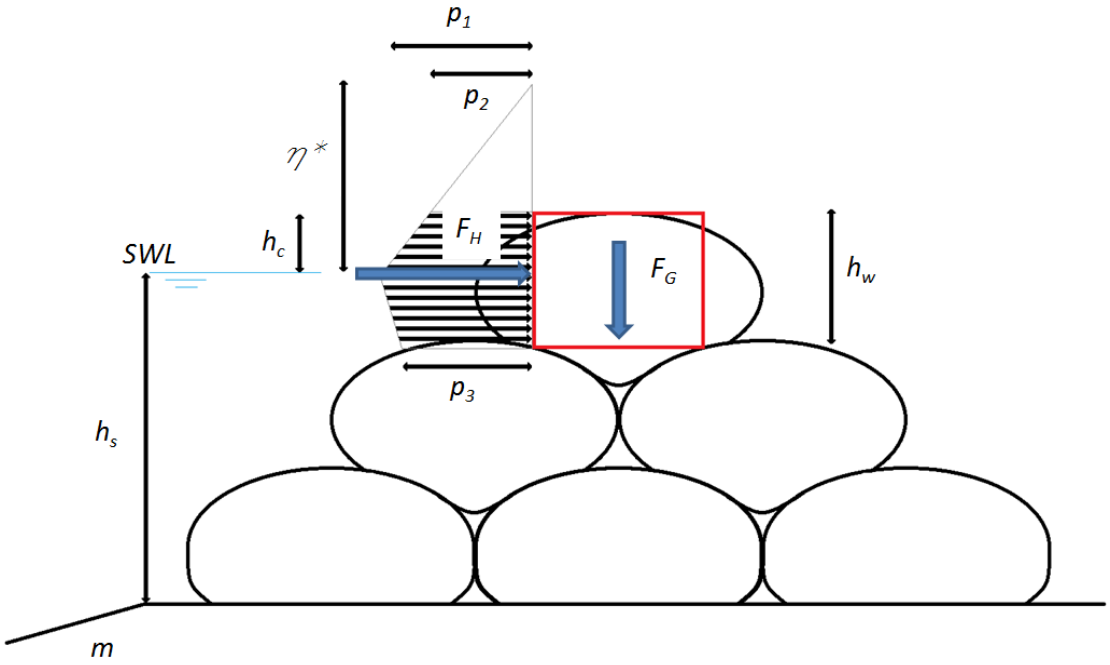

Figure 5.3: Schematisation of forces on the crest tube with the SWL between the base and the crest of the crest tube

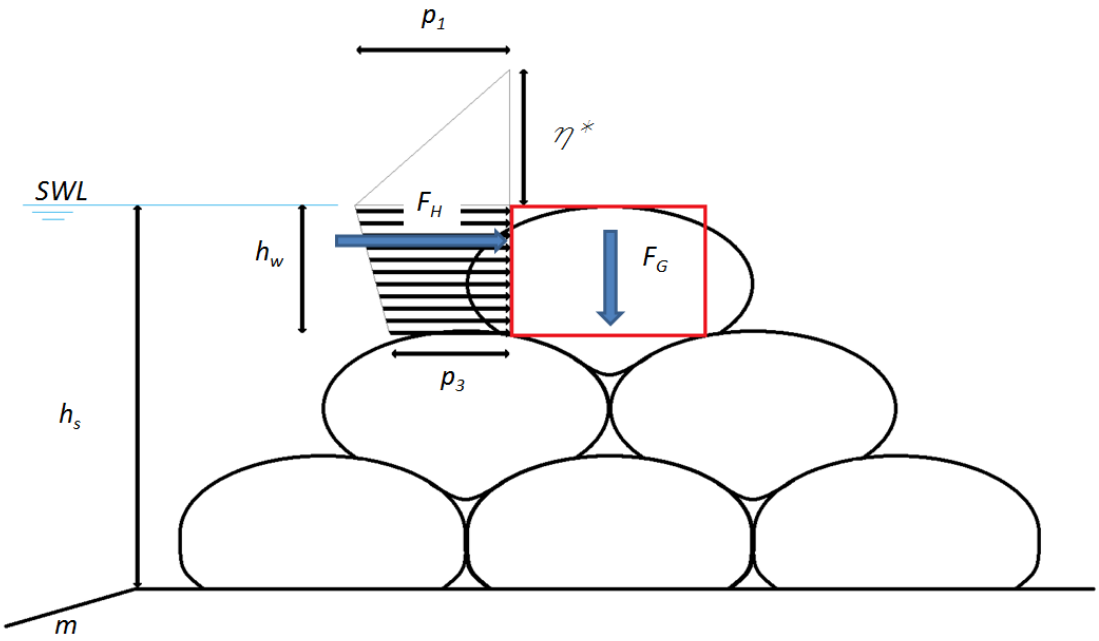

Figure 5.4: Schematisation of forces on the crest tube with the SWL at the crest of the structure

Note: No wave induced uplift force as the tubes are considered to be impermeable.

$$\eta^* = 0.75(1 + cos\beta)(\lambda_1 H_{design})$$

$$\alpha_* = \alpha_2$$

$$\alpha_1 = 0.6 + 0.5\left[\frac{4\pi h_s/L}{sinh(4\pi h_s/L)}\right]^2$$

$$\alpha_2 = \min\left\{\frac{h_b - h_s}{3h_b}\left(\frac{H_{design}}{h_s}\right)^2, \frac{2h_s}{H_{design}}\right\}$$

$$p_1 = 0.5(1 + cos\beta)(\lambda_1\alpha_1 + \lambda_2\alpha_* cos^2\beta)\rho_w g\chi H_{design}$$

$$p_2 = \begin{Bmatrix} \frac{p_1}{cosh(2\pi h/L)} \; for \; h_c > 0 \\ 0 \; for \; h_c = 0 \end{Bmatrix}$$

$$p_3 = \begin{Bmatrix} \alpha_3 p_1 \; for \; h_c < h_w \\ 0 \; for \; h_c \geq h_w \end{Bmatrix}$$

$$\alpha_3 = 1 - \frac{h_w - h_c}{h_s}\left[1 - \frac{1}{cosh(2\pi h_s/L)}\right]$$

with:

H_{design} = *min {max. wave height measured at structure; 1.8H_s}*

H_s = *significant wave height. Assume equal to H_{m0}*

L = $T_p\sqrt{gh_s}$ *wave length at structure*

T_p = *peak wave period*

h' = *submerged depth of tube*

h_c = *crest height above SWL*

h_w = *height of tube, 0.15m*

h_s = *total depth of structure*

h_b = $5(H_s)(m) + h_s$ *depth a distance of 5(H_s) from tube,*

λ_1 = *modification factor*

λ_2 = *modification factor*

λ_3 = *modification factor*

m = *slope*

ρ_w = *water density*

ρ_s = *saturated sand density*

Δ_t = $(\frac{\rho_s - \rho_w}{\rho_w})$ *relative density of the geotextile tube*

β = *angle of incidence of waves*

Wave-induced horizontal force per metre length of the structure:

$F_H = U_{FH}[F]$

F = the resultant force from the pressures p_1, p_2 and p_3

U_{FH} is a stochastic variable signifying the bias and uncertainty in the horizontal force.

Gravity and buoyancy-induced vertical force per metre length of structure:

$F_G = \Delta_t \rho_w A g$

A is the cross-section area of the tube, not the equivalent rectangle

Using the wave force calculated by the modified Goda method in combination with factors derived from the results obtained from the physical modelling produces a new way of calculating the stability of a multi-layered geotextile tube structure against wave attack.

5.7 – Stability against Overturning

From the visual inspection of the physical models during testing it was clear that the top geotextile tube will rock under wave loading during the 0.13m H_s test up to the 0.24m H_s test without overturning. From this observation it was reasoned that the point on which the crest tube pivots moves leeward as it receives impact loading, which increases the restoring moment (see Figure 5.5 below). The rocking at low wave heights did not result in any horizontal displacement. The effect that this rocking of the tube might have on geotextile lifetime and deformation in prototype scale could be problematic.

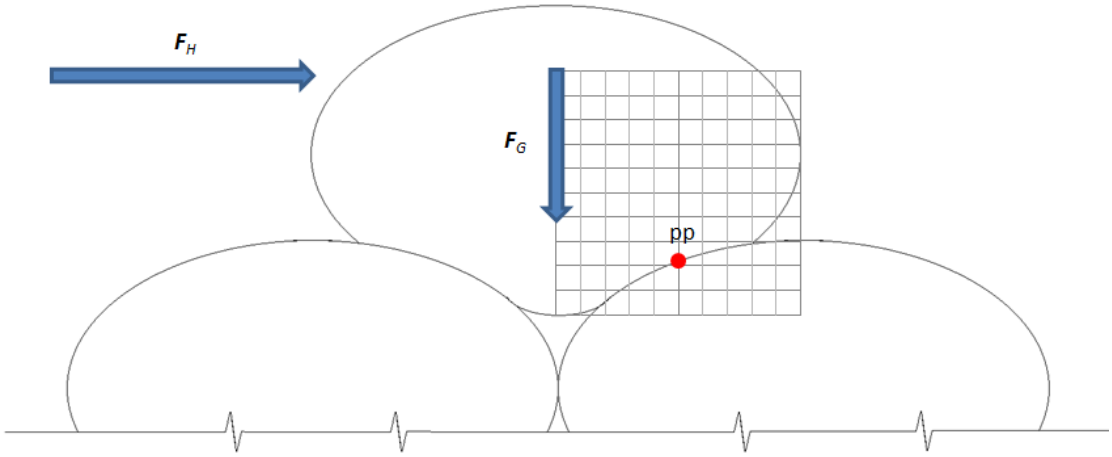

Figure 5.5: Movement of the pivot point under wave loading

Moment corresponding to the horizontal force, F_H, at the leeward pivot point, pp:

$$M_H = U_{MH}(F_H H)$$

U_{MH} is a stochastic variable signifying the bias and uncertainty of the horizontal moment

H is the vertical distance between the resultant horizontal wave force, F_H, and the pivot point of the geotextile tube.

Moment corresponding to the gravity and buoyancy force, F_G

$$M_G = F_G(B)$$

B is the horizontal distance between the centre of gravity of the geotextile tube and the pivot point of the geotextile tube.

With $M_H < M_G$ the structure is stable against overturning

5.8 – Stability against Sliding

Impact loading is in the order of fractions of a second and the movement seen in the physical modelling tests arise from minor shifts as a result of numerous waves impacting on the structure.

The crest tube is not resting on a flat surface, but is wedged in between the crests of the tubes below it. Due to the curved surface of the tube, a single hypothetical angle, α, which is representative of the crest tube's set-up, was chosen for calculation purposes (see Figure 5.6).

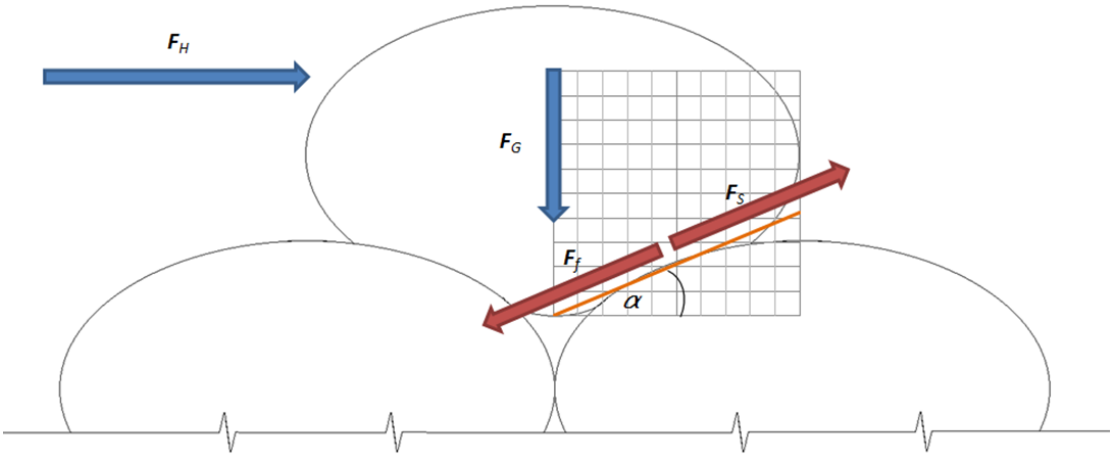

Figure 5.6: Schematisation of forces for sliding instability of the crest tube

The hypothetical angle, α, was selected to correspond to the movement observed from the physical modelling. Initial displacement of the crest tube occurs at much lower wave conditions than critical failure. An angle of approximately 5° appears to best fit the results obtained from the physical modelling for the start of horizontal displacement. The crest tube will move leeward and a new equilibrium for the wave condition will be reached. This movement increases the devised angle α.

By the author's definition, the structure is considered to have failed critically after the crest tube has moved leeward approximately 15% of its own width, as structure collapse occurs soon thereafter. The angle, α, that corresponds to the 15% displacement of the crest tube of the structure is 21° and was derived from results in the physical model.

For the crest tube to resist sliding on the leeward tube below it, the following forces needs to be considered.

Resisting static friction force, F_f

$$F_f = \mu_s(F_G cos\alpha + F_H sin\alpha)$$

Sliding force, F_S

$$F_S = (F_H cos\alpha - F_G sin\alpha)$$

For initial movement $\alpha = 5^\circ$

$$F_{f,i} = \mu_s(F_G cos5^\circ + F_H sin5^\circ)$$

$$F_{S,i} = (F_H cos5^\circ - F_G sin5^\circ)$$

If $F_{s,i} > F_{f,i}$, initial displacement of the crest tube can be expected.

For critical failure $\alpha = 21^\circ$ (Structure collapse)

$$F_{f,c} = \mu_s(F_G cos21^\circ + F_H sin21^\circ)$$

$$F_{S,c} = (F_H cos21^\circ - F_G sin21^\circ)$$

If $F_{s,c} > F_{f,c}$, collapse of the structure can be expected.

Similar to the findings by Van Steeg and Vastenburg (2010), a double crest tube configuration has very little effect on the stability of the structure against sliding. It does, however significantly reduce the energy transferred to the leeside of the structure.

By setting α = 0, the modified Goda method gives results that correlate well with results from previous studies on single geotextile tubes (see Figure 5.7).

5.9 – Deformation and Sand Tightness

No signs that can be related to the loss of sand through the geotextile were observed. The little sand that can be seen in some of the photos from the physical modelling is from wastage during the filling process. Sand tightness is discussed in Chapter 2.4.3.

Using information from Appendix F and Appendix G, the requirements for sand tightness as prescribed by the CUR (2006) are met:

$O_{90} \leq D_{90}$ (CUR requirement)

$0.012mm < 1.14mm$ OK (from Appendix F and G)

$O_{90} < 1.5D_{10}C_u^{1/2}$ (CUR requirement)

$0.012mm < 1.5(0.15)3.3^{1/2}$ (from Appendix F and G)

$0.12mm < 0.409mm$ OK

No deformation of the tubes was observed visually and, due to the small scale, possible unnoticed deformation of the geotextile tubes could not be measured properly.

5.10 – Double vs. Single Tube Crests

The increase in stability provided by an additional tube at the crest of the structure with its crest at the SWL level is negligible. However, by adding additional tubes the wave energy transferred to the leeside is reduced.

Although data is limited, it would appear that double crested structures with their crests sufficiently higher than the SWL are more stable against sliding than structures with a single tube crest (see results for test series 2 and 4). After test series 4, the crest tubes had shifted leeward approximately half of the distance of the movement of the crest tubes in test series 2. This could be due to a lack of hydrostatic force between the crest tubes that is present with higher water levels

5.11 – Comparison with Current Formulae

Comparing the technique for calculating stability in this chapter, to that of studies done in previous research is difficult, due to the different application areas and the lack of important variables in them.

All previous formulae are for applications where the SWL is at the crest of the structure.

The CUR 217 (2006) formula is very general and does not use friction coefficients or wave period.

Van Steeg and Vastenburg's (2010) formula incorporates all the important variables required and was derived from large-scale physical model tests, making it a suitable formula with which to compare results. It is however for single tubes with the SWL at their crests.

By changing the devised angle, α, from the modified Goda method to 0, it is possible to use the method on single tubes.

Figure 5.7 provides a comparison of the results obtained from the different methods for a single tube on a substructure with a slope of 1 in 2.5 and a flat crest, with a friction coefficient of 0.5 between the structure and the geotextile. The SWL is at the crest of the tube. This set-up is similar to that used by Van Steeg and Vastenburg (2010) in their physical modelling.

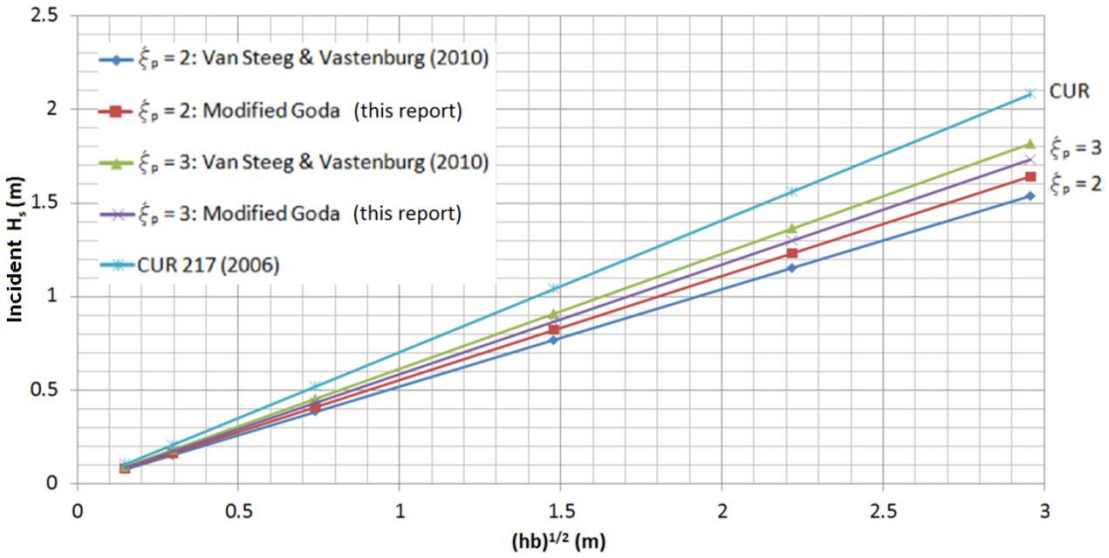

Figure 5.7: Comparison of different methods for single tubes (80% filled)

The formula recommended in the CUR 217 (2006) gives a wave height larger than that calculated by the formulae from Van Steeg and Vastenburg (2010) and the modified Goda method. It is described as being more a rule of thumb, and due to the lack of wave period and friction coefficient, should be used as such.

The formula of Van Steeg and Vastenburg (2010) gives answers with good correlation to that of the modified Goda formulae. The modified Goda method also accurately predicts the failure of the 80% filled tube structures from the data presented in the physical modelling by Van Steeg and Vastenburg (2010).

The formula of Pilarczyk (2000) was a theoretical derivation from studies done on tubes with a very high filling percentage on a substructure with a slope of 1:30. It calculates the stability against overturning, which is not the key failure method of stacked tubes filled to 80%. The absence of wave period from the formula makes it difficult to compare results. The approximation of the formulae that give $H_s \approx \Delta_t b$

does however correlate to the physical model test results for the short-crested waves in test series 11.

All formulae are for structures with the SWL at their crests. The modified Goda method has the advantage that it can be used on any SWL at the structure, which is especially useful since it was found that the SWL at the structure's crest is not always the critical water level because of wave energy transmission.

5.12 – Predicting Results of the Physical Modelling

Presenting the results visually is problematic due to the large number of variables. Tables 5.1 to 5.4 supply the measurements and calculations from the physical modelling for comparative purposes. Appendix C gives an example of the calculation method used to calculate the wave forces.

For initial movement of the tubes, the initial sliding force, $F_{s,initial}$, needs to be larger than the initial friction force, $F_{f,initial}$. For the critical failure of the structure the sliding force at critical failure, $\mathbf{F_{s,crititcal}}$, needs to be larger than the friction force $\mathbf{F_{f,critical}}$. Test series 7 to 11 are shown, as they are the only tests with all the available variables required for the modified Goda method. Test series 8 is excluded because of its double tube crest, but it can be assumed to be the same as test series 7. Results that predict initial movement are highlighted in yellow and results that predict failure are highlighted in red.

Table 5.1: Results of modified Goda method for test series 7

Test Series 7								
Test	7-1	7-2	7-3	7-4	7-5	7-6	7-7	7-8
H_s (m)	0.13	0.15	0.16	0.18	0.18	0.20	0.22	0.24
T_p (s)	1.8	2.1	2.22	2.44	1.72	1.82	1.92	2
H_{design} (m)	0.259	0.29	0.349	0.409	0.328	0.349	0.353	0.397
χ	0.46	0.46	0.46	0.46	0.463	0.457	0.452	0.477
F_G (N/m)	418.23	418.23	418.23	418.23	418.23	418.23	418.23	418.23
F_H (N/m)	163.8	193.45	236.86	285.15	205.8	223.81	238.86	271.44
$F_{s,initial}$ (N/m)	*126.73*	*156.26*	*199.51*	*247.61*	*168.57*	*186.51*	*201.50*	*233.96*
$F_{f,initial}$ (N/m)	*176.67*	*177.73*	*179.29*	*181.01*	*178.18*	*178.82*	*179.36*	*180.52*
$F_{s,critical}$ (N/m)	**3.04**	**30.72**	**71.25**	**116.33**	**42.25**	**59.06**	**73.11**	**103.53**
$F_{f,critical}$ (N/m)	**184.15**	**188.51**	**194.89**	**201.98**	**190.32**	**192.97**	**195.18**	**199.97**
x_{cum} (mm)	0	3	5	6	6	6	7	9
x_{cum} / b	0.000	0.009	0.015	0.018	0.018	0.018	0.021	0.027

Table 5.2: Results of modified Goda method for test series 9

Test Series 9								
Test	9-1	9-2	9-3	9-4	9-5	9-6	9-7	9-8
H_s (m)	0.13	0.15	0.16	0.18	0.18	0.20	0.22	0.24
T_p (s)	1.8	2.1	2.22	2.44	1.72	1.82	1.92	2
H_{design} (m)	0.234	0.27	0.288	0.324	0.324	0.349	0.373	0.397
χ	0.783	0.715	0.67	0.658	0.73	0.695	0.663	0.645
F_G (N/m)	418.23	418.23	418.23	418.23	418.23	418.23	418.23	418.23
F_H (N/m)	225.62	256.34	263.23	303.66	268.65	326.42	341.23	356.63
$F_{s,initial}$ (N/m)	*188.31*	*218.91*	*225.78*	*266.05*	*231.18*	*288.73*	*303.48*	*318.82*
$F_{f,initial}$ (N/m)	*178.88*	*179.98*	*180.23*	*181.67*	*180.42*	*182.49*	*183.02*	*183.57*
$F_{s,critical}$ (N/m)	**60.75**	**89.43**	**95.87**	**133.61**	**100.93**	**154.86**	**168.69**	**183.06**
$F_{f,critical}$ (N/m)	**193.24**	**197.75**	**198.76**	**204.70**	**199.56**	**208.05**	**210.22**	**212.49**
x_{cum} (mm)	0	1	5	18	18	18	18	29
x_{cum} / b	0.000	0.003	0.015	0.055	0.055	0.055	0.055	0.088

Table 5.3: Results of modified Goda method for test series 10

Test Series 10								
Test	10-2	10-4	10-6	10-8	10-1	10-3	10-5	10-7
H_s (m)	0.12	0.14	0.16	0.18	0.16	0.19	0.22	0.24
T_p (s)	2	2.17	2.34	2.46	1.61	1.76	1.9	1.97
H_{design} (m)	0.216	0.252	0.288	0.324	0.251	0.298	0.349	0.342
χ	0.483	0.45	0.472	0.481	0.485	0.48	0.47	0.476
F_G (N/m)	187.1	187.1	187.1	187.1	187.1	187.1	187.1	187.1
F_H (N/m)	104.18	115.91	141.7	164.44	113.48	137.64	157.27	163.30
$F_{s,initial}$ (N/m)	*87.48*	*99.16*	*124.85*	*147.51*	*96.74*	*120.81*	*140.36*	*146.37*
$F_{f,initial}$ (N/m)	*80.14*	*80.56*	*81.48*	*82.30*	*80.47*	*81.34*	*82.04*	*82.25*
$F_{s,critical}$(N/m)	**30.21**	**41.16**	**65.24**	**86.47**	**38.89**	**61.45**	**79.77**	**85.40**
$F_{f,critical}$ (N/m)	**86.92**	**88.65**	**92.44**	**95.78**	**88.29**	**91.84**	**94.72**	**95.61**
x_{cum} (mm)	1.67	4	6.33	9.66	0	4	5.67	8.33
x_{cum} / b	0.008	0.018	0.029	0.044	0.000	0.018	0.026	0.038

Table 5.4: Results of modified Goda method for test series 11

Test Series 11								
Test	11-2	11-4	11-6	11-8	11-1	11-3	11-5	11-7
H_s (m)	0.12	0.14	0.16	0.18	0.16	0.19	0.22	0.24
T_p (s)	2.00	2.15	2.33	2.46	1.72	1.77	1.91	2.00
H_{design} (m)	0.216	0.252	0.288	0.298	0.251	0.271	0.284	0.301
χ	0.684	0.655	0.625	0.617	0.654	0.613	0.624	0.616
F_G (N/m)	187.10	187.10	187.10	187.10	187.10	187.10	187.10	187.10
F_H (N/m)	140.4	163.17	183.83	190.19	154.77	159.47	174.11	185.28
$F_{s,initial}$ (N/m)	*123.56*	*146.24*	*166.82*	*173.16*	*137.87*	*142.56*	*157.14*	*168.27*
$F_{f,initial}$ (N/m)	*81.44*	*82.25*	*82.99*	*83.22*	*81.95*	*82.12*	*82.64*	*83.04*
$F_{s,critical}$ (N/m)	**64.02**	**85.28**	**104.57**	**110.51**	**77.44**	**81.83**	**95.50**	**105.92**
$F_{f,critical}$ (N/m)	**92.24**	**95.59**	**98.63**	**99.56**	**94.36**	**95.05**	**97.20**	**98.84**
x_{cum} (mm)	9.99	11.99	37.30	*	9.66	10.99	16.99	*
x_{cum} / b	0.046	0.055	0.170	*	0.044	0.050	0.078	*

**Structure collapse*

From the above tables it can be seen that the results predicted by the modified Goda method correlate well with the results obtained from the physical modelling. See Figure 5.8 & Figure 5.9 for graphical presentation of selective data from Table 5.4.

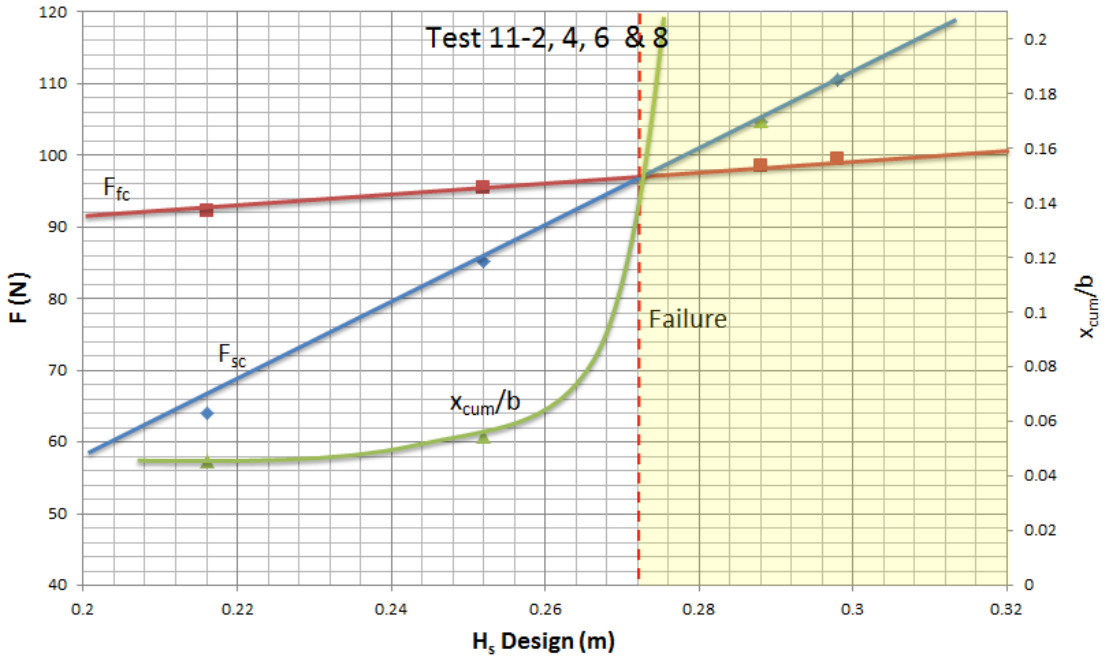

Figure 5.8: Graphical presentation of data from Table 5.4 : Tests 11-2, 4, 6 & 8

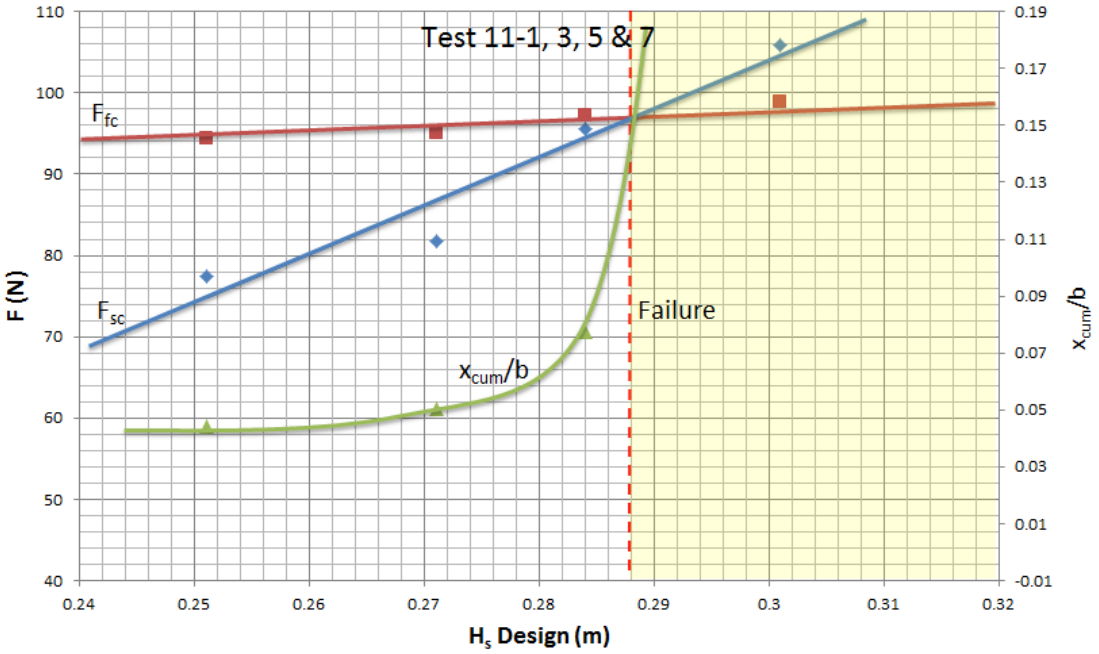

Figure 5.9: Graphical presentation of data from Table 5.4 : Tests 11-1, 3, 5 & 7

Chapter 6 – Conclusions and Recommendations

Conclusions and recommendations based on the findings of this research.

6.1 – Introduction

2D physical modelling in the large wave/current flume of the Stellenbosch University was done to test various set-up and hydraulic conditions to determine the hydraulic stability of a stacked geotextile tube structure against wave attack. Modelling was done on two different scales that had good similitude, despite the fact that the same geotextile and fill material were used in both. A total of 65 tests were completed. All tests consisted of approximately 1,000 waves. Wave conditions were increased incrementally until failure or until the capacity of the wavemaker was reached.

To explain the results obtained from the physical modelling in this study, the tube cross-section was simplified to that of an equivalent rectangle and a modified Goda method was used to determine wave loading that incorporates a wave reduction factor and an angle representative of the position of the crest tube.

6.2 – Stability of Single Tube Structures

By changing the devised angle, α, to 0 the modified Goda method can be used for single tube structures. Using the modified Goda method gives answers that correlate well with those obtained by Van Steeg and Vastenburg (2010) in their large scale physical modelling. However, the modified Goda method is more versatile in its application and is less constrained by limitations.

6.3 – Stability of Multi-layered Structures

6.3.1 – Slip Circle Failure

In the physical model set-up the friction at the flume bed-geotextile interface was extremely high ($\mu_s > 1.2$). This condition would not exist in a prototype application. A normal geotextile-sand interface friction coefficient, μ_s, is approximately 0.57.

It is possible that slip circle failure of the structure will occur before failure due to sliding at heavy wave loading as experienced in the physical modelling. This problem was found by Van Steeg and Vastenburg (2010) in their physical modelling, which had a friction coefficient of 0.5 between the geotextile and the supporting structure.

The possibility of slip circle failure decreases with a decrease in the fill percentage of the geotextile tubes.

Keeping the bottom layer of geotextile tubes from sliding outward to prevent slip circle failure of the structure is important. This can be done by adding additional tubes to the bottom layer, or by using a pre-dredged trench for the bottom layer of tubes.

Future modelling and testing on similar structures can explore the overall stability of the structure and scour at the foot of the structure on movable beds.

6.3.2 – Sliding

Assuming a stable base for the structure, the key failure mechanism under wave loading for a multi-layered geotextile tube structure with an 80% filling percentage of tubes is sliding of the geotextile tube at the crest. With lower filling percentages, deformation of the fill could become a key failure mechanism, as sand transport in the geotextile tube increases. With higher filling percentages, overturning of the crest tube could become the key failure mechanism.

6.4 – Design Considerations

6.4.1 – Forces and Other Variables

There are a multitude of variables and forces that needs to be considered for stability. In addition to the forces covered in this thesis, the additional drag force experienced by a structure at its edges also needs to be taken into account when selecting a tube size.

6.4.2 – Wave Climate

The maximum wave height at the structure is one of the key variables and need to be calculated properly or be known from physical measurement. With the application area of the structure most commonly expected to be inside the surf zone, deep water wave statistics are not sufficient to determine structure stability. Shoaling and depth induced breaking need to be considered to determine accurate wave statistics at the location of the structure.

6.4.3 – Structure Location

The structure is limited to a sand or silt seabed due to the nature of the geotextile. The height of the structure will be directly related to the level of the seabed. The structure therefore needs to have flexible height and alignment requirements, should be built in areas with a regular seabed profile or the construction area should be pre-dredged.

6.4.4 – Water Level

Water level relative to the crest of the structure plays an important role in the wave transmission coefficient and effective wave height factor. Deeper water levels at the structure provide the possibility of bigger waves, but will give rise to higher wave transmission, resulting in a lower effective wave height reduction factor. A lower water level at the structure limits the height of the waves, but will give rise to reduced wave overtopping compared to the condition with the higher water level, resulting in higher wave reduction factors. A critical SWL needs to found to calculate the structure's stability where the combination of wave transmission over the structure and wave condition possible in the specific water depth will give the biggest force on the structure. For structures consisting of four and fewer layers of geotextile tubes, the critical water level should be between the base and the crest of the crest tube of the structure.

6.4.5 – Failure

Depending on the definition of failure for a structure the design will vary immensely. Structural failure is defined very loosely in previous research when compared to definitions relating to conventional rubble mound breakwaters. The CUR 217 (2006) defines failure as the start of movement of the structure. The wave conditions associated with the initial movement is considerably smaller than the wave conditions for the critical failure of the structure. Van Steeg and Vastenburg (2010) recommend that a single geotextile tube structure has failed after the tube has moved more than 5% of its width.

From the results of the physical modelling a structure is deemed to have failed once its crest geotextile tube has been displaced leeward by 15% of its width, as structure collapse occurs soon after the displacements exceeds 15%.

The failure of a structure depends on what the intended purpose is of said structure. A geotextile tube used to heighten a dyke should be allowed very little or no movement during its designed loading, whereas a geotextile tube structure used as an offshore breakwater for retaining sand nourishment for a beach could deform substantially during its design storm conditions and still be considered intact.

References

Battjes, J.A. & Groenendijk, H. (2000) Wave height distributions on shallow foreshores. *Coastal Engineering*, 40, pp.161 – 182.

Bezuijen, A. & Vastenburg, E. (2008) Geosystems, Possibilities and Limitations for applications. *EuroGeo*, 4(282), pp.1–6.

Cantré, S. (2002) Geotextile tubes — analytical design aspects. *Geotextiles and geomembranes*, 20, pp.305–319.

Cantré, S. & Saathoff, F. (2011) Geotextiles and Geomembranes Design method for geotextile tubes considering strain e Formulation and verification by laboratory tests using photogrammetry. *Geotextiles and Geomembranes*, 29.

CIRIA CUR CETMEF (2007) *The Rock Manual. The use of rock in hydraulic engineering* 2nd ed., CIRIA London.

CUR (2006) *CUR 217: Ontwerpen met geotextiele zandelementen*, Stichting CUR, Gouda.

CUR (2004) *CUR214: Geotextiele zandelementen*, Stichting CUR Gouda.

Delft Hydraulics (1994) *Stability of geotubes and geocontainers*, report for Nicolon b.v. Delft.

Elko, N.A. & Mann, D.W. (2007) Implementation of geotextile T-groins in Pinellas County, Florida. *Shore and Beach*, 75(2).

Ergin, A., Pamukçu, A., Derun, B. & Yalçiner, A. (2003) Transmission of Waves Through the Breakwaters Constructed with Geotextile Tubes. In *COP EDEC VI*. pp. 1–13, Paper no. 24.

Fowler, J., Stephens, T., Santiago, M. & De Bruin, P. (2002) Amwaj Islands constructed with Geotubes, Bahrain. In Denver, USA: CEDA Conference, pp. 1–14.

Fowler, J., Gilbert, Paul & Trainer, E. (1997) Construction Productivity Advancement Research (CPAR) Program. Development and Demonstration of Dredged Material Containment Systems Using Geotextiles.

Goda, Y. (1974) New Wave Pressure Formulae for Composite Breakwaters. In *ICCE*. Copenhagen, pp. 1702–1720.

Goda, Y. (2000) *Random seas and design of maritime structures*, Singapore: World Scientific Publishing co. Pte. Ltd.

Hiroi, I. (1920) Evaluation of wave pressure. *JSCE*, 6, pp.435–449.

Honma, M. & Horikawa, K. (1965) Experimental study on total wave force against sea wall. *Coastal Engineering in Japan*, 8, pp.119–129.

Hornsey, W. & Jackman, M. (2005) Limeburners Breakwater - The Innovative Use of Geotextile Sand Containers. *Coasts and Ports: Coastal Living-*, pp.1–4.

Hughes, S.A. (1993) *Physical models and laboratory techniques in coastal engineering*, World Scientific.

Jackson, L.. & Hornsey, W.P. (2003) *An Artificial Reef to Protect Surfers Paradise Beach Developing & Implementing the Science*,

Koerner, G.R. & Koerner, R.M. (2006) Geotextile tube assessment using a hanging bag test. *Geotextiles and Geomembranes*, 24, pp.129–137.

Koerner, R.M. (2005) *Designing with geosynthetics* 5th ed., New Jersey, USA: Pearson Prentice Hall.

Leschinsky, B.A. (2007) Adema Engineering. Available at: http://www.geoprograms.com/geocopsindex.htm [Accessed February 24, 2012].

Leshchinsky, D., Leshchinsky, O., Ling, H. & Gilbert, P. (1996) Geosynthetic Tubes for confining Pressurized slurry: Some design Aspects. *Journal of geotechnical engineering*, (685).

Leshchinsky, D. & Leshchinsky, O. (1996) GeoCoPS (2.0) : Supplemental Notes. Available at: http:/www.geoprograms.com/downloads/GeoCoPS_Supplemental%20Notes.pdf [Accessed February 24, 2012]

Mansard, E.P.D. and Funke, E.R. (1980) 'The measurement of incident waves and reflected spectra using a least square method', 17th Int. Conf. of Coastal Engineering, Proc. ICCE'80, ASCE, pp.154-172, Sydney.

Minikin, R.R. (1963) *Winds, Waves and Maritime Structures: Studies in Harbor making and in the Protection of Coasts* 2nd ed., London: Griffin.

Oh, Y.I. & Shin, E.C. (2006) Using submerged geotextile tubes in the protection of the E . Korean shore. *Coastal Engineering*, 53, pp.879–895.

PIANC (2011) *Report no. 113 - 2011: The Application of Geosynthetics in Waterfront Areas*,

Pilarczyk, K. (2000) *Geosynthetics and Geosystems in Hydraulic and Coastal Engineering* 1st ed., Rotterdam: Balkema.

Pullen, H., Allsop, N., Bruce, T., Kortenhaus, A. & Schuettrumpf, H. & Van der Meer, J. (2007) EurOtop - Wave overtopping of sea defences and related structures: Assessment manual.

Recio, J. (2008) 'Hydraulic Stability of Geotextile Sand containers for Coastal Structures - Effect of Deformations and Stability Formulae' PhD Thesis, Leichtweiss Institute for Hydraulic Engineering and Water resources, www.digibib.tu-bs.de/?docid=00021899

Restall, S., Jackson, L. & Heerten, G. (2002) Case studies showing the growth and development of geotextile sand containers: an Australian perspective. *Geotextiles and Geomembranes*.

Sainflou, G. (1928) Essai sur les diques maritimes verticales. *Annales des Ponts et Chausees*, 98(4).

U.S. Army Corps of Engineers (2006) *Coastal Engineering manual (CEM)*,

U.S. Army Corps of Engineers (1984) *SPM: Shoreline Protection manual*, Mississippi.

Van der Meer, J.W., Wang, B., Wolters, A., Zanuttigh, B. and Kramer, M. (2003) 'Oblique wave transmission over low-crested structures'. In: J.A. Melby (ed) Proc 4th international coastal structures conferenc, Portland, OR, 26-30 Aug 2003. ASCE, reston, VA, pp567-579

Van Steeg, P. & Vastenburg, E. (2010) *Large scale physical model tests on the stability of geotextile tubes*, Deltares report, Delft.

Weggel, J.R. (2005) On the Stability of Shore- • Parallel Geotextile Tubes for Shore Protection. In *ASCE Geofrontiers Conference Proceedings*.

Williams, J.A., (1994) Engineering Tribology. In Cambridge University Press, pp. 134–138.

Appendix A – Facility

Large Wave/Current Flume

Stellenbosch University, Faculty of Engineering, Department of Civil Engineering

Fig. A.1: Large wave flume at the Faculty of Engineering of Stellenbosch University

The 2m wide by 2m deep Stellenbosch University large flume is used for large scale wave/current structure interaction tests, design optimisation and hydrodynamic studies of coastal and offshore structures and wave energy conversion devices. The concrete

flume is 60m long of which 6.5m has glass walls on both sides. If required a 1t overhead gantry crane may be used to build the models. The hinged paddle is fitted with a Dynamic Absorption System that receives HR Wavemaker input signals, enabling fully irregular waves and design spectra on demand

The flume is equipped with a hinged type wave maker with Dynamic Wave Absorption that can simulate: Long and short crested random waves. JONSWAP, Pierson-Moskowitz or a user-defined wave spectrum can be used. Time series of surface elevations are imported from ASCII files. A 4-channel wave gauge system, 4x600mm resistive wave probes and HR DAQ software are used to acquire and analyse the data from model tests: Reflection analysis is done with a four probe array, using HR Wallingford's HR DAQ software.

Maximum wave height: 0.6 m (at 1.5m depth)

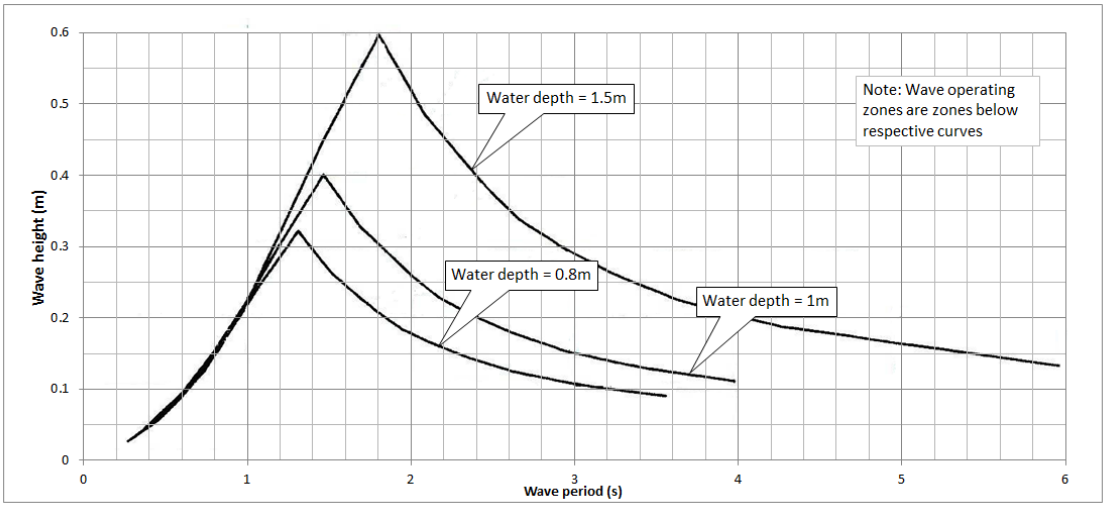

Fig. A.2: Generation curves for the Large Flume

From Fig. A.2 note the sharp drop in generation capacity with the drop in water depth. 1.5m is the recommended water depth, but larger waves are possible with deeper water depths although overtopping of the flumes edges could become problematic. With active absorption turned on the maximum wave height that can be generated drops, depending on the reflection coefficient of the structure being tested.

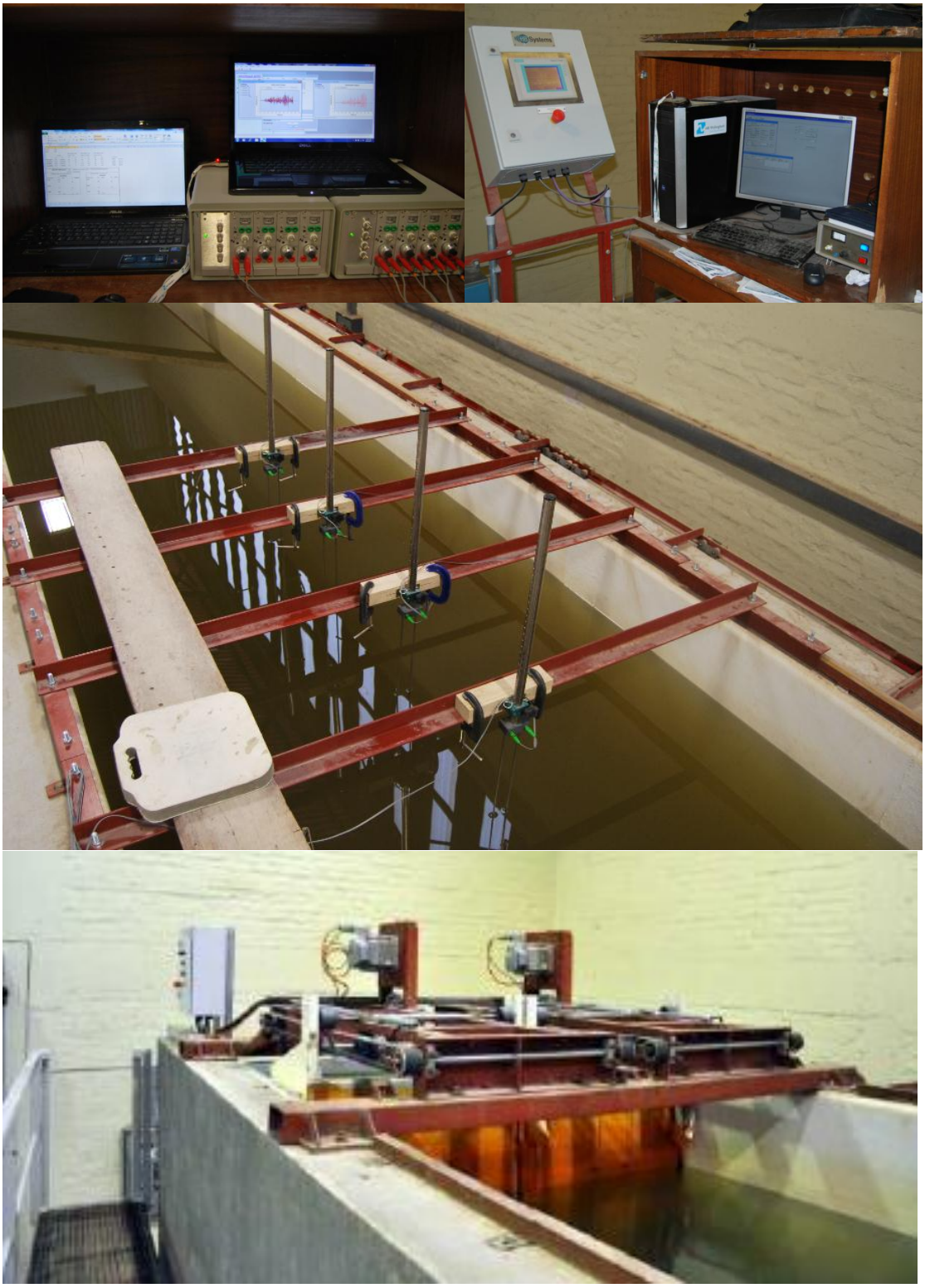

Fig. A.3: Equipment used for wave generation and data acquisition

Appendix B – Wave reduction factor

(after Van Steeg & Vastenburg 2010)

It is assumed that all incoming wave energy (E_i) is transferred into dissipated energy due to depth induced breaking before reaching the structure (E_{ss}), energy dissipated on the structure (E_{tube}) and energy transmitted to the leeside of the structure (E_l). From the physical modelling the wave energy at the structure location is known ($E_i - E_{ss}$).

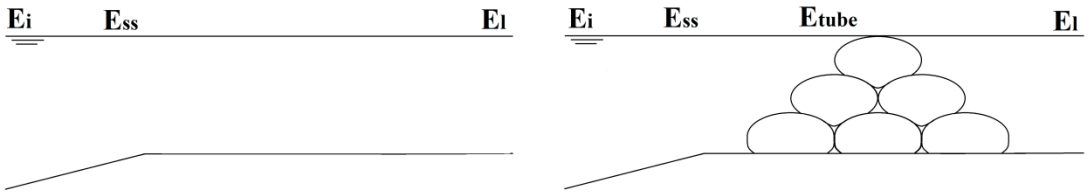

Fig. B.1: Energy positions

Energy balance:

Without structure: $E_i = E_{ss} + E_l$

With structure: $E_i = E_{ss} + E_{tube} + E_{l+tube}$

From the above two equations: $E_{tube} = E_{ss} - E_{l+tube}$

$$\chi = \frac{H_{s,tube}}{H_{s,i}} = \sqrt{\frac{E_{tube}}{E_i}}$$

with:

χ = *ratio between effective wave height and the incoming wave height*

$H_{s,tube}$ = *dissipated energy on tube given as wave height (effective wave height)*

$H_{s,i}$ = *incoming wave height*

The ratio, χ, can be used to adapt the incident wave height to an effective wave height.

The effective wave height on the structure is determined by comparing the situation where no structure is applied to a situation where a structure is applied (Van Steeg & Vastenburg 2010).

The coefficient of transmission, C_t, is the ratio between the transmitted and incident wave height. (CIRIA CUR CETMEF 2007)

$$C_t = H_t/H_i = \sqrt{E_t/E_i}$$

From above equation the equation for the reduction factor can be re-written as:

$$\chi = \sqrt{C_{t,ss}^2 - C_{t,l}^2}$$

with:

$C_{t,ss}$ = transmission coefficient for the foreshore seabed

$C_{t,l}$ = transmission coefficient for the structure

$H_{tube} = C_{t,ss}(C_{t,l}(H_i))$

The relationship between the relative crest freeboard, R_c/H_s, and the coefficient of transmission, C_t, is summarized in the equations below.

$-2.00 < \frac{R_c}{H_s} < -1.13$ $\quad C_t = 0.8$

$-1.13 < \frac{R_c}{H_s} < 1.20$ $\quad C_t = 0.46 - 0.3R_c/H_s$

$1.20 < \frac{R_c}{H_s} < 2.00$ $\quad C_t = 0.1$

$R_c/H_s << -2$ $\quad C_t = 1$

$R_c/H_s >> 2$ $\quad Ct = 0$

R_c = *crest height above SWL*

These relationships give a very simple description, but can be used for preliminary estimates of performance. (CIRIA CUR CETMEF 2007)

The formula below has been developed within the DELOS project (J. W. V. D. Van der Meer et al. 2004) for any smooth low-crested structure. The formula is based on the significant wave height at the toe of the structure and the peak wave period in deep water, with minimum and maximum values of C_t = 0.075 and C_t = 0.8 respectively.

$$C_t = \left(-0.3\frac{R_c}{H_s} = 0.75\left(1 - exp\left(0.5\xi_p\right)\right)\right)cos^{\frac{2}{3}}\beta$$

The formula has the following limitations: $1 < \xi_p < 3$; $0^\circ \leq \beta \leq 70^\circ$; $1 < B/H_s < 4$, where B is the crest width.

A graphic presentation of the reduction parameter by Van Steeg and Vastenburg (2010) can be seen in Figure 2.13

In this thesis the energy at the seaward toe of the structure and leeward of the structure is known and used to determine the effective wave height at the structure as shown in the formulae below.

$$E_{effective} = E_{seaward} - E_{leeward}$$

$$E_{effective} = E_{seaward} - C_t^2 E_{seaward}$$

$$E_{effective} = E_{seaward}(1 - C_t^2)$$

$$H_{effective} = H_{seaward}\sqrt{(1 - C_t^2)}$$

$\chi = H_{effective}/H_{seaward\ toe}$

$$\chi = \sqrt{(1 - C_t^2)}$$

Appendix C – Modified Goda: Calculation Example

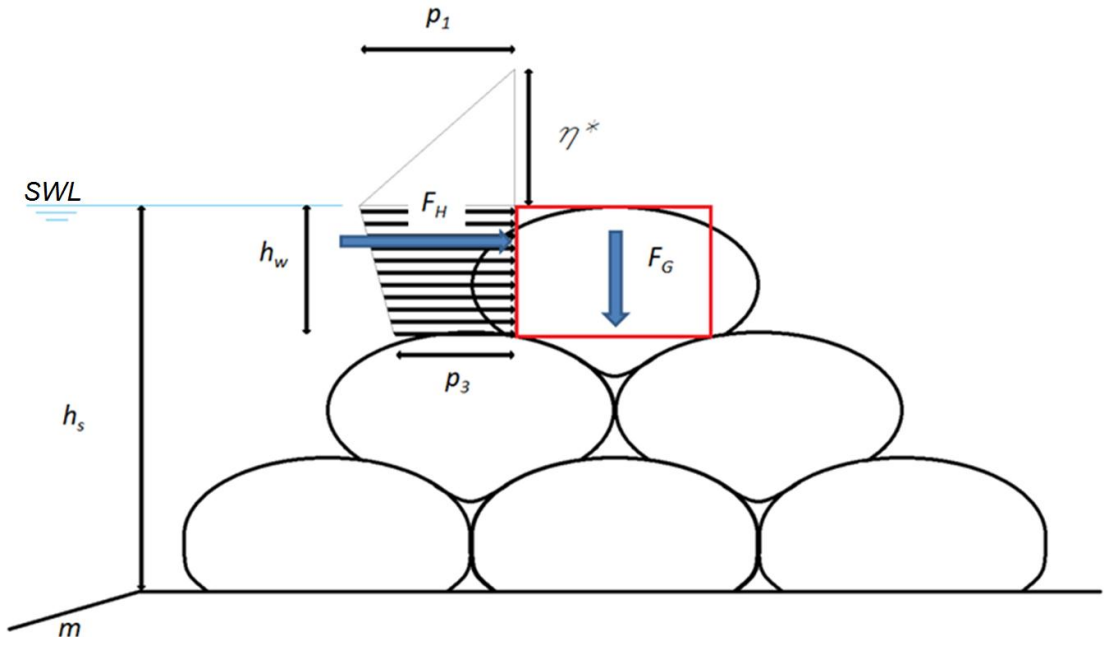

Fig. C.1: Schematisation of forces on a tube at the crest of a breakwater

Given: *Test 7-8 with wave condition 8*

A three layer stacked geotextile tube offshore breakwater with a total height of 0.45m with its crest at SWL.

Tube dimension: h = 0.150m (height)

b = 0.328m (width)

A = 0.041m^2 (cross-section area)

Spectral significant wave height for design, H_{m0} = 0.24m (assume equal to H_s)

Peak wave period, T_p = 2 s

Wave angle of incidence, β = 0°

Water, ρ_w = 1000kg/m^3

Saturated Sand, ρ_s = 2040kg/m^3

Relative density of tube, $\Delta_t = (\frac{\rho_s - \rho_w}{\rho_w}) = 1.04$

Offshore slope of 1 in 20, m = 0.05

Highest wave height at structure location, H_{design} = 0.4m (actual measurement)

Friction coefficient for a wet geotextile-geotextile interface, μ_s = 0.41

Data captured by the probes at the seaward toe and leeward of the structure produces a wave reduction factor, χ, of 0.477.

Solution:

Submerged depth of crest tube, h' = 0.15m

Crest height above SWL, h_c = 0m

Height of tube, h_w = 0.15m

Total structure submerged depth, h_s = 0.45m

Depth a distance of 5(H_s) from geotube, $h_b = 5(H_s)(m) + h_s = 0.513\text{m}$

Wavelength at structure, $L = T_p\sqrt{gh_s} = 2\sqrt{(9.81)(0.45)} = 4.202\text{m}$

Modification factors, $\lambda_1 = \lambda_2 = \lambda_3 = 1$

$$\eta^* = 0.75(1 + cos\beta)\left(\lambda_1 H_{design}\right) = 0.75(2)\left(1(0.4)\right) = 0.6\text{m}$$

$$\alpha_* = \alpha_2 = 0.236$$

$$\alpha_1 = 0.6 + 0.5\left[\frac{4\pi h_s/L}{sinh(4\pi h_s/L)}\right]^2 = 0.6 + 0.5\left[\frac{4\pi(0.45)/4.202}{sinh(4\pi(0.45)/4.202)}\right]^2 = 0.883$$

$$\alpha_2 = \text{the smallest of } \frac{h_b - h_s}{3h_b}\left(\frac{H_{design}}{h_s}\right)^2 \text{ and } \frac{2h_s}{H_{design}} = 0.236$$

$$\alpha_3 = 1 - \frac{h_w - h_c}{h_s}\left[1 - \frac{1}{cosh\left(\frac{2\pi h_s}{L}\right)}\right] = 1 - \frac{0.15}{0.45}\left[1 - \frac{1}{cosh\left(\frac{2\pi(0.45)}{4.202}\right)}\right]$$

$$= 0.937$$

$$p_1 = 0.5(1 + cos\beta)(\lambda_1\alpha_1 + \lambda_2\alpha_* cos^2\beta)\rho_w g\chi H_{design}$$

$$= 0.5(2)(0.883 + 0.236)1000(9.81)(0.477)(0.4)$$

$$= 2093\text{N/m}^2$$

$$p_3 = \alpha_3 p_1 = 1961\text{N/m}^2$$

Wave induced horizontal force: $F_H = U_{FH}\left[\frac{1}{2}(p_1 + p_3)h'\right]$

(per m length of structure) $= 0.9\left[\frac{1}{2}(2093 + 1961)0.15\right]$

$= 274N/\text{m}$

U_{FH} is a stochastic variable signifying the bias and uncertainty in the horizontal force.

Note: No uplift force as the tubes are considered as impermeable.

Gravity and buoyancy induced vertical force: $F_G = \Delta_t \rho_w A g$

(per m length of structure) $= (1.04)(1000)(0.041)(9.81)$

$= 418.298\text{N/m}$

Stability against Overturning

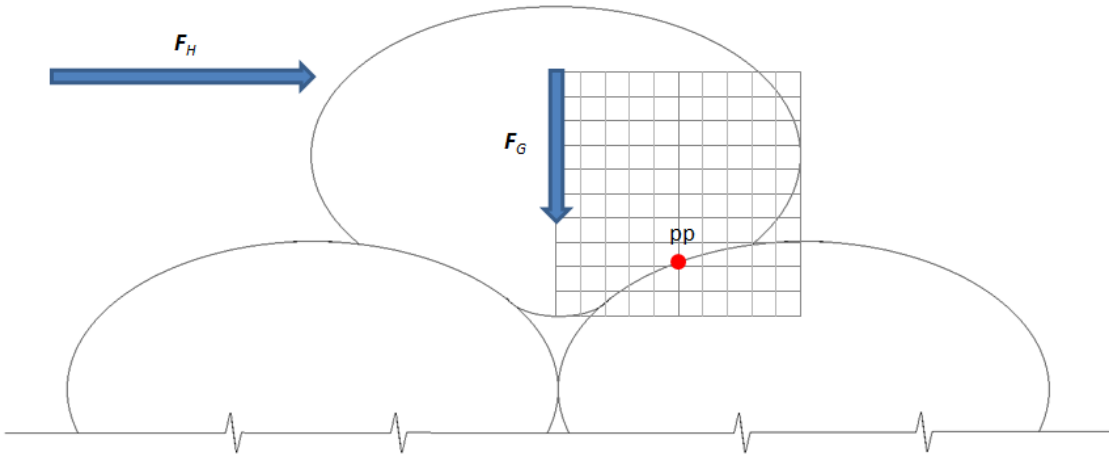

Fig. C.2: Pivot point for crest tube

M_H and M_G relate to the pivot point, *pp*, in Fig. C.2

Moment corresponding to the horizontal force, F_H, at the pivot point:

$$M_H = U_{MH}\left[\frac{1}{6}p_1 + \frac{1}{3}p_3\right]h'^2$$

$$= 0.81\left[\frac{1}{6}(2093) + \frac{1}{3}(1961)\right](0.15)^2$$

$$= 19\text{Nm/m}$$

U_{MH} is a stochastic variable signifying the bias and uncertainty of the horizontal moment

Moment corresponding to the gravity and buoyancy force, F_G

$$M_G = F_G(B)$$

$$= 418.298(B)$$

B is the horizontal distance between the centre of gravity of the tube and the pivot point of the tube.

B = 0.082m (0.25b)

$$M_{Gmin} = 29.281\text{Nm/m}$$

$M_H < M_G$, ∴ the crest tube is stable against overturning

Stability against Sliding

The crest tube is not resting on a flat surface, but is wedged in between the two crests of the tubes below it. The structure becomes more stable after initial movement. Initial displacement of the crest tube occurs at much lower wave conditions than failure. For initial movement, $\alpha = 5^\circ$ should be used, and for critical failure $\alpha = 21^\circ$.

For the crest tube to resist sliding on the leeward tube below it, the following forces needs to be considered (see Fig. C.3).

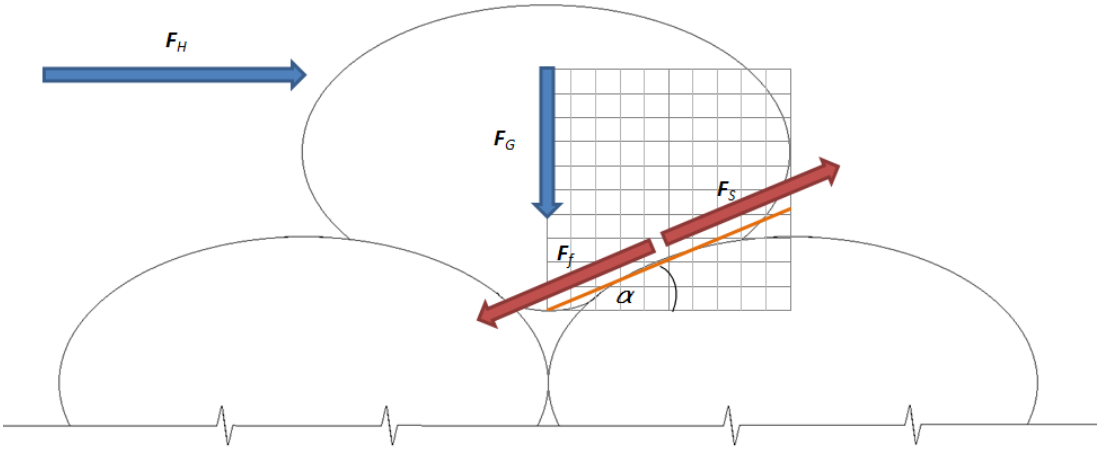

Fig. C.3: Schematisation of forces for sliding instability of the crest tube

Resisting static friction force, F_f

$$F_f = \mu_s(F_G cos\alpha + F_H sin\alpha)$$

Sliding force, F_S

$$F_S = (F_H cos\alpha - F_G sin\alpha)$$

For initial movement $\alpha = 5^\circ$

$$F_{f,i} = 0.41(418cos5^\circ + 274sin5^\circ)$$

$$= 181\text{N/m}$$

$$F_{S,i} = (274cos5^\circ - 418sin5^\circ)$$

$$= 236\text{N/m}$$

$F_{s,i} > F_{f,i}$, therefore initial displacement of the top tube can be expected.

For critical failure $\alpha = 21^\circ$

$$F_{f,c} = 0.41(418cos21^\circ + 274sin21^\circ)$$

$$= 200\text{N/m}$$

$$F_{S,c} = (274cos21^\circ - 418sin21^\circ)$$

$$= 106\text{N/m}$$

$F_{s,c} < F_{f,c}$, therefore the structure will reach stability after initial displacement.

In the physical model the crest tube was displaced leeward by 29mm during the tests, but it did not fail.

Appendix D – Wave Data

Tab. D.1: Hydraulic conditions for test series 0-9

Wave condition	Incident					At structure			
	H_s (m)	T_p (s)	H_{max} (m)	s_{0p}	$\xi_{m-0,p}$	Depth (m)	H_s (m)	T_p (s)	H_{max} (m)
1	0.13	1.79	0.242	0.026	0.310	0.15	0.13	1.75	0.184
						0.225	0.145	1.75	0.249
						0.3	0.13	1.75	0.21
						0.375	0.133	1.75	0.25
						0.45	0.13	1.85	0.259
2	0.15	2.01	0.279	0.024	0.324	0.15	0.147	2	0.208
						0.225	0.174	2	0.263
						0.3	0.164	2.13	0.289
						0.375	0.171	2.13	0.305
						0.45	0.161	2.13	0.29
3	0.16	2.24	0.298	0.020	0.350	0.15	0.159	2.38	0.239
						0.225	0.19	2.38	0.29
						0.3	0.204	2.22	0.339
						0.375	0.197	2.27	0.364
						0.45	0.189	2.22	0.349
4	0.18	2.46	0.335	0.019	0.362	0.15	0.168	2.44	0.235
						0.225	0.208	2.44	0.304
						0.3	0.231	2.38	0.382
						0.375	*	*	*
						0.45	0.225	2.33	0.409
5	0.18	1.73	0.335	0.039	0.255	0.45	0.177	1.82	0.328
6	0.2	1.82	0.372			0.45	0.205	1.79	0.349
7	0.22	1.91	0.409			0.45	0.229	1.89	0.353
8	0.24	1.99	0.446			0.45	0.25	2.13	0.397

* Flume capacity exceeded

Tab. D.2: Hydraulic conditions for test series 10 & 11

Wave condition	Incident					At structure			
	H_s (m)	T_p (s)	H_{max} (m)	s_{0p}	$x_{m-0,p}$	Depth (m)	H_s (m)	T_p (s)	H_{max} (m)
S1	0.16	1.63	0.298	0.039	0.255	0.3	0.163	1.72	0.251
						0.4	0.152	1.61	0.251
S2	0.19	1.77	0.353			0.3	0.182	1.72	0.271
						0.4	0.19	1.85	0.298
S3	0.22	1.91	0.409			0.3	0.203	2.04	0.284
						0.4	0.223	1.89	0.339
S4	0.24	1.99	0.446			0.3	0.212	1.96	0.301
						0.4	0.24	2.13	0.342
L1	0.12	2.01	0.223	0.019	0.362	0.3	0.139	2	0.239
						0.4	0.134	1.89	0.25
L2	0.14	2.17	0.260			0.3	0.17	2.08	0.272
						0.4	0.158	2.13	0.298
L3	0.16	2.32	0.298			0.3	0.196	2.38	0.292
						0.4	0.204	2.27	0.359
L4	0.18	2.46	0.335			0.3	*	*	*
						0.4	0.233	2.63	0.368

* Flume capacity exceeded

Appendix E – Construction

While being filled the bottom layer of geotextile tubes were packed in between large bricks that were set-out according to the width of the tube to help keep them in place (see Fig. E.1 left). A secondary pump was used to top up the sand container and to help suspend the sand particles (see Fig. E.1 right). Filling the tubes in the correct position was extremely important as moving them after filling was completed was near impossible due to their weight (approx. 175kg) and their long, unwieldy shape.

Fig. E.1: Filling of geotextile tube

The filling of tubes on the upper layers did not require help to prevent unwanted movement, as the lower tubes created a wedge keeping the upper tubes in place.

As the tube filled, the permeability of the tube decreased. This results in an increase in the pressure in the tube. The pressure was controlled by pulling the filling pipe further out of the relatively long filling port to provide additional area for the pressure to be released. The planned function of the second filling port, which can be seen on the first set of tubes, was to help with the pressure release at the end of the filling process. It did not work quite as intended, however, as large amounts of sand washed out when it was opened and it therefore was kept closed. Tube rupturing was uncommon, but occurred around the stitching of the filling port.

As in prototype filling of tubes, a low spot forms around the filling port at the end of the filling process. This low area was remedied by taking the pipe from the pump almost completely out of the filling port and bending the filling port so that most of

the pumping pressure to the tube was lost or by washing in a final handful of sand manually.

See Fig E.2 below for the progression of the tube structure.

Fig. E.2: 3-2-1 Structure construction steps

After the tubes had been filled, the filling ports were sewn shut and the excess material was tucked in beneath the tubes on the lower levels and stitched fast to the leeward side of the tube on the crest level.

Positions were cross-sections were measured was marked with a black cross.

Appendix F – Characteristics of Sand

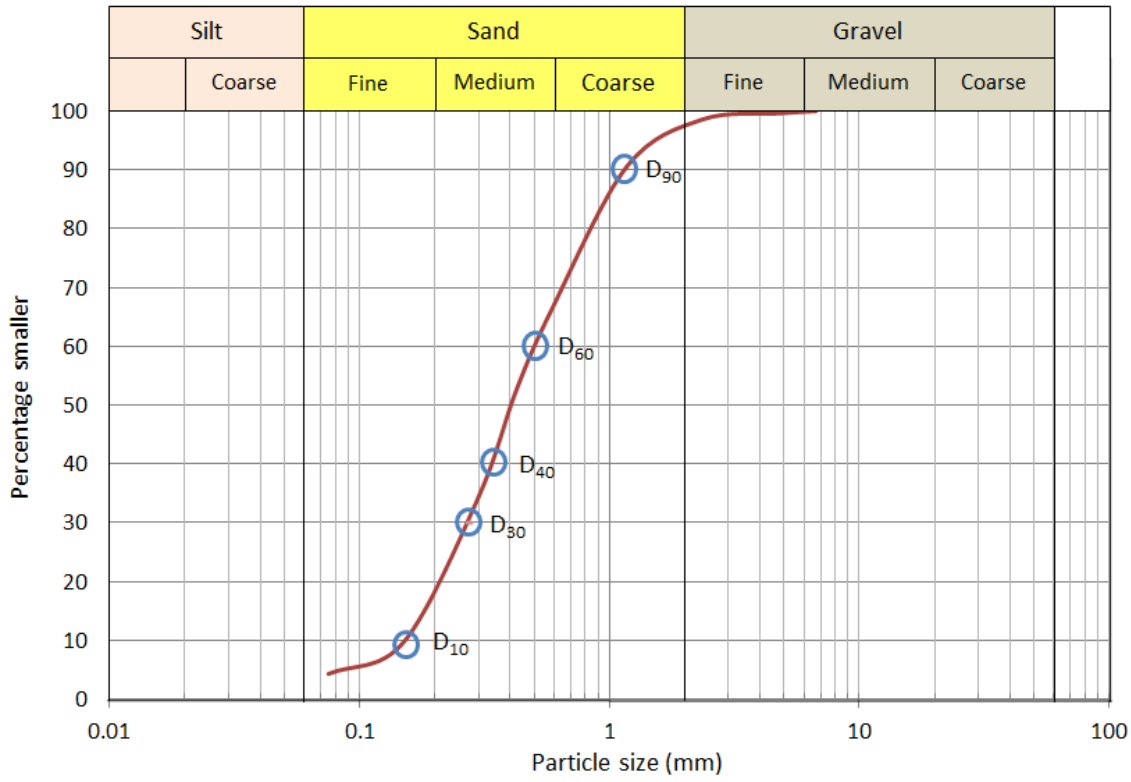

Fig. F.1: Sieving curve

From above sieving curve: D_{10} = 0.15mm (Effective size)

D_{30} = 0.27mm

D_{40} = 0.34mm

D_{60} = 0.50mm

D_{90} = 1.14mm

C_U = $\frac{D_{60}}{D_{10}} = 3.33$ (coefficient of uniformity)

C_Z = $\frac{D_{30}^2}{D_{60}D_{10}} = 0.972$ (coefficient of curvature)

From actual weighing: ρ_s = 2040kg/m3

Δ = 1.04

Appendix G – Secudrän® Specifications

The geotextile tubes were made of a nonwoven polypropylene material, sponsored by the company: NAUE Geotechnics and Geosystems (Germany).

The textile has the following characteristics:

- Mass per unit area: ≥ 180 g/m2

- Thickness at 2 kPa: ≥ 2.2 mm

- Maximum tensile strength: longitudinally / transversally: 7.2 kN/m / 10.8 kN/m

- Elongation at max. strength (longitudinal) / (transversally): 45 % / 36 %

- Static puncture test: 1.5 kN/m

- Opening size: 0.12 mm

- Water permeability: 3 x 10^{-3} m/s

- Friction angle geotextile-geotextile: 20° to 25°; geotextile-sand: > 30°

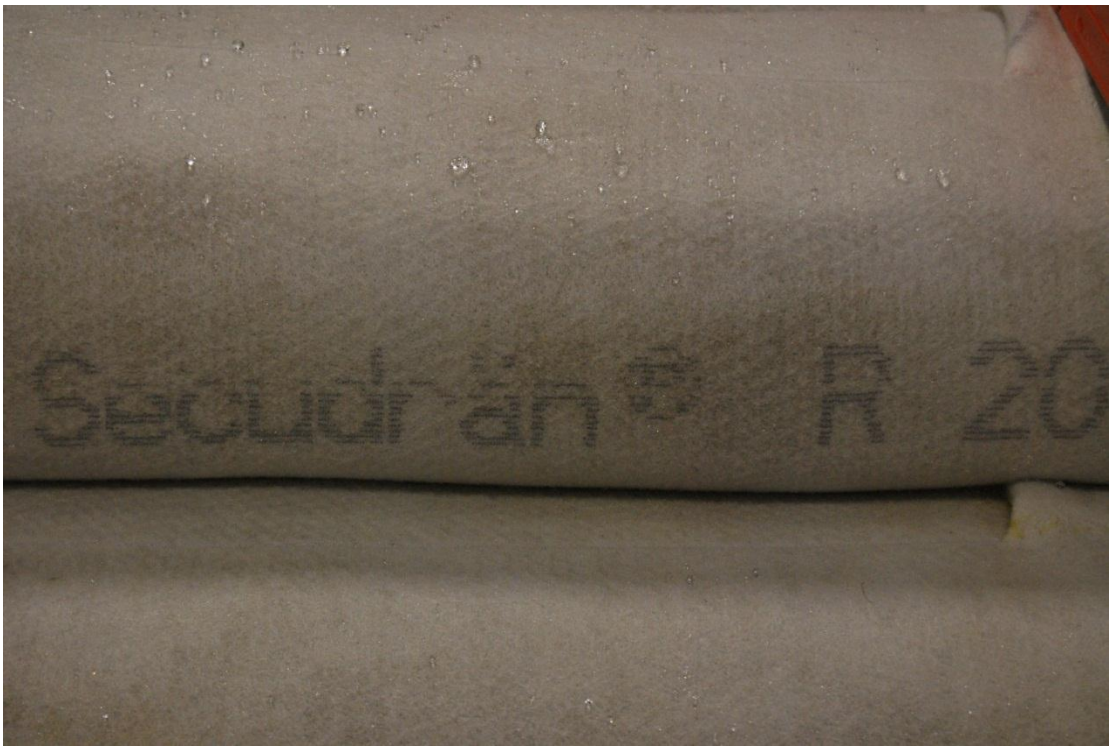

Fig. G.1: Close-up of geotextile tube

Appendix H – Static Friction

H.1 – Amonton's Laws (Williams 1994)

Amonton's First Law: The force of friction is directly proportional to the applied load.

Assume an arbitrary object lying on an arbitrary flat surface. With greater mass (greater weight as g is constant) the object would then exert a greater force on the surface it is resting on (the increased load causes the separation distance of the nuclei to decrease, the force of repulsion becomes stronger and more of the atoms of the object and the surface would be in contact).

Amonton's law applies to any two surfaces, regardless of their orientation.

Amonton's Second Law: The force of friction is independent of the area of contact.

What this law means is that if two equivalent masses made of similar material are resting on the same surface with different areas of contact, they would require the same amount of force to start moving (overcome static friction) and to move at constant speed.

For example: Consider two equal masses and the area in contact in situation 1 is greater than in situation 2. This means that in situation 1, the load is distributed over a greater area then in situation 2. However, the applied load is still the same. Therefore to move both masses, we would require the same amount of applied force to overcome friction. (Amonton's First Law)

In summary: $F = \mu_s.N$

with:

μ_s: *Static coefficient of friction*

N: *Force normal to surface*

H.2 – Experiment

An experiment to determine the friction coefficient between concrete and Secudrän® > 180g/m^2 polypropylene needle punched geotextile was performed by placing a flat element on a slope and slowly increasing that slope. Imbalance in the gravitational and frictional forces is reached when the element starts to slide. The angle was

determined using basic trigonometry. See Fig. H.1 for the experiment setup. Both a heavy concrete block (25kg) and a much lighter geotextile sand bag (4kg) were used in the experiment to determine whether the compression of the geotextile has any influence on the friction coefficient. No difference in the friction coefficient was noticed with compression in the geotextile. See Fig. H.2 for the force diagram of friction and gravitation forces on an object.

Fig. H.1: Experiment setup for attaining friction coefficients

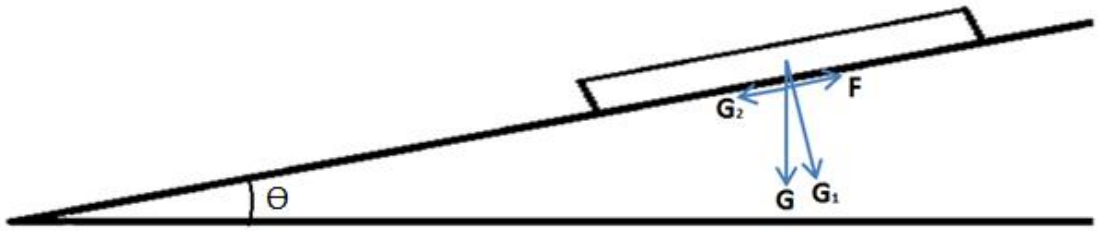

Fig. H.2: Forces on object on a sloped surface

G = gravitational force of element

$G_1 = G.\cos\theta$

$G_2 = G.\sin\theta$

$F = \mu_s.G_1$

μ_s = *static friction coefficient*

For the balance of forces $G_2 = F$.

Thus $\mu_s = tan\Theta$

Tab. H.1: Summary of friction coefficients

Interacting surfaces	Wet/Dry	Friction coefficient (μ_s)
Geotextile-geotextile	Dry	0.57
Geotextile-concrete	Dry	0.59
Geotextile-geotextile	Wet	0.41
Geotextile-concrete	Wet	0.58
Geotextile-flume bed	Wet	>1.2

Tab. H.2: Results of friction experiment

Concrete - Geotextile (Dry)		**Geotextile - Geotextile (Dry)**	
Test	tanΘ at failure	Test	tanΘ at failure
1	0.58	1	0.55
2	0.61	2	0.56
3	0.59	3	0.59
4	0.58	4	0.57
5	0.59	5	0.55
6	0.59	6	0.57
Average	0.59	Average	0.57
Geotextile - Geotextile (Wet)		**Concrete - Geotextile (Wet)**	
Test	tanΘ at failure	Test	tanΘ at failure
1	0.4	1	0.58
2	0.41	2	0.6
3	0.42	3	0.59
4	0.41	4	0.57
5	0.42	5	0.58
6	0.42	6	0.58
Average	0.41	Average	0.58

Friction coefficient obtained from supplier for geotextile-geotextile interface: 0.36 – 0.47.

The friction coefficient between the flume bed and geotextile was much higher than the friction coefficient between the initially tested geotextile and the concrete. A mixture of sand, cement and very little water was used to construct the slope bed. The mixture gets compacted and floated which results in a finished surface with a texture similar to that of fine sand paper. A piece was broken out from the bed and tested after the physical modelling. The geotextile and bed surface reacted almost like Velcro, with a friction coefficient greater than 1.2. See Fig. H.3.

Fig. H.3: High friction angle between wet geotextile and flume slope surface.

Appendix I – Froude Scaling Laws

The Froude number is a parameter that expresses the relative influence of inertial and gravity forces in a hydraulic flow.

Froude number:

$$\sqrt{\frac{inertial\ force}{gravity\ force}} = \sqrt{\frac{\rho L^2 V^2}{\rho L^3 g}} = \frac{V}{\sqrt{gL}}$$

with:

ρ = *fluid density*

L = *length*

V = *velocity*

The requirement for Froude scaling is that the Froude number should be the same in the model as in the prototype. Therefore:

$$\left(\frac{V}{\sqrt{gL}}\right)_p = \left(\frac{V}{\sqrt{gL}}\right)_m$$

This leads to:

$$\frac{V_p}{V_m} = \sqrt{\left(\frac{g_p}{g_m}\right)\left(\frac{L_p}{L_m}\right)}$$

See Tab. I.1 for full list of similitude ratios.

with:

L = *measurement of length*

M = *measurement of mass*

T = *measurement of time*

N_L = *length/geometric scale*

N_ρ = *density scale*

N_γ = *specific weight scale*

Tab. I.1: Froude similitude ratios after Hughes 1993

Characteristic	Dimension	Froude
Geometric		
Length	L	N_L
Area	L^2	N_L^2
Volume	L^3	N_L^3
Kinematic		
Time	T	$N_L^{1/2} N_\rho^{1/2} N_\gamma^{-1/2}$
Velocity	LT^{-1}	$N_L^{1/2} N_\rho^{-1/2} N_\gamma^{1/2}$
Acceleration	LT^{-2}	$N_\gamma N_\rho^{-1}$
Discharge	L^3T^{-1}	$N_L^{5/2} N_\rho^{-1/2} N_\gamma^{1/2}$
Kinematic Viscosity	L^2T^{-1}	$N_L^{3/2} N_\rho^{-1/2} N_\gamma^{1/2}$
Dynamic		
Mass	M	$N_L^3 N_\rho$
Force	MLT^{-2}	$N_L^3 N_\gamma$
Mass Density	ML^{-3}	N_ρ
Specific weight	$ML^{-2}T^{-2}$	N_γ
Dynamic viscosity	$ML^{-1}T^{-1}$	$N_L^{3/2} N_\rho^{1/2} N_\gamma^{1/2}$
Surface Tension	MT^{-2}	$N_L^2 N_\gamma$
Volume Elasticity	$ML^{-1}T^{-2}$	$N_L N_\gamma$
Pressure and Stress	$ML^{-1}T^{-2}$	$N_L N_\gamma$
Momentum, Impulse	MLT^{-1}	$N_L^{7/2} N_\rho^{1/2} N_\gamma^{1/2}$
Energy, Work	ML^2T^{-2}	$N_L^4 N_\gamma$
Power	ML^3T^{-3}	$N_L^{7/2} N_\rho^{-1/2} N_\gamma^{1/2}$